OPEN ACCESS

TRANSLATIONAL SCIENCE

Taxonomy of fibroblasts and progenitors in the synovial joint at single-cell resolution

Fraser L Collins [1], Anke J Roelofs [1], Rebecca A Symons [1], Karolina Kania,[1] Ewan Campbell,[2] Elaina S R Collie-duguid,[2] Anna H K Riemen,[1] Susan M Clark,[1] Cosimo De Bari [1]

Handling editor Josef S Smolen

► Additional supplemental material is published online only. To view, please visit the journal online (http://dx.doi.org/10.1136/ard-2021-221682).

[1]Arthritis and Regenerative Medicine Laboratory, Centre for Arthritis and Musculoskeletal Health, University of Aberdeen, Aberdeen, UK
[2]Centre for Genome-Enabled Biology and Medicine, University of Aberdeen, Aberdeen, UK

Correspondence to
Professor Cosimo De Bari and Dr Fraser L Collins, Institute of Medical Sciences, University of Aberdeen, Aberdeen, UK; c.debari@abdn.ac.uk, fraser.collins@abdn.ac.uk

FLC and AJR contributed equally.

Received 15 October 2021
Accepted 5 October 2022
Published Online First 22 November 2022

To cite: Collins FL, Roelofs AJ, Symons RA, *et al*. *Ann Rheum Dis* 2023;**82**:428–437.

ABSTRACT

Objectives Fibroblasts in synovium include fibroblast-like synoviocytes (FLS) in the lining and *Thy1*+ connective-tissue fibroblasts in the sublining. We aimed to investigate their developmental origin and relationship with adult progenitors.

Methods To discriminate between *Gdf5*-lineage cells deriving from the embryonic joint interzone and other *Pdgfrα*-expressing fibroblasts and progenitors, adult *Gdf5-Cre;Tom;Pdgfrα-H2BGFP* mice were used and cartilage injury was induced to activate progenitors. Cells were isolated from knees, fibroblasts and progenitors were sorted by fluorescence-activated cell-sorting based on developmental origin, and analysed by single-cell RNA-sequencing. Flow cytometry and immunohistochemistry were used for validation. Clonal-lineage mapping was performed using *Gdf5-Cre;Confetti* mice.

Results In steady state, *Thy1*+ sublining fibroblasts were of mixed ontogeny. In contrast, *Thy1-Prg4*+ lining fibroblasts predominantly derived from the embryonic joint interzone and included *Prg4*-expressing progenitors distinct from molecularly defined FLS. Clonal-lineage tracing revealed compartmentalisation of *Gdf5*-lineage fibroblasts between lining and sublining. Following injury, lining hyperplasia resulted from proliferation and differentiation of *Prg4*-expressing progenitors, with additional recruitment of non-*Gdf5*-lineage cells, into FLS. Consistent with this, a second population of proliferating cells, enriched near blood vessels in the sublining, supplied activated multipotent cells predicted to give rise to *Thy1*+ fibroblasts, and to feed into the FLS differentiation trajectory. Transcriptional programmes regulating fibroblast differentiation trajectories were uncovered, identifying Sox5 and Foxo1 as key FLS transcription factors in mice and humans.

Conclusions Our findings blueprint a cell atlas of mouse synovial fibroblasts and progenitors in healthy and injured knees, and provide novel insights into the cellular and molecular principles governing the organisation and maintenance of adult synovial joints.

WHAT IS ALREADY KNOWN ABOUT THIS TOPIC

⇒ Synovial fibroblasts, consisting of lining fibroblast-like synoviocytes (FLS) and sublining connective tissue fibroblasts, play a critical role in joint health and arthritis pathology. However, their phenotypic diversity, developmental origin and relationship with adult progenitors is incompletely understood.

WHAT THIS STUDY ADDS

⇒ This study reveals the relationship between ontogeny and phenotypic diversity of synovial fibroblasts, and shows at single-cell level the cellular and molecular pathways involved in the response to injury. Findings also identify *Prg4*-expressing FLS progenitors in the lining and facultative progenitors in sublining that are activated by cartilage injury and give rise to FLS and *Thy1*+ sublining fibroblasts.

HOW THIS STUDY MIGHT AFFECT RESEARCH, PRACTICE OR POLICY

⇒ This study provides novel insight into the hierarchical pathways and molecular regulation that govern synovial fibroblast cell fate in the adult joint.

INTRODUCTION

The synovium consists of two layers, lining and sublining. The sublining is composed of Thy1+ fibroblasts, immune cells, blood vessels and nerves in a meshwork of extracellular matrix (ECM). The lining consists of type A macrophage-like synoviocytes and type B fibroblast-like synoviocytes (FLS). The FLS are specialised fibroblasts, negative for Thy1, which are unique to the synovium and critical for the maintenance of joint homeostasis through secretion of lubricating factors including lubricin (encoded by *Prg4*) and hyaluronic acid.[1] Here, we will use the term synovial fibroblasts to collectively refer to Thy1-Prg4+ FLS in the lining and Thy1+ fibroblasts in the sublining.

Synovial fibroblasts express platelet-derived growth factor receptor α (*Pdgfrα*),[2] a pan-fibroblast marker[3] also expressed by skeletal progenitors.[4] They are ontogenetically heterogeneous and derive in part from the growth differentiation factor 5 (*Gdf5*)-expressing cells of the embryonic joint interzone.[2] The joint-interzone cells give rise to joint tissues during development, including articular cartilage and synovium.[5–7] Tracing of *Gdf5*-expressing cell progeny into adulthood, using *Gdf5* regulatory sequence to control *Cre* expression that is active in the embryonic knee joint interzone but not in healthy, injured or osteoarthritic adult knees,[8–10] revealed that the *Gdf5*-lineage cells in adult mouse knees proliferate following cartilage injury and

repair cartilage.[2] More recently, we identified within the adult *Gdf5*-lineage cell population two progenitor cell subsets, *Prg4*-expressing cells in synovial lining and *Sox9*-expressing cells in periosteum, which cooperate to form osteophytes during osteoarthritis.[11] FLS express *Prg4*, and whether the progenitor activity of *Prg4*+ cells in the lining reflects FLS plasticity or true progenitor cells exist that are distinct from FLS, remains to be determined. Furthermore, it is not known whether a common adult stem/progenitor cell lineage or distinct pools of progenitors supply the different subsets of synovial fibroblasts.

Here, we used transgenic mice allowing the separation of ontogenetically distinct *Gdf5*-lineage mesenchymal stromal cells from other *Pdgfrα*-expressing fibroblasts and progenitors, we analysed at the single-cell level the transcriptome of these lineages in healthy and injured adult knees to construct a stromal cell atlas of the joint and elucidate the relationships between fibroblasts and progenitors in synovium.

METHODS

Materials and methods are available inonline supplemental materials and tables 1–4

RESULTS

Developmental origin and taxonomy of adult synovial fibroblasts in steady state.

To investigate the developmental origin of adult synovial fibroblasts, we used *Gdf5-Cre;Tom;Pdgfrα-H2BGFP* mice to trace cells from the *Gdf5*-expressing embryonic joint interzone based on tdTomato (Tom) expression and to identify fibroblasts and progenitors based on *Pdgfrα*-promoter-driven green fluorescent protein (GFP) expression (figure 1A). Cells isolated from adult mouse knees were sorted by FACS into Tom+ *Gdf5*-lineage cells, which coexpressed GFP, and Tom-GFP+ cells, and analysed independently by scRNA-seq, to ensure high purity (figure 1B; online supplemental figures 1 and 2). Unsupervised clustering of integrated datasets (figure 1C) and analysis of differentially expressed genes (DEGs) (figure 1D; online supplemental figure 3; table 5) identified FLS, osteoblast-lineage cells, chondrocyte-lineage cells, tenocyte-lineage cells, and 6 fibroblast clusters (F1–F6) expressing the synovial sublining fibroblast markers *Thy1* and *Cd34* (figure 1E, F).[12 13] Gene Ontology (GO) analysis of significant cluster genes indicated functional diversity between the *Thy1*+ fibroblast clusters (figure 1G). The two ontogenetic lineages made variable contributions to the different fibroblast clusters, and within each cluster, Tom+ and Tom-GFP+ cells were highly transcriptomically similar (online supplemental figure 4). Strikingly, FLS were only detected in the Tom+ population, deriving from the embryonic joint interzone (figure 1C).

To identify putative developmental relationships among cell clusters, we performed unsupervised Slingshot lineage inference.[14] This predicted, for both ontogenetic cell lineages, trajectories that emerged from the F4 fibroblast cluster towards the specialised cells of the skeletal joint (figure 1H). The transcriptome of the F4 cluster was characterised by *Pi16* and *Cd55* expression (figure 1I), and correlated with the transcriptome of a population of *Pi16*+ fibroblasts recently identified across multiple tissues that has been postulated to represent a reservoir of non-specialised, universal fibroblasts that can develop into specialised, tissue-specific fibroblasts (figure 1J).[15]

Collectively, these data reveal that the adult joint contains functionally distinct fibroblast subsets of heterogeneous developmental origin, with each ontogenetic lineage comprising a universal fibroblast population predicted to give rise to specialised cells.

Identification of FLS and progenitors in synovial lining

Analysis of the scRNA-seq data showed that the FLS cluster only included Tom+ cells deriving from the embryonic joint interzone (figure 1C). We sought to confirm this in a larger cohort of mice and other synovial joints. Tom+ cells were present in synovial lining in all joints analysed (online supplemental figure 5). Flow cytometry confirmed that Thy1-Itga6+ FLS were enriched in the Tom+GFP+ population, while Thy1+Cd55+ universal fibroblasts were similarly or less abundant in the Tom+GFP+ compared with the Tom-GFP+ population (figure 2A; online supplemental figure 6). Furthermore, immunofluorescence staining on tissue sections showed that the vast majority of FLS, identified by Clic5 expression, expressed Tom (figure 2B; online supplemental figure 7). These findings show that, consistent with the scRNA-seq data, the FLS in the adult synovial joints predominantly derive from the embryonic joint interzone.

To define the spatial patterns of adult synovial fibroblasts by their derivation from individual embryonic joint interzone cells, we carried out clonal-lineage mapping using *Gdf5-Cre* mice crossed with Confetti multi-colour reporter mice.[16] This revealed clonal fibroblast clusters in synovium to be typically aligned longitudinally, along the proximal-distal axis, parallel to the lining (figure 2C). This indicates that parallel clonal cell stacking underpins synovial tissue architecture and suggests that lining fibroblasts are a self-maintaining cell population throughout life.

Interestingly, we observed Tom+ cells in synovial lining that were negative for the FLS marker Clic5 (figure 2B), raising the possibility of the existence of distinct progenitors within the *Gdf5*-lineage synovial lining fibroblast population. Consistent with this notion, we identified in the scRNA-seq data a Tom+ subcluster of *Thy1-Prg4*+ cells, which were distinct from mature FLS (defined by expression of *Cd44*, *Cd55*, *Hbegf*, *Has1*, *Tspan15*, *Itga6* and *Clic5*)[17] and superficial zone chondrocytes[18–21] (figure 2D and E; online supplemental figure 8, table 6). We additionally identified growth plate chondrocytes and vascular smooth muscle cells (figure 2D; online supplemental figure 8, table 6), and a putative progenitor subset within the osteoblast-lineage cluster (online supplemental figure 9). These findings further define the mouse synovial joint stromal cell atlas and identify *Prg4*-expressing synovial lining cells distinct from FLS.

Activation of synovial fibroblasts following joint injury

To study fibroblast activation, we used a mouse model whereby injury to articular cartilage triggers a healing response characterised by fibroblast proliferation that underpins synovial hyperplasia and chondrogenesis to repair cartilage.[2] We analysed cells 6 days after cartilage injury, a time when synovial hyperplasia peaks (figure 3A),[2] and integrated the data with steady-state data (figure 3B; online supplemental figure 10). Clusters identified by unsupervised clustering were annotated by analysing the top DEGs for each cluster and mapping cells from each steady-state cluster onto the integrated UMAP (figure 3C; online supplemental figures 11-13; table 7). Relative abundance analysis revealed increases in FLS and *Prg4*+ progenitor populations post-injury within both ontogenetic lineages (figure 3D), and FLS expansion was confirmed by flow cytometry (figure 3E; online supplemental file 14). The injured-state Tom+ and Tom-GFP+ FLS were transcriptomically highly

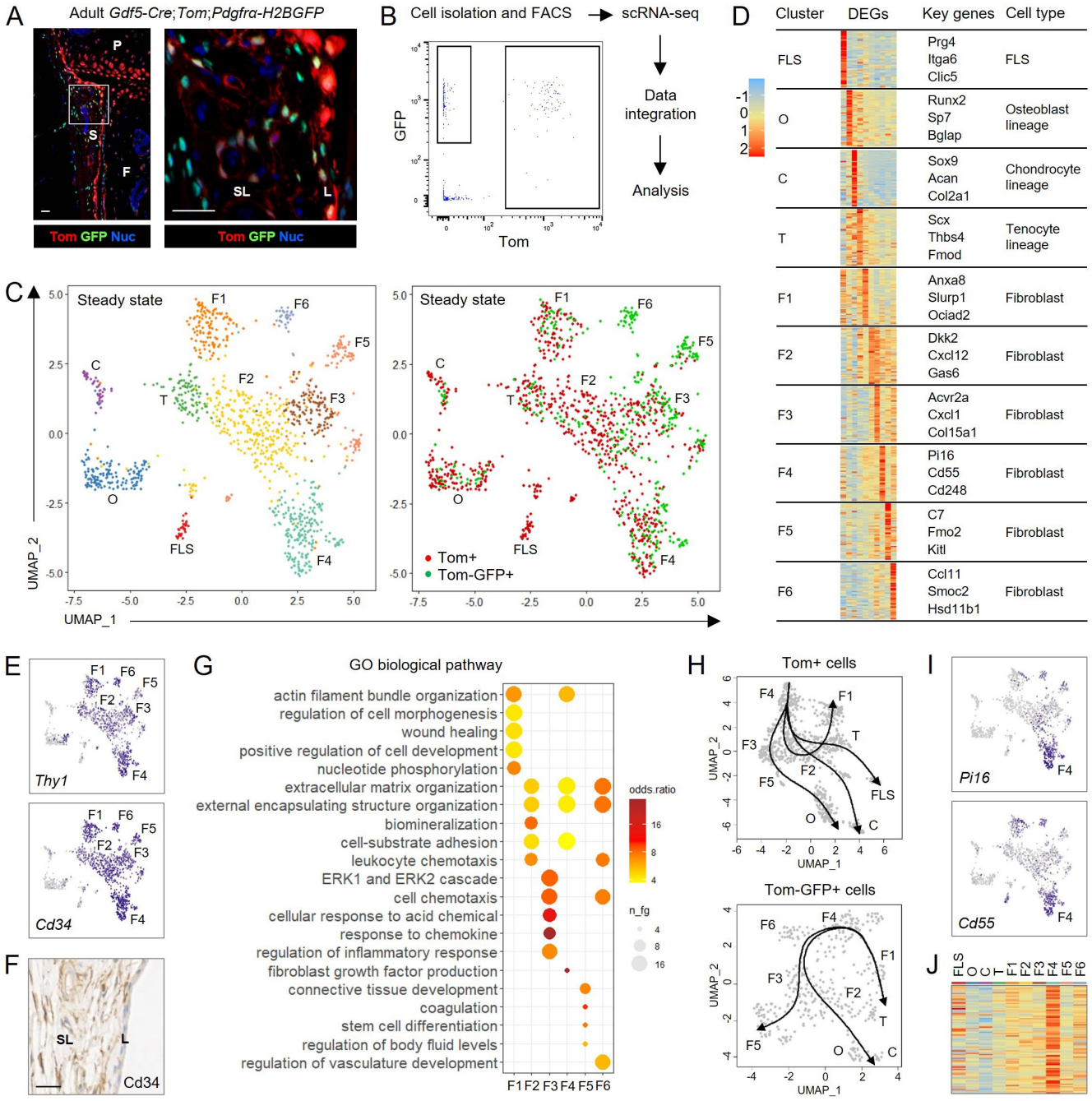

Figure 1 Single-cell transcriptomic atlas of adult mouse synovial fibroblasts. Cells were isolated from knees of 11-week-old *Gdf5-Cre;Tom;Pdgfrα-H2BGFP* mice, sorted by FACS into *Gdf5*-lineage cells (Tom+) and other cells expressing the pan-fibroblast marker *Pdgfrα* (Tom-GFP+), and analysed by scRNA-seq. (A) Histology showing Tom+GFP+ and Tom-GFP+ cells in synovium of 15-week-old *Gdf5-Cre;Tom;Pdgfrα-H2BGFP* mouse knee (n=3). Blue: DAPI nuclear counterstain. White outline on left shown at higher magnification on right. scale bars: 20 µm. S: synovium; P: patella; F: femur; SL: synovial sublining; L: synovial lining. (B) Experimental workflow with flow cytometry scatter plot showing cell populations sorted by FACS. See online supplemental figure 1 for extended data. (C) Unsupervised UMAP plot of integrated scRNA-seq data from 786 Tom+ cells (n=2 mice) and 376 Tom-GFP+ cells (n=1 matched mouse). Left: unsupervised clustering. Right: colour-coded by analysed cell population. See online supplemental figure 2 for extended data. (D) Analysis of differentially expressed genes (DEGs) to identify clusters. Heatmaps show expression of top 50 DEGs for each cluster. Key genes indicate selected DEGs that identify cell types or are dominant cluster-specific genes. See online supplemental figure 3 for UMAP plots of key genes and online supplemental table 5 for top 10 DEGs for each cluster. (E) UMAP plots showing expression of *Thy1* and *Cd34* by fibroblast clusters F1-F6. (F) Immunohistochemical detection of Cd34 in synovial sublining (SL) of 11-week-old mouse knee (n=7). Scale bar: 20 µm. (G) Over-representation analysis of gene ontology (GO) categories for the identified *Thy1*+ fibroblast clusters. (H) Inferred lineage trajectories within the Tom+ and the Tom-GFP+ cell populations based on Slingshot unbiased pseudotime analysis visualised using principal curves. Within both ontogenetic cell lineages, the F4 fibroblast cluster was predicted to represent a root state. (I) UMAP plots showing expression of the cross-tissue universal fibroblast marker *Pi16* and *Cd55* by fibroblast cluster F4. (J) Heatmap showing expression of top 100 DEGs of the *Pi16*+ cross-tissue fibroblast cluster identified by Buechler *et al*[15] by the clusters identified in the adult mouse knee. UMAP, uniform manifold approximation and projection; FLS, fibroblast-like synoviocytes; C, chondrocyte-lineage cells; O, osteoblast-lineage cells; T, tenocyte-lineage cells; F, fibroblasts.

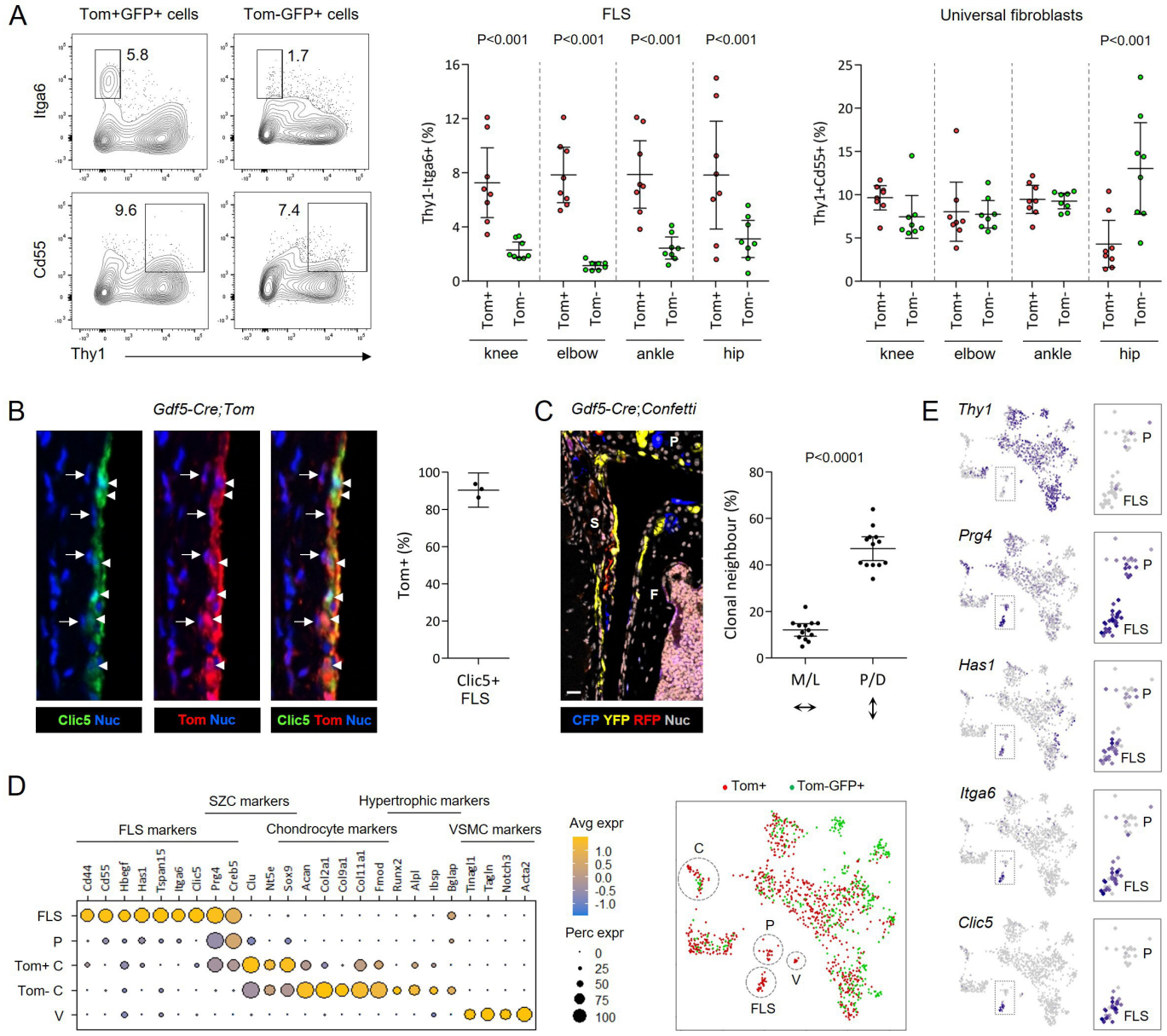

Figure 2 Ontogenetic compartmentalisation of synovial lining and sublining fibroblasts. (A) Detection of Thy1-Itga6+ FLS and Thy1+Cd55+ universal fibroblasts within Tom+GFP+ and Tom-GFP+ cell populations in indicated joints of 21–23 week old *Gdf5-Cre;Tom;Pdgfrα-H2BGFP* mice (n=8) by flow cytometry. Flow plots show gating to identify cell populations. See online supplemental figure 6 for full gating strategy and controls. Graphs show percentage of Thy1-Itga6+ FLS and Thy1+Cd55+ fibroblasts within Tom+GFP+ and Tom-GFP+ cell populations in each of the joints. P values: two-way repeated-measures ANOVA with Holm-Sidak post-test after log-transformation. (B) Tom+cells expressing the FLS marker Clic5 (arrowheads) and adjacent Tom+Clic5- cells (arrows) in synovial lining of 10-week-old *Gdf5-Cre;Tom;Pdgfrα-H2BGFP* mice detected by immunofluorescence staining. Scale bars: 10 µm. Graph shows the percentage of Clic5+ FLS that are Tom+ (n=3). See online supplemental figure 7 for low magnification image and isotype negative control staining. (C) Clonal lineage analysis in 13–16 week old *Gdf5-Cre;Confetti* mouse knees. Clonal cell clusters in synovium, marked by expression of cerulean fluorescent protein (CFP), yellow fluorescent protein (YFP) or red fluorescent protein (RFP), show alignment along the proximal-distal axis parallel to synovial lining. Scale bar: 20 µm. S: synovium; P: patella; F: femur. Graph shows percentage of labelled cells with at least one neighbouring cell expressing the same fluorescent protein in medial or lateral (M/L), or proximal or distal (P/D), direction (n=13; seven unoperated mice and six unoperated contralateral knees from injured mice). P value: paired two-tailed t-test. (D) Expression of selected marker genes to identify subclusters in the steady-state scRNA-seq data, as indicated on the UMAP plot on the right. Cells within a *Prg4*+ progenitor subcluster (P) expressed *Prg4* and *Creb5,* but were largely negative for other FLS and chondrocyte-lineage markers. Tom+ cells in the chondrocyte-lineage cluster (C) displayed a superficial zone chondrocyte (SZC) phenotype, while Tom- cells displayed a mature/hypertrophic chondrocyte phenotype and likely derived from growth plate. An additional Tom+ subcluster was identified as vascular smooth muscle cells (V). See online supplemental figure 8 for extended data. (E) UMAP plots showing expression of indicated genes. Dotted outline indicates enlarged region shown on right to highlight expression in FLS and the *Prg4*+ progenitor subcluster (P). All graphs show mean ± 95% CI. ANOVA, analysis of variance; UMAP, uniform manifold approximation and projection; FLS, fibroblast-like synoviocyte; SZC, superficial zone chondrocytes; VSMC, vascular smooth muscle cells.

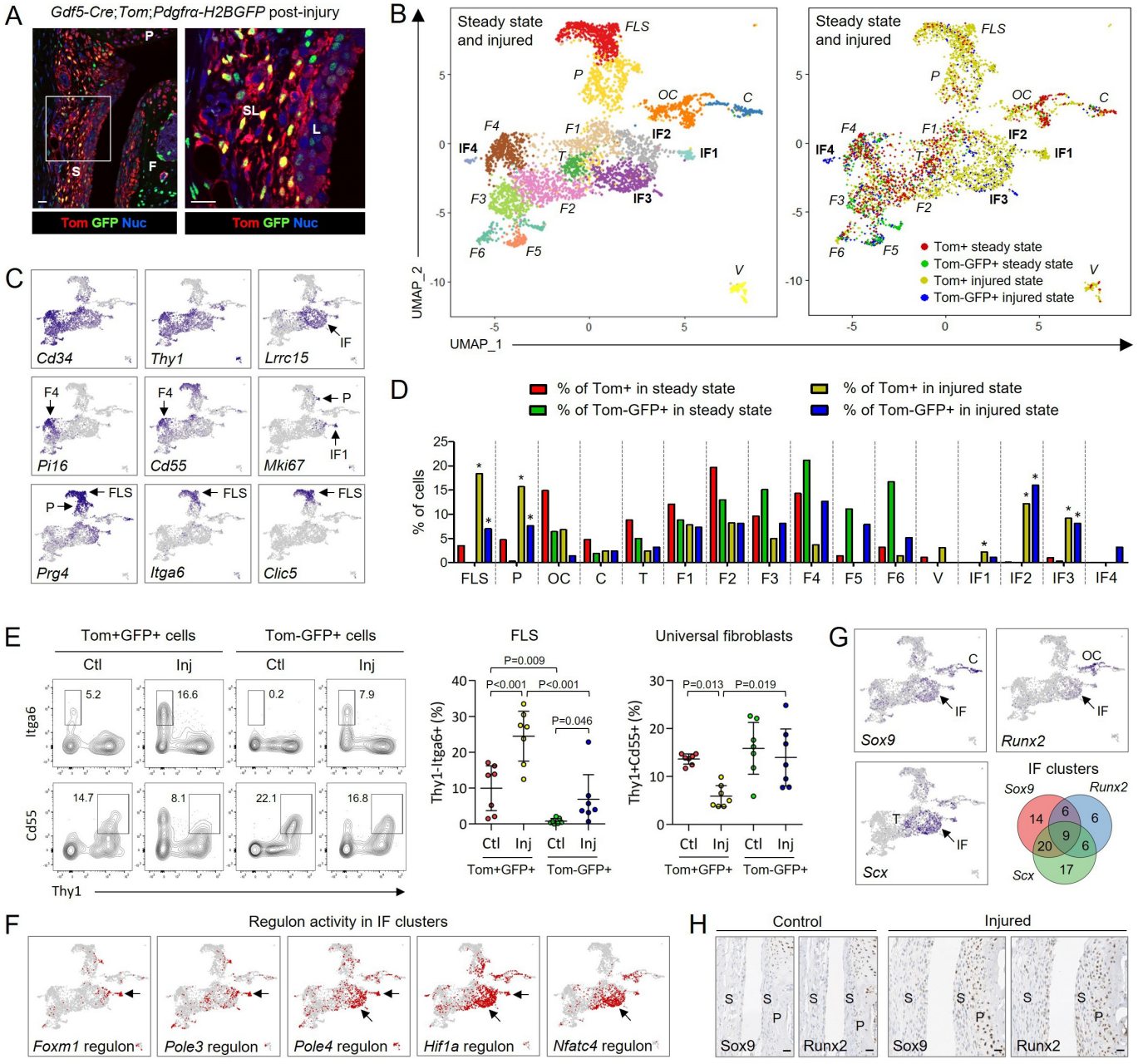

Figure 3 Single-cell transcriptomic atlas of synovial fibroblasts from 12-week-old *Gdf5-Cre;Tom;Pdgfrα-H2BGFP* mice 6 days after joint surface injury, integrated with steady-state data shown in figure 1. (A) Histology showing Tom+GFP+ and Tom-GFP+ cells in synovium 6 days after injury (n=3). Blue: DAPI nuclear counterstain. White outline on left shown at higher magnification on right. Scale bars: 20 µm. S: synovium; P: patella; F: femur; SL: synovial sublining; L: synovial lining. (B) UMAP plot of integrated scRNA-seq data from 786 steady-state Tom+ cells (n=2 mice), 376 steady-state Tom-GFP+ cells (n=1 matched mouse), 2383 injured-state Tom+ cells (n=4 mice) and 651 injured-state Tom-GFP+ cells (n=2 matched mice). Left: unsupervised clustering. Right: colour-coded by analysed cell population and state. Injury-induced fibroblast (IF) clusters are in bold; clusters with steady-state analogues in italics. See online supplemental figure 10–12 for extended data. (C) Expression of key genes that identify clusters. See online supplemental figure 13 for extended data. (D) Relative abundance of cells across identified cell clusters. *FDR<0.05 vs steady-state, negative binomial generalised linear model with Benjamini-Hochberg post-test. (E) Detection by flow cytometry of Thy1-Itga6+ FLS and Thy1+Cd55+ universal fibroblasts within the Tom+GFP+ and Tom-GFP+ cell populations in control (Ctl) and injured (Inj) knees of 15–19 week old *Gdf5-Cre;Tom;Pdgfrα-H2BGFP* mice 6 days post-injury (n=7). See online supplemental figure 14 for gating strategy and controls. Graphs show percentage of cells within the respective cell populations that are Thy1-Itga6+ FLS or Thy1+Cd55+ fibroblasts. Lines and error bars: mean ± 95% CI. P values: two-way repeated-measures ANOVA with Holm-Sidak post-test. (F) Regulons active in injury-induced fibroblast clusters IF1-3. (G) Expression of lineage-specifying transcription factors. Venn diagram shows percentage of cells in injury-induced clusters IF1-IF3 expressing *Sox9*, *Runx2* and *Scx*. See online supplemental figure 17 A,B for other cell clusters. (H) Immunohistochemical detection of Sox9 and Runx2 in synovium (S) and periosteum (P) in consecutive tissue sections of control and injured knees of 11–13 week old mice 7 days post injury (n=5). Scale bars: 20 µm. ANOVA, analysis of variance; UMAP, uniform manifold approximation and projection; FDR, false discovery rate; C, chondrocyte-lineage cells; F, fibroblasts; FLS, fibroblast-like synoviocytes; IF, injury-induced fibroblasts; OC, osteochondral-lineage cells; T, tenocyte-lineage cells; VSMC, vascular smooth muscle cells.

similar to each other and to the steady-state Tom+ FLS (online supplemental figure 15). Transcriptomic comparisons between steady-state and injured-state cells within the fibroblast clusters revealed upregulation of genes involved in ECM remodelling and fibroblast migration, such as *Cthrc1*, *Postn*, *Timp1*, *Bgn*, *Lum*, *Sparc*, *Lox* and various collagens (online supplemental figure 16).[13 22–24]

Four injury-induced fibroblast (IF) clusters were identified with no steady-state analogous cluster (figure 3B–D; online supplemental figures 11-13), which were characterised by activity of regulons associated with cell proliferation and activation (figure 3F; online supplemental tables 8-12). Individual cells in these clusters coexpressed *Sox9* (chondrocyte-lineage), *Runx2* (osteoblast-lineage) and *Scx* (tenocyte-lineage) transcription factors (figure 3G; online supplemental figure 17A, B), suggestive of multilineage differentiation potential. In addition, the cluster analogous to the osteoblast-lineage cluster in steady state displayed an osteochondral phenotype after injury (online supplemental figure 17C, D), similar to the hybrid skeletal cells that form the early osteophyte in osteoarthritis.[11] Immunostaining confirmed upregulation of Sox9 and Runx2 expression after injury, especially at the joint margin where synovium and periosteum merge and chondrophyte formation is typically observed (figure 3H).

Altogether, these data indicate that injury triggers expansion of the *Prg4*+ progenitor and FLS populations, which in part involves recruitment of cells that do not derive from the *Gdf5*-expressing joint interzone, and induces activation of fibroblasts expressing genes indicative of multi-lineage differentiation potency.

Context-dependent activated fibroblast phenotypes

Next, we sought to determine the specificity of the synovial fibroblast response to cartilage injury. Recently, Buechler *et al* analysed single-cell transcriptomic data of fibroblasts from multiple injured or diseased mouse tissues and identified three perturbed-state fibroblast (PF) populations.[15] Two of these showed transcriptomic similarity to the injury-induced clusters in our study (online supplemental figure 18).

We then focused on a comparison with fibroblasts from joints of mice with serum transfer-induced inflammatory arthritis (STIA), by integrating our injured-state dataset with the STIA dataset published by Croft *et al*.[25] Unsupervised clustering revealed five perturbed-state fibroblast clusters (PF1-5) (figure 4A–C; online supplemental figures 19, 20), which showed expression of lineage-specifying transcription factors (*Sox9*, *Runx2* and *Scx*) in both models (figure 4D). Strikingly, few FLS were present in STIA, while *Thy1-Prg4*+ cells

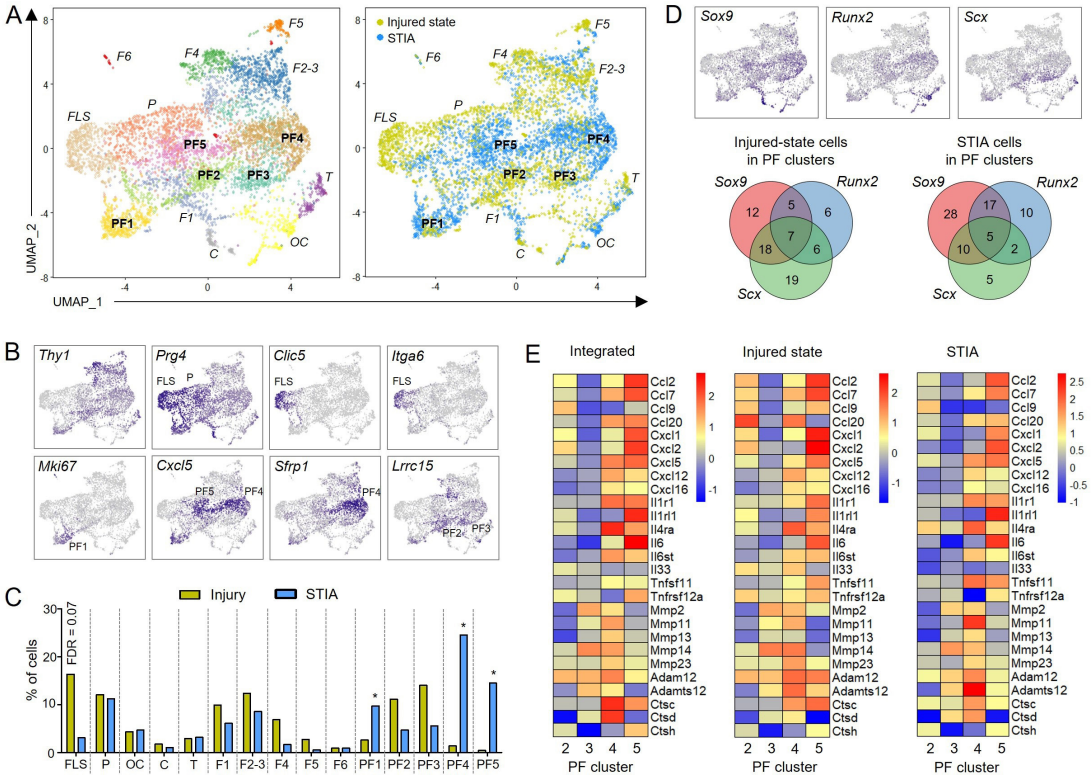

Figure 4 Integrated single-cell transcriptomic analysis of synovial fibroblasts from mice 6 days after joint surface injury (data shown in figure 3) and day 9 serum-transfer induced arthritis (STIA) mice.[25] (A) UMAP plot of integrated scRNA-seq data from 2955 Tom+ and Tom-GFP+ injured-state cells and 3549 STIA cells. Left: unsupervised clustering. Right: colour-coded by state. See online supplemental figures 19, 20 for cluster annotation. Perturbed-state fibroblast (PF) clusters are in bold; clusters with steady-state analogues in italics. (B) Expression of key genes that identify steady-state analogous clusters (top) and perturbed-state clusters (bottom). (C) Relative abundance of cells across identified clusters. *FDR<0.05 vs injured-state, negative binomial generalised linear model with Benjamini-Hochberg post-test. (D) Expression of lineage-specifying transcription factors. Venn diagrams show percentage of STIA cells and injured-state cells in perturbed-state clusters (PF1-PF5) expressing *Sox9*, *Runx2* and *Scx*. (E) Heatmaps showing expression of differentially expressed genes (DEGs) involved in inflammation and catabolism in non-proliferating perturbed-state fibroblast clusters (PF2-PF5). Left: integrated injured-state and STIA cells. Middle: Injured-state cells only. Right: STIA cells only. UMAP, uniform manifold approximation and projection; FDR, false discovery rate.

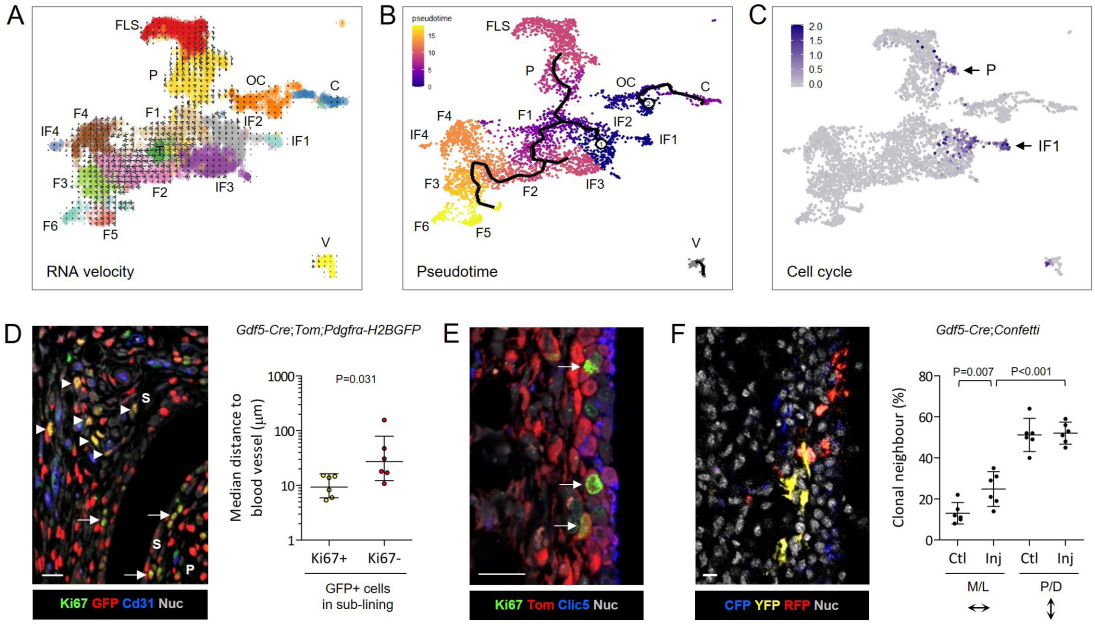

Figure 5 Stromal cell proliferation and differentiation trajectories after injury. (A) RNA velocity analysis using the dynamical model projected onto the integrated steady-state and injured-state uMAP plot as shown in figure 3B. Arrows show the local average velocity and direction. (B) Monocle3 lineage inference showing differentiation trajectories originating from injury-induced fibroblast clusters with a branchpoint towards *Thy1*+ fibroblasts or FLS. Colouring of plot represents pseudotime. (C) UMAP plot of cell cycle gene module score based on expression of *Mki67*, *Ccna2*, *Ccnb1*, *Ccnb2* and *Cdk1*. Arrows indicate proliferating cells. See online supplemental figure 21 for separate analysis of injured-state Tom+, injured state Tom-GFP+, and steady-state populations. (D, E) Immunofluorescence staining in 12–14 week old *Gdf5-Cre;Tom;Pdgfrα-H2BGFP* mouse synovium 6 days after injury (n=6) to locate proliferating fibroblasts. (D) Ki67+GFP+ proliferating fibroblasts in synovial lining (arrows), and near Cd31+blood vessels in synovial sublining (arrowheads). See online supplemental figure 22A for split channel images and isotype negative control staining. Graph shows the median distance to the nearest Cd31+ blood vessel for Ki67+GFP+ proliferating fibroblasts and Ki67-GFP+ non-proliferating fibroblasts in synovial sublining. Lines and error bars indicate geometric mean ± 95% CI. P value: Wilcoxon signed rank test. (E) Ki67+Tom+ proliferating *Gdf5*-lineage cells in synovial lining (arrows), adjacent to Clic5+Tom+ FLS. see online supplemental figure 22B for split channel images and isotype negative control staining. (F) Clonal lineage analysis in 13–14 week old *Gdf5-Cre;Confetti* mouse knees 6 days after injury (n=6). Ctl: unoperated contralateral control knees. Cerulean fluorescent protein (CFP), yellow fluorescent protein (YFP), red fluorescent protein (RFP) and TO-PRO-3 nuclear counterstain were detected by confocal fluorescence microscopy. Graph shows percentage of labelled cells with at least one neighbouring cell expressing the same fluorescent protein in the medial or lateral (M/L), or the proximal or distal (P/D), direction. Lines and error bars indicate mean ± 95% CI. P value: two-way repeated-measures ANOVA with Holm-Sidak post-test. ANOVA, analysis of variance; UMAP, uniform manifold approximation and projection.

extended from the progenitor cluster into the perturbed-state clusters (figure 4A–C).

PF clusters included one proliferating cluster (PF1), and four clusters predominant in either the injured state (PF2 and PF3) or STIA (PF4 and PF5) (figure 4A–C), the latter characterised by *Cxcl5* expression (figure 4B). Cells in STIA-dominant PF clusters showed a more inflammatory and catabolic transcriptome compared with cells in injury-dominant PF clusters, and this remained true when injured-state and STIA cells were analysed separately (figure 4E).

These findings indicate that different perturbed-state synovial fibroblast phenotypes exist, in varying proportions, both after injury and during immune-mediated inflammation, and suggest that adoption of multilineage potency by fibroblasts is a generic response to a perturbed state.

Identification and molecular regulation of progenitor cell differentiation trajectories

We next analysed differentiation trajectories using RNA velocity and lineage reconstruction[14 26 27] (figure 5A) and by pseudotemporally ordering the cells based on changes in gene expression using Monocle 3[27] (figure 5B). This revealed inferred differentiation trajectories originating from cells in injury-induced fibroblast clusters IF1 and IF2, with a branchpoint towards either *Thy1-Prg4*+ lining fibroblasts (P and FLS) or *Thy1*+ sublining fibroblasts (F1–F6 and tenocytes) (figure 5A and B). Cell cycle analysis revealed two clusters of cycling cells after injury supplying new cells feeding into the differentiation trajectories, one in IF1 and IF2 clusters, and one in the *Thy1-Prg4*+ progenitor cluster extending into the FLS cluster (figure 5C; online supplemental figure 21).

To confirm these findings in situ, we costained for GFP and the proliferation marker Ki67, together with the endothelial marker Cd31. Proliferating fibroblasts were detected in lining, and in sublining enriched near blood vessels (figure 5D, online supplemental figure 22A). To further determine the identity of proliferating fibroblasts in the lining, we costained for Tom and Ki67, together with the FLS marker Clic5. We observed Tom+Ki67+ proliferating cells in the lining located immediately adjacent to Clic5+ FLS (figure 5E, online supplemental figure 22B), and occasional Tom+Ki67+Clic5+ FLS (online supplemental figure 22B), supporting the notion that the *Thy1-Prg4*+ progenitors identified by scRNA-seq (P cluster) are located in the lining where they proliferate and give rise to new FLS after injury. Clonal-lineage tracing using the *Gdf5-Cre;Confetti* model indicated clonal expansion along the medial-lateral axis (figure 5F), although clones typically remained locally confined to either lining or sublining compartments . Altogether, these data indicate that synovial lining hyperplasia after injury in large part results from proliferation of *Gdf5*-lineage FLS progenitors in the lining, with additional

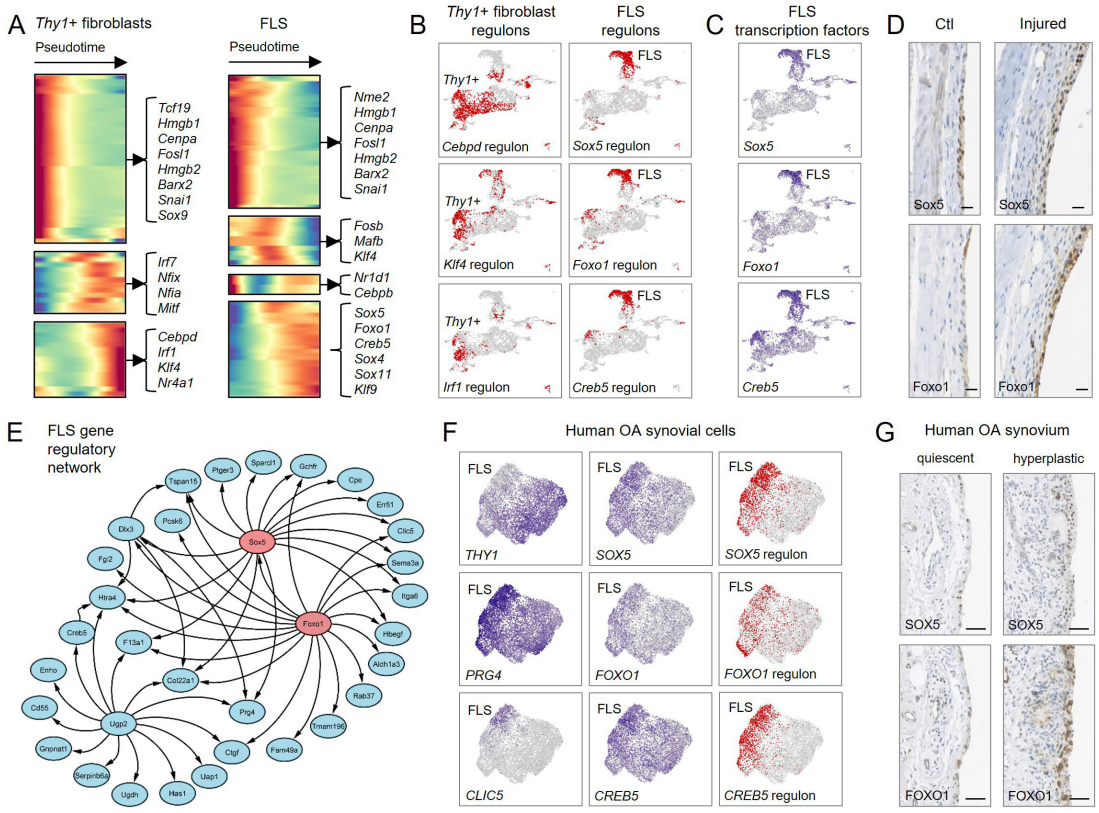

Figure 6 Transcriptional programmes regulating fibroblast differentiation trajectories. (A–C) Transcription factors and regulons associated with the two fibroblast differentiation trajectories (*Thy1+* fibroblasts and FLS) identified in figure 5. (A) Heatmaps showing expression across pseudotime of transcription factors whose expression changed significantly across either trajectory. Transcription factors are clustered by pseudotemporal expression pattern. Top differentially expressed transcription factors are indicated. (B) Activity of selected regulons associated with transcription factors identified by pseudotime analysis, projected onto the integrated steady-state and injured-state UMAP plot as shown in figure 3B. See online supplemental figure 23 for regulon activity analysed independently in steady state and injured state. (C) Expression of selected FLS-associated transcription factors identified from the pseudotime analysis projected onto the integrated steady-state and injured-state UMAP plot. Expression of *Sox5* and *Foxo1* is mostly restricted to the FLS, while *Creb5* shows a wider expression pattern. (D) Immunohistochemical detection of SOX5 and FOXO1 in near-consecutive tissue sections of 11–13 week old mice 7 days post-injury (n=5) showing expression in synovial lining of control (unoperated contralateral control knee) and injured knees. Scale bars: 20 µm. See online supplemental figure 24A for lower magnification images and isotype negative control stainings. (E) Predicted FLS-associated gene regulatory network based on the mouse scRNA-seq data, constructed using GENIE3 and Cytoscape, indicating that the transcription factors Sox5 and Foxo1 drive key FLS-associated genes. (F) UMAP plots of scRNA-seq data from human OA synovium obtained at arthroplasty (n=3; 2 female and one male, mean age 68)[28] showing from left to right expression of indicated marker genes to identify FLS (THY1-PRG4+CLIC5+), expression of transcription factors *SOX5*, *FOXO1 and CREB5*, and activity of associated regulons. See online supplemental figure 25 for analysis of two additional human OA synovial cell datasets.[13 29] (G) Immunohistochemical detection of SOX5 and FOXO1 in near-consecutive tissue sections of human OA synovium obtained at arthroplasty (n=6; see online supplemental table 1 for donor information), showing expression in quiescent and active areas of synovial lining. Scale bars: 20 µm. See online supplemental figure 24B for lower magnification images and isotype negative controls. UMAP, uniform manifold approximation and projection; FLS, fibroblast-like synoviocytes; OA, osteoarthritis.

recruitment from proliferating cells in injury-induced clusters into the FLS trajectory.

To gain insight into the molecular regulation of synovial fibroblast differentiation, we identified transcription factors that significantly changed in expression across pseudotime (figure 6A). SCENIC analysis revealed regulon activity associated with these transcription factors along their respective differentiation trajectories, suggesting they are key to driving this process (figure 6B; online supplemental figure 23; tables 13-18). FLS-associated transcription factors included *Sox5*, *Foxo1 and Creb5* (figure 6C), with *Sox5* and *Foxo1* detectable by immunostaining in the lining of normal and injured knee synovium (figure 6D; online supplemental figure 24A). Reconstruction of gene regulatory networks revealed that *Sox5* and *Foxo1* transcription factors interact with key FLS genes (figure 6E), supporting their potentially critical role in FLS fate determination.

For clinical relevance, we extended our analysis to published data from knee synovial tissues of osteoarthritis patients,[13 28 29] which similarly showed that *THY1-PRG4+CLIC5+* FLS exhibited *SOX5*, *FOXO1* and *CREB5* regulon activity (figure 6F, online supplemental figure 25). Immunohistochemistry confirmed SOX5 and FOXO1 expression in both quiescent and hyperplastic lining of human synovium (figure 6G, online supplemental figure 24B). These data indicate that molecular regulation of the FLS phenotype is conserved across species and states.

DISCUSSION

Comprehensive cell atlases from diseased joints with inflammatory or degenerative arthritis have documented heterogeneity of synovial fibroblasts, identifying perturbed-state subsets.[13 15 25 30]

We previously reported that in the adult knee synovium, the *Gdf5*-lineage cell population contains fibroblasts that become pathogenic in inflammatory arthritis[31] and progenitors that form cartilage after injury.[2 11] However, little was known about the fibroblasts in healthy joints, and it remained to be determined whether progenitors and fibroblasts are distinct cells, or plastic fibroblasts adopt progenitor activity. In this study, single-cell transcriptomic analysis of ontogenetically distinct stromal cell lineages from steady-state mouse knee joints led to the identification of FLS and distinct *Prg4*-expressing progenitors in the lining, both largely deriving from the embryonic joint interzone. Joint surface injury, employed to study repair mechanisms,[2] triggered proliferation of progenitors in the lining, and additional cells located near blood vessels in sublining predicted to supply specialised fibroblasts.

Traditionally, *Prg4*-expressing synovial lining fibroblasts are considered to be specialised FLS that maintain joint homeostasis through secretion of lubricating factors.[1] Here, we disentangle the identity of the lining fibroblasts and show that they comprise two distinct cell subsets, FLS and progenitors postulated to replenish FLS lost to physiological turnover. The observation that in synovium, clonal fibroblasts are arranged longitudinally parallel to the lining, supports this notion. We also show that the synovial lining hyperplasia following joint surface injury[2 32] is largely underpinned by an expansion of FLS driven by proliferating *Prg4*-expressing progenitors. A previous study tracing the progeny of cells expressing *Prg4* showed their proliferation and expansion in synovium after cartilage injury.[32] Our data identify a population of *Prg4*-expressing progenitors in synovial lining that are distinct from FLS and respond to injury with proliferation to supply new FLS.

The FLS population is further expanded after injury by differentiation of cells that do not derive from the *Gdf5*-lineage population. Although the non-*Gdf5* lineage FLS are transcriptomically highly similar to their *Gdf5*-lineage counterparts, to which extent they are functionally equivalent remains to be determined. Similarly, while *Gdf5*-lineage cells are the main progenitors that form articular cartilage during development, repair cartilage after injury in adulthood,[2] and form osteophytes in osteoarthritis,[11] other cells can give rise to new chondrocytes, especially ectopically in synovium after injury.[2] Thus, while the *Gdf5*-lineage cells are the natural progenitors for FLS and articular chondrocytes, under conditions of stress, other cells in the joint supply FLS and chondrocytes in a compensatory mechanism.

The quiescent cells from which the injury-induced cells with multipotent phenotype originate remain to be determined. A recent study identified a population of fibroblasts that reside near blood vessels in many tissues, marked by expression of *Pi16*. These cells were postulated to be unspecialised reservoir cells giving rise to tissue-specific specialised fibroblasts.[15] We identified a transcriptomically similar *Pi16*+ fibroblast cluster in the adult mouse knee, which was predicted to give rise to specialised cells of the steady-state skeletal joint. After injury, proliferating cells feeding into differentiation trajectories were found to be enriched in a sublining perivascular niche, and we previously showed these perivascular cells to be distinct from pericytes.[33] While these cells could be progeny of the *Pi16*+ fibroblasts, we speculate that quiescent fibroblasts in the joint, under the stress resulting from damage, would be opportunistically recruited to function as facultative progenitors, showing a plasticity that has been reported in other tissues.[34]

A comparative analysis of synovial fibroblasts in joint surface injury and various perturbed states revealed an overall similar fibroblast response. Fibroblasts with an inflammatory phenotype were detected in our injury model, although at a much lower prevalence compared with the STIA mouse model of inflammatory arthritis. Inflammation plays a crucial role in repair.[35] Likewise, activated cells with a multipotent phenotype were detected in both injury and STIA models. These data suggest that inflammatory and multipotent fibroblast transcriptional states reflect a generic response to insult, although their prevalence and level of activation would be context-dependent and likely to determine structural outcome. It was interesting to observe that while few FLS were present in the STIA dataset, *Prg4*-expressing progenitors were abundant and extended into the PF clusters. This suggests that under inflammatory conditions such as rheumatoid arthritis, *Prg4*-expressing progenitors are shifted towards pathogenic fibroblasts.

Our data define the molecular identity of FLS distinct from *Prg4*+ progenitors, and reveal the transcriptional programmes underpinning synovial fibroblast differentiation. Notably, both mouse and human FLS are characterised by *Sox5*, *Foxo1* and *Creb5* regulon activity. This suggests that the identified gene regulatory networks are crucial for the FLS phenotype and that their disruption could result in dysregulation of FLS formation or function. The transcription factors Foxo1 and Sox5 have been linked to skeletal cell survival and fate.[36 37] Creb5 was shown to be required for the induction of *Prg4* expression in articular chondrocytes.[19] Since the synovial lining shares many properties with the superficial zone of the articular cartilage, including production of lubricin (encoded by *Prg4*), it is likely that the *Creb5* regulon has similar functions in FLS and superficial zone chondrocytes.

In summary, our analysis at single-cell resolution of stromal cells isolated from steady-state and injured mouse knees provides novel insights into the ontogeny and taxonomy of fibroblast and progenitor populations in synovium and defines differentiation trajectories and their molecular regulation. This study critically advances our knowledge of the cell populations that maintain the synovial joint in adult life.

Acknowledgements The authors thank all members of the Arthritis and Regenerative Medicine Laboratory at the University of Aberdeen, with special thanks to Alison Richmond, Iain Cunningham and Megan Robertson for technical assistance. The authors are also grateful to Animal Facility staff for care of our animals, the NHS Grampian Biorepository for facilitating the collection of human tissue samples, and staff in the Centre for Genome-Enabled Biology and Medicine, the Microscopy and Histology Facility, and the Iain Fraser Cytometry Centre, for their expert support. Part of this work has been previously presented at OARSI 2022 World Congress: FLC, AJR, KK, EC, ESRC-D, CDB. Defining the Hierarchy of Fibroblasts and Their Stem Cells in the Adult Synovial Joint At Single Cell Resolution. Osteoarthr Cartil 2022;30:S40. doi:10.1016/j.joca.2022.02.041.

Contributors FLC and AJR: conceptualisation, experimental design, data acquisition, analysis and interpretation, and writing of the manuscript. RS, KK and SMC: data acquisition and analysis. EC: data acquisition. AHKR: provision of human tissue samples. ESRC-D: experimental design and data interpretation. CDB: conceptualisation, experimental design, data analysis and interpretation, and writing of the manuscript. All authors edited and approved the manuscript. CDB is acting as guarantor.

Funding This work was supported by funding from Versus Arthritis (grants 20775, 21156, 21800), Medical Research Council (grant MR/L020211/1) and Tenovus Scotland (grant G18.11).

Competing interests None declared.

Patient and public involvement Patients and/or the public were not involved in the design, or conduct, or reporting, or dissemination plans of this research.

Patient consent for publication Not applicable.

Ethics approval Human synovial tissue samples were obtained from patients with a clinical diagnosis of osteoarthritis after informed consent, under the auspices of the NHS Grampian Biorepository, during knee arthroplasty. Animal experimental protocols were approved by the UK Home Office and the Animal Welfare and Ethical Review Committee of the University of Aberdeen.

Provenance and peer review Not commissioned; externally peer reviewed.

Data availability statement Data are available in a public, open access repository. Data are available on reasonable request. Single-cell RNA sequencing data that support the findings of this study have been deposited in Gene Expression Omnibus (GEO) with the accession code GSE214500. All data relevant to the study are included in the article or uploaded as online supplemental information.

ORCID iDs
Fraser L Collins http://orcid.org/0000-0002-1156-6873
Anke J Roelofs http://orcid.org/0000-0001-8993-1984
Rebecca A Symons http://orcid.org/0000-0002-2811-7919
Cosimo De Bari http://orcid.org/0000-0002-5113-862X

REFERENCES

1 Veale DJ, Firestein GS. *Synovium*. 10th edn. Elsevier Inc, 2017.
2 Roelofs AJ, Zupan J, Riemen AHK, *et al*. Joint morphogenetic cells in the adult mammalian synovium. *Nat Commun* 2017;8:15040.
3 Driskell RR, Lichtenberger BM, Hoste E, *et al*. Distinct fibroblast lineages determine dermal architecture in skin development and repair. *Nature* 2013;504:277–81.
4 Park D, Spencer JA, Koh BI, *et al*. Endogenous bone marrow MSCs are dynamic, fate-restricted participants in bone maintenance and regeneration. *Cell Stem Cell* 2012;10:259–72.
5 Shwartz Y, Viukov S, Krief S, *et al*. Joint development involves a continuous influx of Gdf5-Positive cells. *Cell Rep* 2016;15:2577–87.
6 Storm EE, Kingsley DM. Joint patterning defects caused by single and double mutations in members of the bone morphogenetic protein (BMP) family. *Development* 1996;122:3969–79.
7 Koyama E, Shibukawa Y, Nagayama M, *et al*. A distinct cohort of progenitor cells participates in synovial joint and articular cartilage formation during mouse limb skeletogenesis. *Dev Biol* 2008;316:62–73.
8 Chen H, Capellini TD, Schoor M, *et al*. Heads, shoulders, Elbows, knees, and toes: modular Gdf5 enhancers control different joints in the vertebrate skeleton. *PLoS Genet* 2016;12:e1006454–27.
9 Pregizer SK, Kiapour AM, Young M, *et al*. Impact of broad regulatory regions on Gdf5 expression and function in knee development and susceptibility to osteoarthritis. *Ann Rheum Dis* 2018;77:450.
10 Kania K, Colella F, Riemen AHK, *et al*. Regulation of GDF5 expression in joint remodelling, repair and osteoarthritis. *Sci Rep* 2020;10:1–11.
11 Roelofs AJ, Kania K, Rafipay AJ, *et al*. Identification of the skeletal progenitor cells forming osteophytes in osteoarthritis. *Ann Rheum Dis* 2020;79:1625–34.
12 Stephenson W, Donlin LT, Butler A, *et al*. Single-Cell RNA-seq of rheumatoid arthritis synovial tissue using low-cost microfluidic instrumentation. *Nat Commun* 2018;9:1–10.
13 Mizoguchi F, Slowikowski K, Wei K, *et al*. Functionally distinct disease-associated fibroblast subsets in rheumatoid arthritis. *Nat Commun* 2018;9:1–11.
14 Street K, Risso D, Fletcher RB, *et al*. Slingshot: cell lineage and pseudotime inference for single-cell transcriptomics. *BMC Genomics* 2018;19:477.
15 Buechler MB, Pradhan RN, Krishnamurty AT, *et al*. Cross-tissue organization of the fibroblast lineage. *Nature* 2021;593:575–9.
16 Snippert HJ, van der Flier LG, Sato T, *et al*. Intestinal crypt homeostasis results from neutral competition between symmetrically dividing LGR5 stem cells. *Cell* 2010;143:134–44.
17 Lomholt S, Nielsen M A, Aspari M P. Fibroblast-Like Synovial Cell Subsets in Rheumatoid Arthritis. In: Bertoncelj MF, Lakota K, eds. *Fibroblasts - Advances in Inflammation, Autoimmunity and Cancer*. London: IntechOpen, 2021.
18 Schumacher BL, Block JA, Schmid TM, *et al*. A novel proteoglycan synthesized and secreted by chondrocytes of the superficial zone of articular cartilage. *Arch Biochem Biophys* 1994;311:144–52.
19 Zhang C-H, Gao Y, Jadhav U, *et al*. Creb5 establishes the competence for PRG4 expression in articular cartilage. *Commun Biol* 2021;4:332.
20 Khan IM, Salter DM, Bayliss MT, *et al*. Expression of clusterin in the superficial zone of bovine articular cartilage. *Arthritis Rheum* 2001;44:1795–9.
21 Li L, Newton PT, Bouderlique T, *et al*. Superficial cells are self-renewing chondrocyte progenitors, which form the articular cartilage in juvenile mice. *Faseb J* 2017;31:1067–84.
22 Shekhani MT, Forde TS, Adilbayeva A, *et al*. Collagen triple helix repeat containing 1 is a new promigratory marker of arthritic Pannus. *Arthritis Res Ther* 2016;18:1–14.
23 You S, Yoo S-A, Choi S, *et al*. Identification of key regulators for the migration and invasion of rheumatoid synoviocytes through a systems approach. *Proc Natl Acad Sci U S A* 2014;111:550–5.
24 Winkler J, Abisoye-Ogunniyan A, Metcalf KJ, *et al*. Concepts of extracellular matrix remodelling in tumour progression and metastasis. *Nat Commun* 2020;11:1–19.
25 Croft AP, Campos J, Jansen K, *et al*. Distinct fibroblast subsets drive inflammation and damage in arthritis. *Nature* 2019;570:246–51.
26 Bergen V, Lange M, Peidli S, *et al*. Generalizing RNA velocity to transient cell states through dynamical modeling. *Nat Biotechnol* 2020;38:1408–14.
27 Trapnell C, Cacchiarelli D, Grimsby J, *et al*. The dynamics and regulators of cell fate decisions are revealed by pseudotemporal ordering of single cells. *Nat Biotechnol* 2014;32:381–6.
28 Chou C-H, Jain V, Gibson J, *et al*. Synovial cell cross-talk with cartilage plays a major role in the pathogenesis of osteoarthritis. *Sci Rep* 2020;10:1–14.
29 Zhang F, Wei K, Slowikowski K, *et al*. Defining inflammatory cell states in rheumatoid arthritis joint synovial tissues by integrating single-cell transcriptomics and mass cytometry. *Nat Immunol* 2019;20:928–42.
30 Wei K, Korsunsky I, Marshall JL, *et al*. Notch signalling drives synovial fibroblast identity and arthritis pathology. *Nature* 2020;582:259–64.
31 Symons RA, Colella F, Collins FL, *et al*. Targeting the IL-6-Yap-Snail signalling axis in synovial fibroblasts ameliorates inflammatory arthritis. *Ann Rheum Dis* 2022;81:214–24.
32 Decker RS, Um H-B, Dyment NA, *et al*. Cell origin, volume and arrangement are drivers of articular cartilage formation, morphogenesis and response to injury in mouse limbs. *Dev Biol* 2017;426:56–68.
33 Kurth TB, Dell'accio F, Crouch V, *et al*. Functional mesenchymal stem cell niches in adult mouse knee joint synovium in vivo. *Arthritis Rheum* 2011;63:1289–300.
34 Stange DE, Koo B-K, Huch M, *et al*. Differentiated Troy+ chief cells act as reserve stem cells to generate all lineages of the stomach epithelium. *Cell* 2013;155:357–68.
35 Cooke JP. Inflammation and its role in regeneration and repair. *Circ Res* 2019;124:1166–8.
36 Lefebvre V. Roles and regulation of SOX transcription factors in skeletogenesis. *Curr Top Dev Biol* 2019;133:171–93.
37 van Gastel N, Stegen S, Eelen G, *et al*. Lipid availability determines fate of skeletal progenitor cells via SOX9. *Nature* 2020;579:111–7.

Supplementary Materials for

The taxonomy of fibroblasts and progenitors in the synovial joint at single-cell resolution

Authors:

Fraser L. Collins[1#*], Anke J. Roelofs[1#], Rebecca A. Symons[1], Karolina Kania[1], Ewan Campbell[2], Elaina S. R. Collie-Duguid[2], Anna H. K. Riemen[1], Susan M. Clark[1], Cosimo De Bari[1*]

Author Affiliations:

[1]Arthritis & Regenerative Medicine laboratory, Aberdeen Centre for Arthritis and Musculoskeletal Health, Institute of Medical Sciences, University of Aberdeen, Aberdeen AB25 2ZD.

[2]Centre for Genome-Enabled Biology and Medicine, University of Aberdeen, Aberdeen AB25 2ZD.

[#]Contributed equally

Correspondence:

Cosimo De Bari, Institute of Medical Sciences, University of Aberdeen, Foresterhill, Aberdeen AB25 2ZD, UK. Tel: +44-1224-437477, E-mail: c.debari@abdn.ac.uk.

Fraser Collins, Institute of Medical Sciences, University of Aberdeen, Foresterhill, Aberdeen AB25 2ZD, UK, E-mail: fraser.collins@abdn.ac.uk

This PDF file includes:

Methods

Suppl. Figs. 1-25

Tables 1 - 18

Methods

Human tissue collection

Human synovial tissue samples were obtained from patients with a clinical diagnosis of osteoarthritis after informed consent, under the auspices of the NHS Grampian Biorepository, during knee arthroplasty. Patient information is provided in Supplementary Table 1.

Mice

All animal experimental protocols were approved by the UK Home Office and the Animal Welfare and Ethical Review Committee of the University of Aberdeen. All animal experiments were performed at the University of Aberdeen Medical Research Facility after a minimum acclimatisation period of 6 days. Experiments were designed to ensure that minimum numbers of mice were used to obtain biologically significant results. *Gdf5-Cre* mice (Tg(Gdf5-cre-ALPP)1Kng)[1] were donated by Dr David Kingsley (Stanford, CA, USA). *Cre*-inducible *tdTomato* (*Tom*) (B6.Cg-Gt(ROSA)26Sortm14(CAG-tdTomato)Hze/J) reporter mice,[2] *Cre*-inducible *Confetti* (STOCK Gt(ROSA)26Sortm1(CAG-Brainbow2.1)Cle/J) reporter mice[3] and *Pdgfrα-H2BGFP* (B6.129S4-Pdgfratm11(EGFP)Sor/J) mice were obtained from The Jackson Laboratory. *Gdf5-Cre* mice were maintained on an FVB background, *Tom* and *Pdgfrα-H2BGFP* mice on a C57BL/6 background, and Confetti mice on a partly backcrossed C57BL/6 background. Mice within each experiment were maintained in the same temperature-controlled room on a 12h:12h light-dark cycle and provided with food and water *ad libitum*. Female *Gdf5-Cre*;*Tom;Pdgfrα-H2BGFP* mice or *Gdf5-Cre*;*Confetti* mice with a hemizygous or heterozygous transgene status were used for experiments. Mice that showed widespread (leaky) *Tom* expression were excluded *a priori* via detection of Tom expression in peripheral blood.[4] Mice whose genotype at the time of analysis did not correspond with the genotype determined *a priori* were excluded. Mice were either left unoperated (steady-state), or underwent joint surface injury on one knee (injured) with the contralateral knee left unoperated (control), as detailed below. No formal randomisation procedure was performed. Mice were humanely killed at 10-23 weeks of age by overdose of CO_2 followed by cervical dislocation and knee joint dissection. No randomisation was carried out for this study. Donor-matched samples (injured and contralateral knees, or cell populations) were compared. Blinding was not applicable to this study as mice within each experiment were all the same genotype.

Joint surface injury

Surgery was performed to create a joint surface injury as previously described.[4,5] Briefly, mice were anaesthetized with ketamine (50 mg/kg) and medetomidine (0.67 mg/kg) with atipamezole (1 mg/kg) post-operatively, or isoflurane with 0.1 mg/kg buprenorphine and in some experiments paracetamol (200 mg/kg) mixed with soft food for two days post-surgery. Medial parapatellar arthrotomy was

performed on the right knee under a dissection microscope. Using a 25G needle, a full-cartilage-thickness scratch was made along the exposed cartilage of the trochlear groove following lateral dislocation of the patella. The patella was re-located and incisions were closed by suturing. For some experiments, the unoperated contralateral knee served as control knee. Mice were humanely killed 6 or 7 days after surgery.

Tissue processing and histology

Mouse knee joints for histology were PFA-fixed, EDTA-decalcified, and paraffin or cryosectioned, as described.[4] Fluorescent proteins were detected either by their native fluorescence in cryosections, or via immunofluorescence staining on paraffin sections. Immunohistochemistry and immunofluorescence stainings were performed as described[6] using antibodies in Supplementary Table 2. For immunofluorescence detection of Clic5, after incubation with primary antibody against Clic5, tissue sections were sequentially incubated with biotinylated anti-rabbit antibody, streptavidin-AF647 (ThermoFisher, cat. no. S32357), biotinylated anti-streptavidin antibody, and again streptavidin-AF647, for signal amplification. Images were acquired on a Zeiss Axioscan Z1 slide scanner or Zeiss 710 META Laser Scanning Confocal microscope. Image analysis was performed using Zen v3 software. Cell counting was performed manually using ImageJ 1.47v or Zen 2.1 Lite software on at least 3 tissue sections per sample.

Isolation of synovial joint cells

Isolation of cells from mouse synovial joints was performed as previously described.[4] Briefly, dissected joints were incubated with 1 mg/ml collagenase type IV in culture media (high-glucose DMEM with 10% foetal bovine serum (FBS;) and 100 U/ml penicillin and 0.1 mg/ml streptomycin) for 50 minutes at 37°C under agitation. Cells were disassociated by vortexing and cell suspensions passed through a 40 µm cell strainer. Cells were centrifuged at 300g for 5 minutes and resuspended in 1 ml of culture media before further processing and analysis.

Immunophenotyping by flow cytometry

Cells were stained with antibodies listed in Supplementary table 3. Data were acquired on a BD Fortessa flow cytometer and analysed using FlowJo v10 software. Unstained and single-labelled cells or antibody-labelled UltraBeads (eBioscience) were used to set compensation and gates were applied based on fluorescence-minus-one (FMO) controls. Erythrocytes and debris were excluded based on forward and side scatter parameters. Doublets and aggregates were gated out based on forward-scatter parameters. Staining with Fixable Viability Dye eFluor 455UV (eBioscience, cat. no. 65-0868-18) was used to exclude dead cells as indicated. See Supplementary Fig. 6 for gating strategies.

Fluorescence-activated cell sorting

Cells isolated from the knees of steady-state or injured female *Gdf5-Cre*;*Tom;Pdgfrα-H2BGFP* mice at 11-13 weeks of age were sorted for Tom+ (*Gdf5*-lineage) and Tom-GFP+ (non-*Gdf5*-lineage, *Pdgfrα*-expressing) cells on an BD Influx Cell Sorter. Cells from each mouse were sorted and processed independently. Erythrocytes and debris were excluded based on forward and side-scatter profiles. Doublets and aggregates were gated out based on forward-scatter parameters, and non-viable cells excluded by 4',6-diamidino-2-phenylindole (DAPI) staining. Cells were sorted based on Tom and GFP fluorescence into separate FBS-coated tubes containing 1 ml culture media to maintain cell viability. Immediately following sorting, small aliquots of sorted cells were analysed on a BD Fortessa flow cytometer to confirm sample purity. Cells were kept on ice in the dark, for a maximum period of 2 hours, until further processing.

Generation of scRNA-seq data

Following sorting, Tom+ cells (n=2) and donor-matched Tom-GFP+ cells (n=1) from steady-state mice, and Tom+ cells (n=4) and donor-matched Tom-GFP+ cells (n=2) from mice 6 days after joint surface injury, were captured independently using the 10x Genomics Chromium system. Steady-state and injured mice were age- and sex-matched. Generation of data was performed separately for each mouse and across 3 experiments as detailed in Suppl. Table 4. Sequencing libraries were generated using the 10x Genomics Single Cell 5' Library and Gel Bead Kit (version 2) and sequenced on the Illumina NextSeq 500. Alignment and quantification of sequencing data was performed using the 10x Genomics Cell Ranger pipeline (version 2.2.0) and mouse reference genome (GRCm38.p6) obtained from NCBI and modified to contain the *tdTom* and *H2BGFP* transgenes.[7]

Analysis of scRNA-seq data

Quality control of scRNA-seq data was performed using the default parameters of the SoupX package[8] to estimate and remove ambient RNA. Analysis of scRNA-seq data was performed using the Seurat R package (version 4.03) and associated SeuratWrappers for the Velocyto, scVelo and Slingshot packages.[9–13] For samples obtained from steady-state mice, cells with fewer than 200 genes, more than 4000 genes, or greater than 5% mitochondrial reads were excluded from analysis. For samples obtained after injury, cells with fewer than 200 genes, more than 6000 genes, or greater than 5% mitochondrial reads were excluded from analysis. Gene expression measurements were normalised by the total expression, multiplied by a scale factor (10,000) and log-transformed. Cells expressing either haematopoietic cell markers *Ptprc* or *Fcer1g* that were also negative for the fibroblast marker *Pdpn* were subset out from all samples to remove haematopoietic contamination.

Cells expressing *Tom* were subset out from the Tom-GFP+ samples to remove Tom+ cell contamination.

Datasets were integrated using the reciprocal PCA (RPCA) method using 2000 integration anchor features that were repeatedly variable across datasets. To mitigate cell cycle heterogeneity, cell cycle scoring, and regression were performed using the Seurat CellCycleScoring function to calculate G2M and S phase scores. The difference between these scores was used to regress out signal associated with cell cycle.

Fifty principal components were determined to account for the majority of variation and, along with the previously identified 2000 variable genes, were used for uMAP and clustering analysis (original Louvain algorithm). For steady-state and integrated steady-state and injured datasets clustering resolution was set to 0.8. For analysis of individual experimental conditions or comparison of ontogenetic lineages within steady-state or injured-state knees, data were subset from the main integrated file and re-clustered at a resolution of 0.7. Following clustering, clusters corresponding to adipocytes, based on high *Adipoq* expression, were removed using the subset function.

Cluster markers were calculated using the non-parametric Wilcoxon rank sum test with Bonferroni correction using all features in the dataset. Only genes detected in 25% of cells either within or outside the cluster of interest and that demonstrated a minimum log-fold difference of 0.25 were tested for differential expression.

To map steady-state clusters onto the fully integrated dataset we first obtained the barcodes for cells that constituted each steady-state cluster using the Seurat WhichCells function. These barcodes were mapped onto the fully integrated dataset using the Seurat Dimplot function with cells.highlight specified.

Gene Ontology analysis

For gene set over-representation analysis, the R package ‘gsfisher’ was utilised. Cluster-specific gene universes were constructed as those genes expressed by 25% of the cells in the cluster or 25% of all cells. Cluster-specific differentially expressed genes were tested against these gene universes for gene ontology (GO) category enrichments using one-sided Fisher’s exact tests with multiple testing correction, with ‘biological process’ gene sets obtained from the GO database. Results were filtered to discard GO categories with less than 3 genes or more than 500 genes in the foreground list, or an over-representation odds ratio of less than 2.

Pseudo-bulk analysis

For pseudo bulk analysis, average gene expression was calculated using the Seurat AverageExpression function. Briefly, for each cluster, gene expression log values were averaged then scaled so that gene variance across clusters is 1. Correlation between cluster gene expression was performed using the R pairs function with Pearson correlation coefficient.

Differential abundance analysis

For differential abundance analysis, the contribution of each replicate / sample to cluster composition was calculated. Differential abundance was calculated by the negative binomial generalised linear model, using the R package edgeR.[14] Briefly, data were normalised using the relative log expression (RLE) method and design matrix specified. Dispersion was estimated and estimation of quasi-likelihood (QL) dispersions performed using the glmQLFit function. Comparisons between cell types was made using the glmQLFTest function. To control the false discovery rate (FDR), multiple testing correction was performed using the Benjamini-Hochberg method.

Venn diagram generation

For analysis of cells expressing multiple master regulator genes, cells expressing selected genes were identified using the Seurat WhichCells function and passed to the R package VennDiagram.

Single-cell gene regulatory network analysis

For single-cell gene regulatory network analysis we utilised the SCENIC package,[15] using the standard R pipeline. Briefly, the expression matrix was isolated from the Seurat object and loaded into GENIE3 for building the initial co-expression gene regulatory network (GRN). RcisTarget was used to analyse the regulon data along with the mm9-tss-centred-10kb (mouse) or hg19-500bp-upstream-7species (human) database to create transcription factor (TF) motifs. Regulon activity scores were calculated using the AUCell package. A binary output for each regulon (active or inactive) was determined by setting a threshold based upon the ranked distribution of AUCell scores across cells. Regulons were then ranked within clusters for level of activity, and the highest ranked regulons that displayed cluster-specificity were identified as potentially important for regulating cell phenotype. Visualisation of gene regulatory networks was performed using Cytoscape 3 and associated R package RCy3.[16]

MA plot analysis

For MA plot generation, gene log sums were first calculated using the R log2 function and Seurat GetAssayData function. Calculation of gene differential expression was performed via the Seurat FindMarkers function with logfc.threshold set to 0 using the Wilcoxon rank sum test. P-value

adjustment was performed using Bonferroni correction based on the total number of genes in a dataset. Gene log sum was plotted against avg_log2FC using ggplot2. Genes with greater than two-fold change and adjusted p value <0.01 were highlighted.

RNA velocity analysis

The package scVelo was utilised for the analysis of RNA velocity.[11] Briefly, loom files were generated from the 10x Genomics cellranger output files using the velocyto python implementation,[10] loaded into Seurat and converted into a Seurat object. Files were merged and the scTransform command run to normalise, scale and find variable features. Fifty principal components were used. Data was subset based on barcode ID to match cell identities between RNA velocity and the standard Seurat analysis. uMAP co-ordinates from the standard Seurat analysis were used to ensure comparable projections. Data was converted to .h5ad format and loaded into the scVelo package. Analysis of RNA velocity in the scVelo package was performed using the default settings for the dynamical model with differential kinetics.[11]

Pseudotime lineage inference

Single-cell pseudotime trajectories were computed using the Slingshot[13] and Monocle3[12] algorithms. Pre-computed cell embeddings and clusters from the Seurat pipeline served as input.

For Slingshot analysis of ontogenetically separated steady-state datasets, no start or end clusters were defined. Lineage inference was performed by the construction of a minimum spanning tree (MST) between clusters (nodes). Pseudotime was visualised by fitting principal curves to these lineages.[13]

For Monocle 3 analysis of injured datasets, gene expression data was isolated from the Seurat object using the Seurat GetAssayData function and a Monocle cell data set (cds) created using the Monocle3 new_cell_data_set function. The cds was pre-processed, dimensions reduced, and cells clustered using the Monocle3 preprocess_cds, reduce_dimension and cluster_cells functions. Seurat cluster IDs and uMAP settings were then imported into the monocle cds. Trajectories were determined and cells ordered in pseudotime using the Monocle3 learn_graph and order_cells functions. Identification of genes whose expression changed significantly along trajectories, as a function of pseudotime, was determined using graph-auto correlation analysis using the Monocle3 choose_cells and graph_test functions. Selected genes, listed as being transcription factors in the AnimalTFDB3.0 database,[17] that varied significantly in their pseudo-temporal expression pattern (Moran's I > 0.1 and q value < 0.01) were plotted on a heatmap of expression over pseudotime.

Cell cycle analysis

For analysis of cell cycle score, a gene module containing Cdk1, Ccna2, Ccnb1, Ccnb2 and Mki67 was generated and the average expression level in each cluster calculated using the Seurat AddModuleScore function.

Analysis of scRNA-seq data from the mouse serum transfer-induced arthritis (STIA) model

Mouse serum transfer-induced arthritis (STIA) scRNA-seq datasets were obtained from NCBI GEO GSE129087.[18] Cells with fewer than 200 genes, more than 6000 genes, or greater than 5% mitochondrial reads were excluded from analysis. Gene expression measurements were normalised by the total expression, multiplied by a scale factor (10,000) and log-transformed.

For the identification of annotated clusters in the Croft *et al*. study[18] the dataset was processed in a comparable manner. Immune cells were removed and the STIA dataset was down sampled to consist of 1,725 cells. Thirty principal components were used for uMAP generation and clustering performed at a resolution of 0.4. Fibroblast clusters were identified according to the Croft *et al*. study[18] based on the expression of: F1 – *Sfrp2*, *Col11a1*, *Mfap4*; F2 – *Tnfaip6*, *Inhba*, *Prg4*; F3 – *Apod*, *Clec3b*, *Cd34*; F4 – *Top2a*, *Hmgb2*, *Cdk1*; F5 – *Clic5*, *Col22a1*, *Tspan15*. Identification of cells in these clusters was determined using the Seurat WhichCells function and mapped onto the integrated STIA and injured dataset using the Seurat Dimplot function with cells.highlight specified.

For the integration of the STIA and injured datasets we used the reciprocal PCA (RPCA) method using 2000 integration anchor features that were repeatedly variable across datasets. To mitigate cell cycle heterogeneity, cell cycle scoring and regression were performed using the Seurat CellCycleScoring function to calculate G2M and S phase scores. The difference between these scores was used to regress out signal associated with cell cycle. Fifty principal components were determined to account for the majority of variation and, along with the previously identified 2000 variable genes, were used for uMAP and clustering analysis (original Louvain algorithm). Clustering resolution was set to 0.8. Non-fibroblasts were removed based on the expression of *Ptprc*, *Pecam1*, *Myh11* and *Adipoq*.

Analysis of scRNA-seq data from human osteoarthritis patients

Human osteoarthritis scRNA-Seq datasets were obtained from Chou *et al*., NCBI GEO GSE152805 (n = 3 patients),[19] Mizoguchi *et al*., NCBI GEO GSE109449 (n = 2 patients),[20] and Zhang *et al*., ImmPort SDY998 (n = 3 patients).[21] For the Chou *et al*.[19] dataset, cells with fewer than 200 genes, more than 7,500 genes or greater than 30% mitochondrial reads were excluded from analysis, as per original publication.[19] For the Mizoguchi *et al*.[20] dataset, cells with fewer than 200 genes, more than 16,000 genes or greater than 20% mitochondrial reads were excluded from analysis. For the Zhang *et*

al.[21] dataset, cells with fewer than 1000 genes or greater than 25% mitochondrial reads were excluded from analysis, as per original publication.[21] Patient samples from within each study were integrated using the reciprocal PCA (RPCA) method with 2000 repeatedly variable integration anchor features. Cell cycle effects were regressed out and fifty principal components used for uMAP and clustering analysis (original Louvain algorithm, resolution set to 0.4, 0.5 and 0.5 respectively). Haematopoietic, endothelial and smooth muscle cells were excluded based on the expression of PTPRC, PLVAP and ACTA2. Regulon analysis was performed using the SCENIC algorithm as previously described.

Statistical analysis

All data points on graphs, and n-numbers in text, indicate individual human donors or mice, except for graphical visualisations of scRNA-seq data. SigmaPlot v14 and GraphPad Prism v5 software were used for statistical analysis. Tests used to determine statistical significance ($p<0.05$) are indicated in figure legends. Normality and equality of variance were tested in Sigmaplot using the Shapiro-Wilk and Brown-Forsythe tests, respectively. Log-transformation was used to equalise variance prior to statistical testing as indicated.

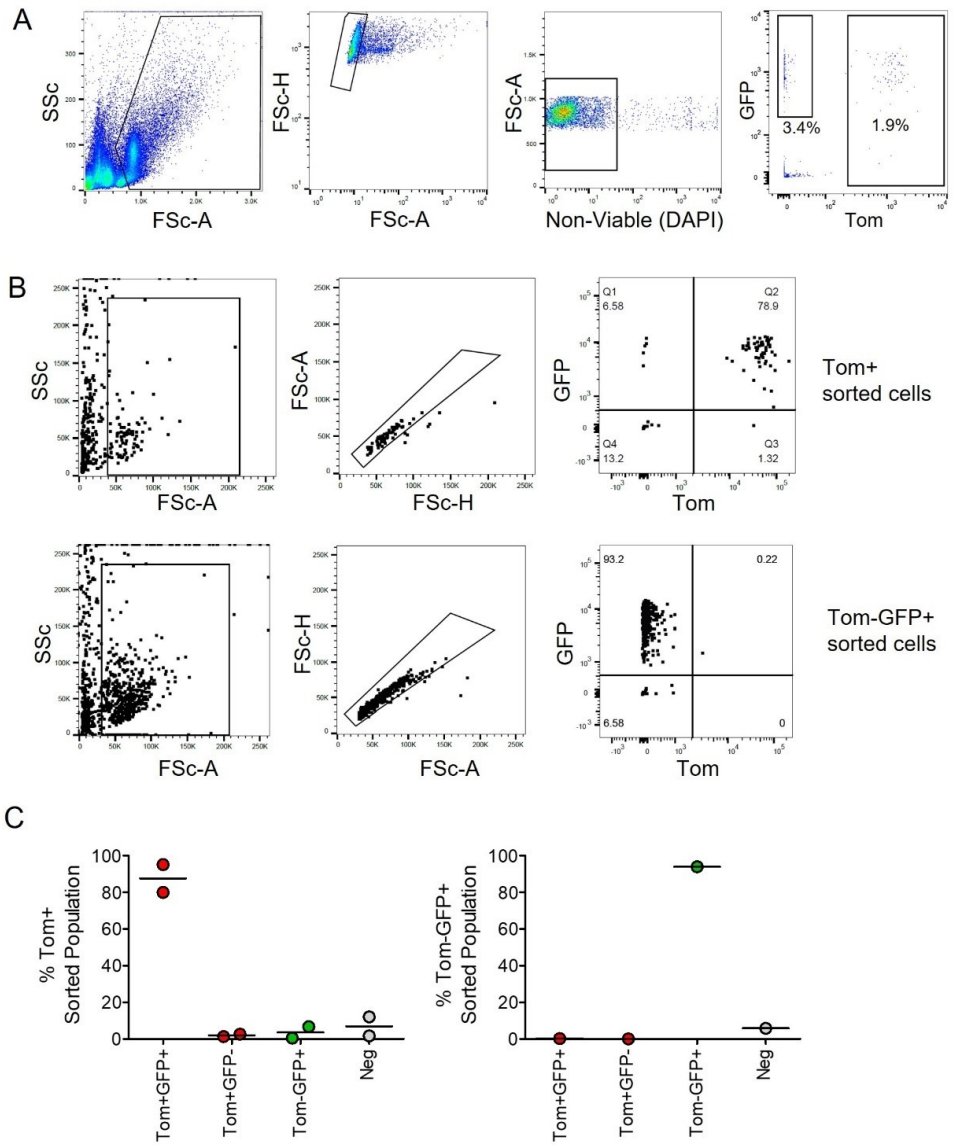

Supplementary Figure 1. Extended data Figure 1B. Cell sorting strategy for isolation of adult *Gdf5*-lineage and non-*Gdf5*-lineage *Pdgfrα*-expressing cells. (**A**) Gating strategy to sort Tom+ (*Gdf5*-lineage) and Tom-GFP+ (non-*Gdf5*-lineage *Pdgfrα+*) cells within single live cells freshly isolated from knees of adult *Gdf5-Cre*;*Tom*;*Pdgfrα-H2BGFP* mice using a BD Influx cell sorter. Erythrocytes and debris were gated out based on Forward and Side Scatter profile. Doublets and aggregates were excluded based on Forward Scatter parameters. Dead cells were excluded based on DAPI staining. Tom+ and Tom-GFP+ cells were sorted based on fluorescence. (**B,C**) Following sorting, aliquots of Tom+ and Tom-GFP+ collected cells were analysed on a BD Fortessa flow cytometer to confirm cell purity. Data in (**C**) show the purity of sorted cells used for scRNA-seq analysis. Note that while Tom+ cells were sorted regardless of GFP expression, the vast majority of Tom+ cells also expressed GFP.

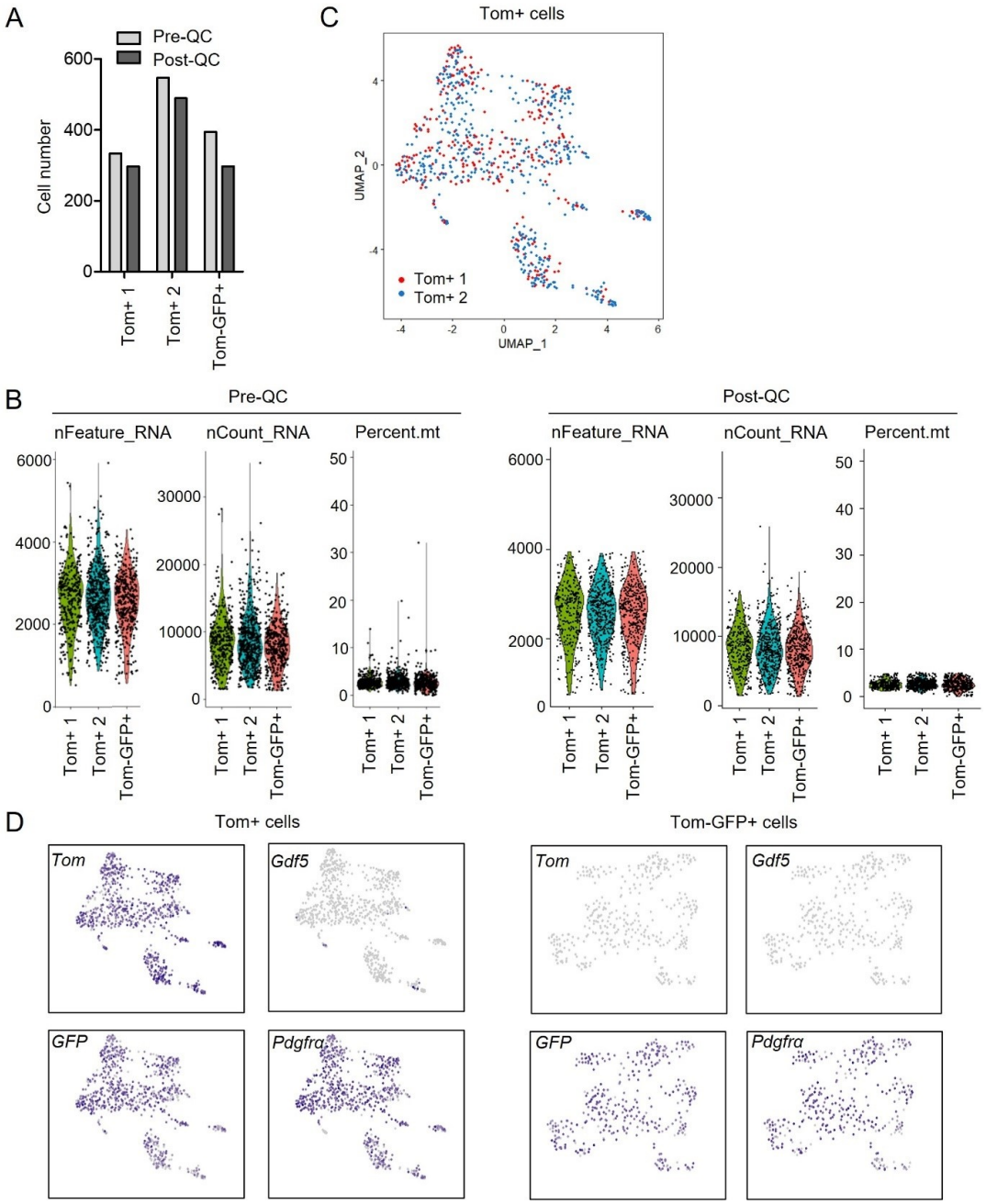

Supplementary Figure 2. Extended data Figure 1C. Single-cell RNA-sequencing analysis of cells isolated from knee joints of adult *Gdf5-Cre*;*Tom*;*Pdgfrα-H2BGFP* mice. scRNA-seq data of Tom+ (n=2 mice) and donor-matched Tom-GFP+ (n=1 mouse) sorted cells was obtained using the 10x Genomics Chromium system. (**A**) Number of cells present in each sample before and after QC processing. (**B**) Features, counts and percent mitochondrial genes before and after QC processing. (**C**) Unsupervised uMAP of the Tom+ cells coloured by biological replicate (mouse). (**D**) Detection of *Tom, Gdf5, GFP* and *Pdgfrα* expression in the analysed cell populations.

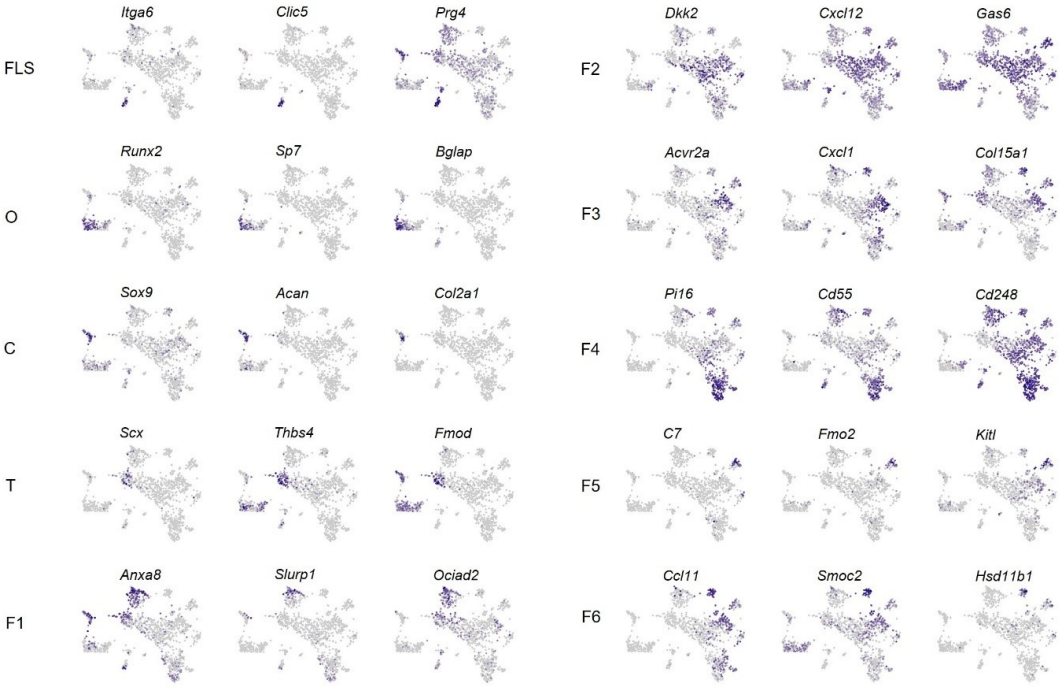

Supplementary Figure 3. Extended data Fig. 1D. UMAP plots showing the expression of selected DEGs for each cluster that identify specialised cell types or are dominant cluster-specific genes. FLS: Fibroblast-like synoviocytes; O: Osteoblast-lineage cells; C: Chondrocyte-lineage cells; T: Tenocyte-lineage cells; F: Fibroblasts.

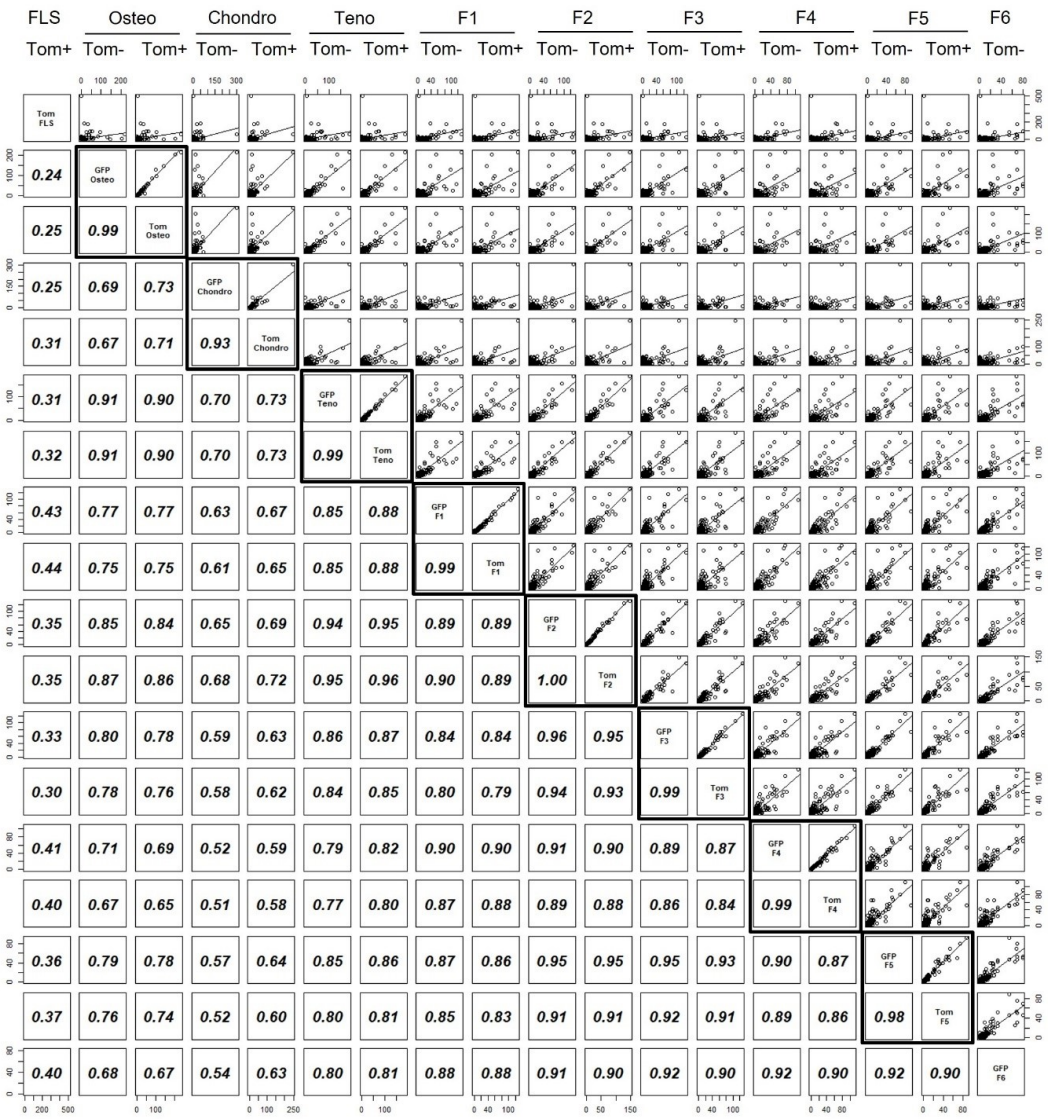

Supplementary Figure 4. Data relating to Figure 1. Pseudo-bulk transcriptome comparisons between Tom+ and Tom-GFP+ cells within the cell sub-populations identified in steady-state. Average gene expression levels were calculated for the Tom+ and Tom-GFP+ cells within each identified cell cluster. Black outlines indicate comparisons between Tom+ and Tom-GFP+ cells within each cluster. FLS: Fibroblast-like synoviocytes; Osteo: Osteoblast-lineage cells; Chondro: Chondrocyte-lineage cells; Teno: Tenocyte-lineage cells; F: Fibroblasts.

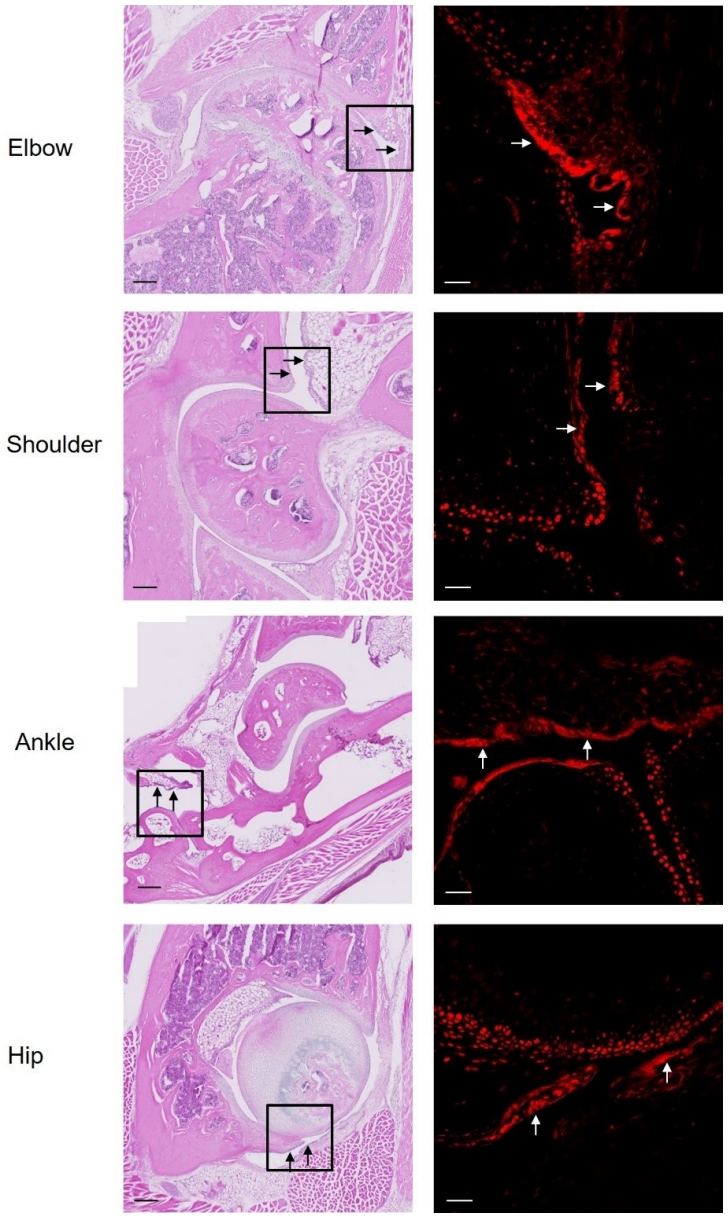

Supplementary Figure 5. Data relating to Figure 2A. Detection of Tom+ cells in synovial lining (arrows) of elbow, shoulder, ankle and hip from 15-week-old *Gdf5-Cre*;*Tom;Pdgfrα-H2BGFP* mice by histology (n=3). Left: H&E-stained sections. Scale bars: 200 µm. Right: Confocal fluorescence microscopy images of near-consecutive sections showing Tom fluorescence in red. Scale bars: 50 µm. Boxed areas in H&E images indicate approximate region shown on the right.

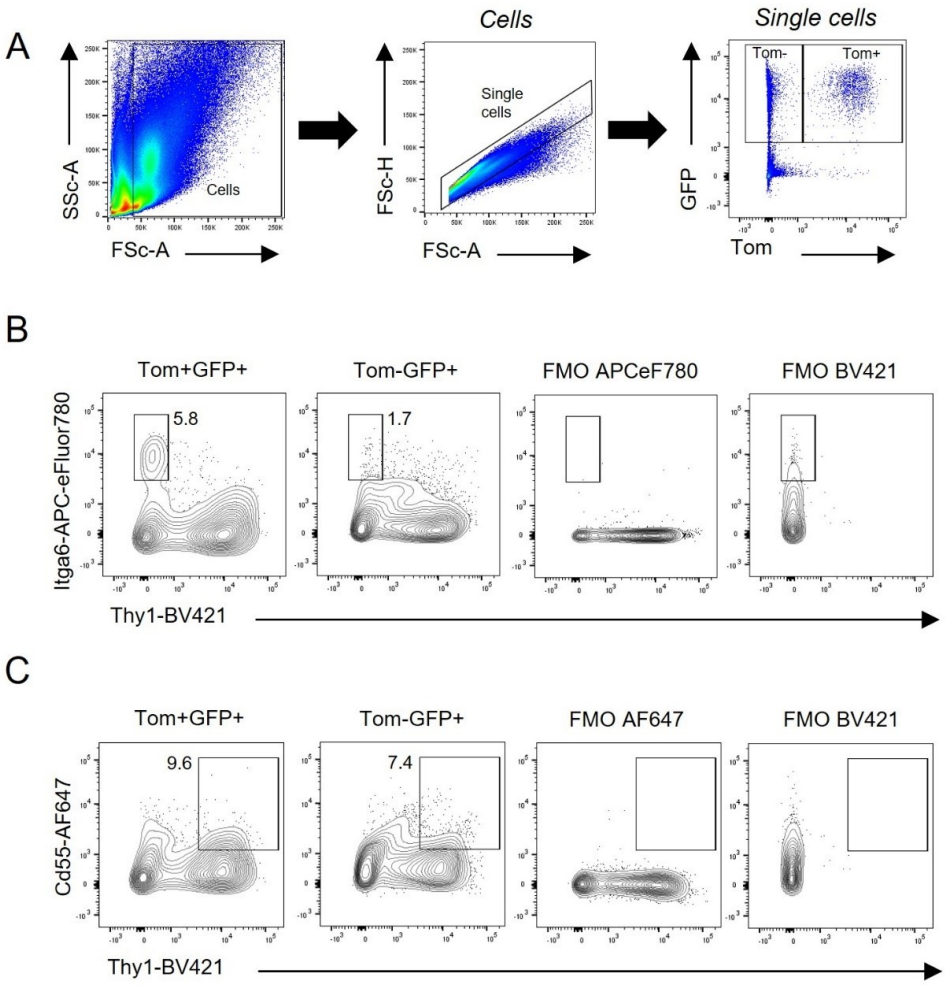

Supplementary Figure 6. Extended data Figure 2A. Cells were isolated from knees, elbows, ankles and hips of 21-to-23-week-old *Gdf5-Cre*;*Tom;Pdgfrα-H2BGFP* mice (n=8) and analysed by flow cytometry. (**A**) Gating strategy to identify Tom+GFP+ and Tom-GFP+ cells. Erythrocytes and debris were excluded based on Forward and Side Scatter profile. Doublets and aggregates were excluded based on Forward Scatter parameters. Tom+GFP+ and Tom-GFP+ cells were identified based on fluorescence. (**B,C**) Representative flow cytometry plots showing gating that was used to identify Thy1-Itga6+ FLS (**B**) and Thy1+Cd55+ fibroblasts (**C**) within the Tom+GFP+ and Tom-GFP+ cell populations. Gates were verified using fluorescence-minus-one (FMO) controls.

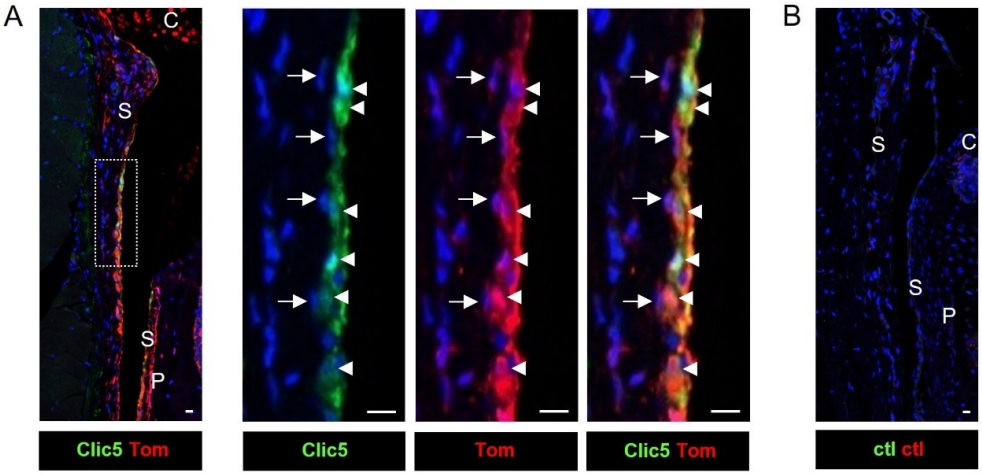

Supplementary Figure 7. Extended data Figure 2B. (**A**) Tom+ cells expressing Clic5 (arrowheads) and adjacent Tom+Clic5- cells (arrows) in synovial lining of 10-week-old *Gdf5-Cre*;*Tom;Pdgfrα-H2BGFP* mice detected by immunofluorescence staining (n=3). Note absence of Clic5 staining in cartilage. Boxed area on the left is shown enlarged on the right as separate and merged channel images. (**B**) Section stained with isotype negative control antibodies (ctl). Scale bars: 10 µm. Blue: DAPI nuclear counterstain. S: Synovium; P: Periosteum; C: Cartilage.

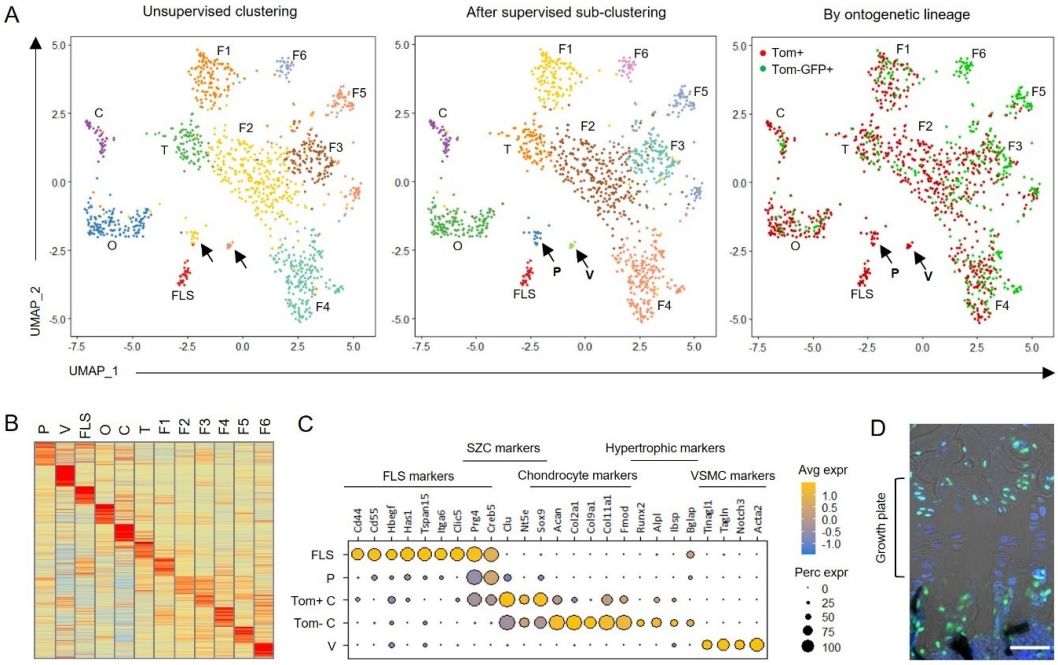

Supplementary Figure 8. Extended data Figure 2D. (**A**) UMAPs of the steady-state scRNA-seq data (see Fig. 1 for details). Left: Unsupervised clustering. Arrows indicate two small cell populations not identified as separate clusters by the unsupervised clustering algorithm. Middle: After supervised sub-clustering of the two clusters indicated by arrows. Right: Coloured by analysed cell populations showing that the two sub-clusters consisted of Tom+ cells. (**B**) Heatmap showing average expression of top 50 DEGs for all clusters identified after supervised sub-clustering. (**C**) Heatmap showing expression of selected marker genes. Cells within the P sub-cluster expressed *Prg4* and *Creb5,* but were largely negative for other FLS, superficial zone chondrocyte (SZC), and chondrocyte markers. Tom+ cells within the chondrocyte-lineage cluster expressed the superficial zone chondrocyte (SZC) markers *Prg4,*[22] *Creb5,*[23] *Clusterin,*[24] and *Nt5e,*[25] the chondrocyte-lineage transcription factor *Sox9*, and limited expression of mature chondrocyte genes, indicative of a SZC phenotype. Of note, the short collagenase digestion protocol that was used is insufficient to release chondrocytes from the deeper zones of articular cartilage, as previously shown.[4] The small number of Tom-GFP+ cells in the chondrocyte-lineage cluster did not express *Prg4* or *Creb5* and showed a mature / prehypertrophic chondrocyte phenotype. These cells likely derived from the growth plate, which was used as an incision point during knee joint dissection. The second sub-cluster was identified as vascular smooth muscle cells (V). (**D**) Histology of the tibial growth plate of an adult *Gdf5-Cre*;*Tom;Pdgfrα-H2BGFP* mouse, showing GFP expression, but not Tom expression, by chondrocytes in the upper part (proliferative/pre-hypertrophic) zone of the growth plate. Scale bar indicates 50 µm. FLS: Fibroblast-like synoviocytes; O: Osteoblast-lineage cells; C: Chondrocyte-lineage cells; T: Tenocyte-lineage cells; F: Fibroblasts.

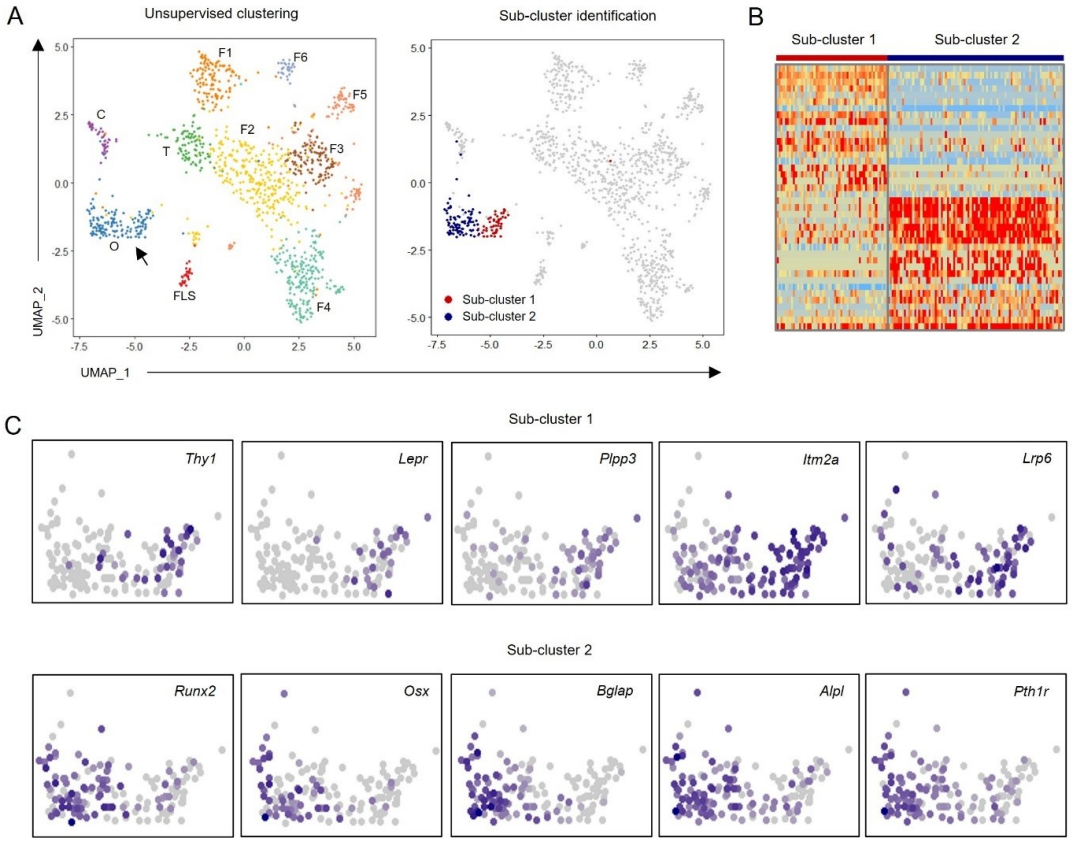

Supplementary Figure 9. Data relating to Figure 2. Osteoblast-lineage sub-cluster analysis. (**A**) UMAPs of the steady-state scRNA-seq data. Left: Unsupervised clustering. Arrow indicates osteoblast-lineage (O) cluster. Right: Osteoblast-lineage cluster was subset and re-clustered to identify sub-clusters. Two sub-clusters were identified and barcodes of cells that composed each sub-cluster were obtained and are shown in red and blue on the UMAP. (**B**) Heatmap showing expression of top 20 DEGs for the two sub-clusters. (**C**) UMAP plots showing expression of selected DEGs that were cluster-specific for the two sub-clusters, putatively identifying sub-cluster 1 as osteochondral progenitors and sub-cluster 2 as osteoblasts. FLS: Fibroblast-like synoviocytes; O: Osteoblast-lineage cells; C: Chondrocyte-lineage cells; T: Tenocyte-lineage cells; F: Fibroblasts.

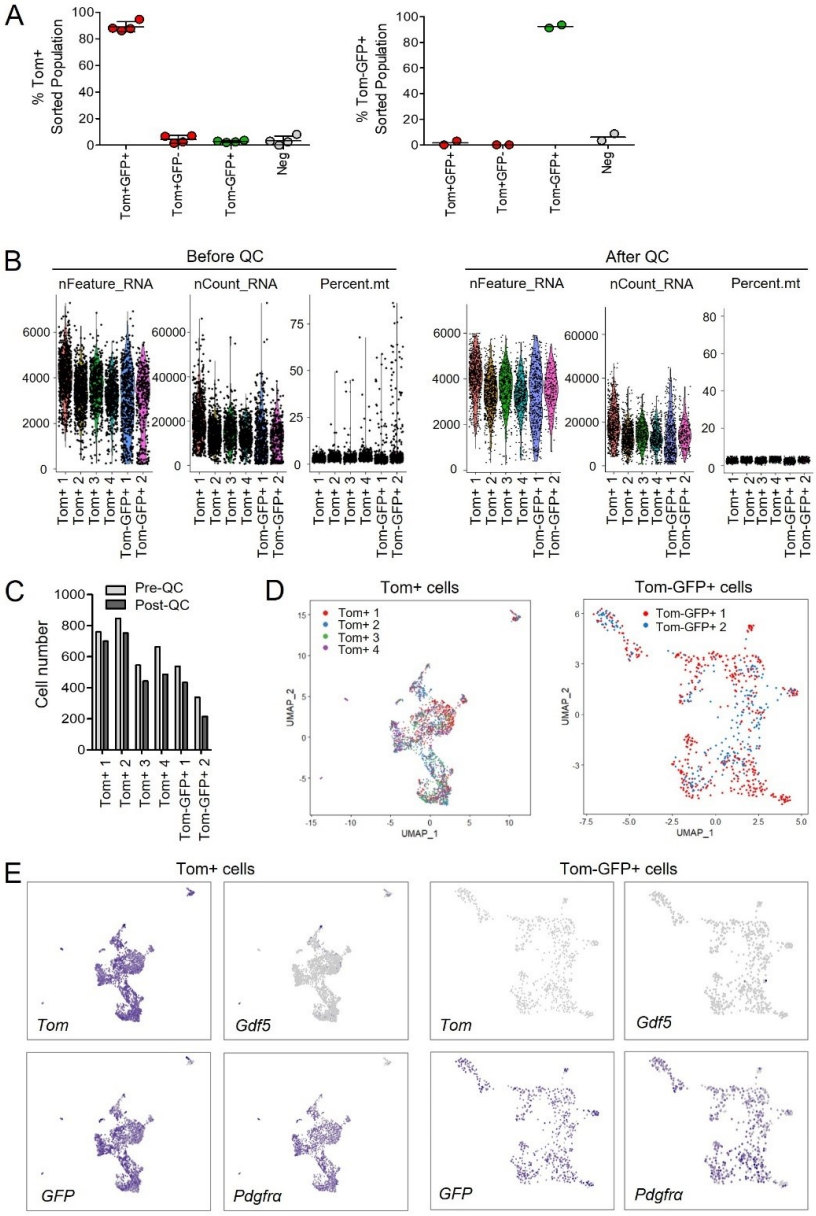

Supplementary Figure 10. Extended data Figure 3B. ScRNA-seq analysis of cells isolated from knee joints of adult *Gdf5-Cre*;*Tom*;*Pdgfrα-H2BGFP* mice after joint surface injury. scRNA-seq data of Tom+ (n=4 mice) and donor-matched Tom-GFP+ (n=2 mice) sorted cells was obtained using the 10x Genomics Chromium system. (**A**) Following sorting by FACS, aliquots of Tom+ and Tom-GFP+ collected cells were analysed on a BD Fortessa flow cytometer to confirm cell purity. Lines and error bars indicate mean ± SD. (**B**) Features, counts and percent mitochondrial genes before and after QC processing. (**C**) Number of cells present in each sample before and after QC processing of the scRNA-seq data. (**D**) Unsupervised uMAP of the Tom+ cells and Tom-GFP+ cells coloured by biological replicate (mouse). (**E**) Detection of *Tom, Gdf5, GFP* and *Pdgfrα* expression in the analysed cell populations.

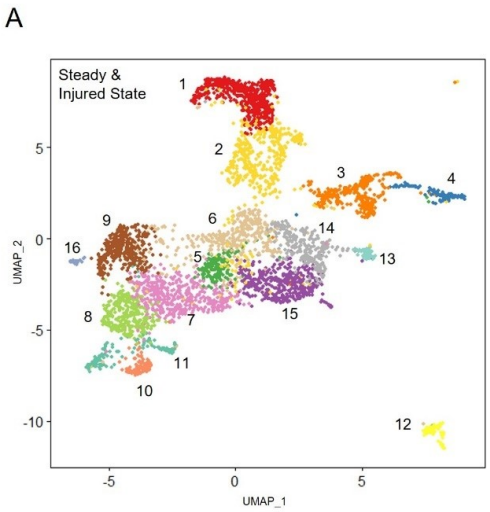

B

Integrated cluster	Expression of DEGs by steady state clusters	Cluster name	Key genes	Function
1		FLS	Itga6 Clic5 Tspan15	FLS
2		P	Megf10 Enpp5 Prg4	Progenitor
3		O	Runx2 Sp7 Chad	Osteoblast lineage
4		C	Sox9 Acan Col2a1	Chondrocyte lineage
5		T	Scx Thbs4 Fmod	Tenocyte lineage
6		F1	Anxa8 Slurp1 Ociad2	Fibroblast
7		F2	Dkk2 Cxcl12 Gas6	Fibroblast
8		F3	Acvr2a Cxcl1 Col15a1	Fibroblast
9		F4	Pi16 Cd55 Cd248	Fibroblast
10		F5	C7 Fmo2 Kitl	Fibroblast
11		F6	Ccl11 Smoc2 Hsd11b1	Fibroblast
12		V	Mcam Notch3 Tagln	VSMC
13		IF1	Mki67 Top2a Mcm5	Proliferating Injury-induced Fibroblast
14		IF2	Gjb5 Glipr1 Acta2	Injury-induced Fibroblast
15		IF3	Tnn Lrrc15 Fbn2	Injury-induced Fibroblast
16		IF4	Mmp27 Dlk1 Ccl8	Injury-induced Fibroblast

Supplementary Figure 11. Extended data Figure 3B,C. (**A**) UMAP plot of integrated scRNA-seq data from steady-state and injured-state cells showing unsupervised clustering identifying 16 cell clusters. (**B**) Analysis of differentially expressed genes (DEGs) (see Suppl. Table 6) used to identify clusters equivalent to the clusters identified in steady-state (see Fig. 1). Heatmaps show expression of the top 50 DEGs from each integrated cluster by the 10 steady-state clusters identified by unsupervised analysis (Fig. 1C) and the two steady-state clusters identified by supervised sub-clustering (Fig. 2D and Suppl. Fig. 8). Heatmap order: FLS, *Prg4*+ progenitors, osteoblast-lineage, chondrocyte-lineage, tenocyte-lineage, fibroblast clusters 1-6 and vascular smooth muscle cells. Key genes indicate selected DEGs that identify specialised cell types or are dominant cluster-specific genes. (**C**) UMAP with cluster annotation. Twelve clusters were annotated according to equivalent cluster identified in steady-state (see also Suppl. Fig. 12), with the osteoblast-lineage cluster identified as osteochondral (OC) lineage after injury (see also Suppl. Fig. 17). Four clusters only identified after injury were annotated as injury-induced fibroblasts (IF1-IF4). Injury-induced fibroblast (IF) clusters are in bold; clusters with steady-state analogues in italics.

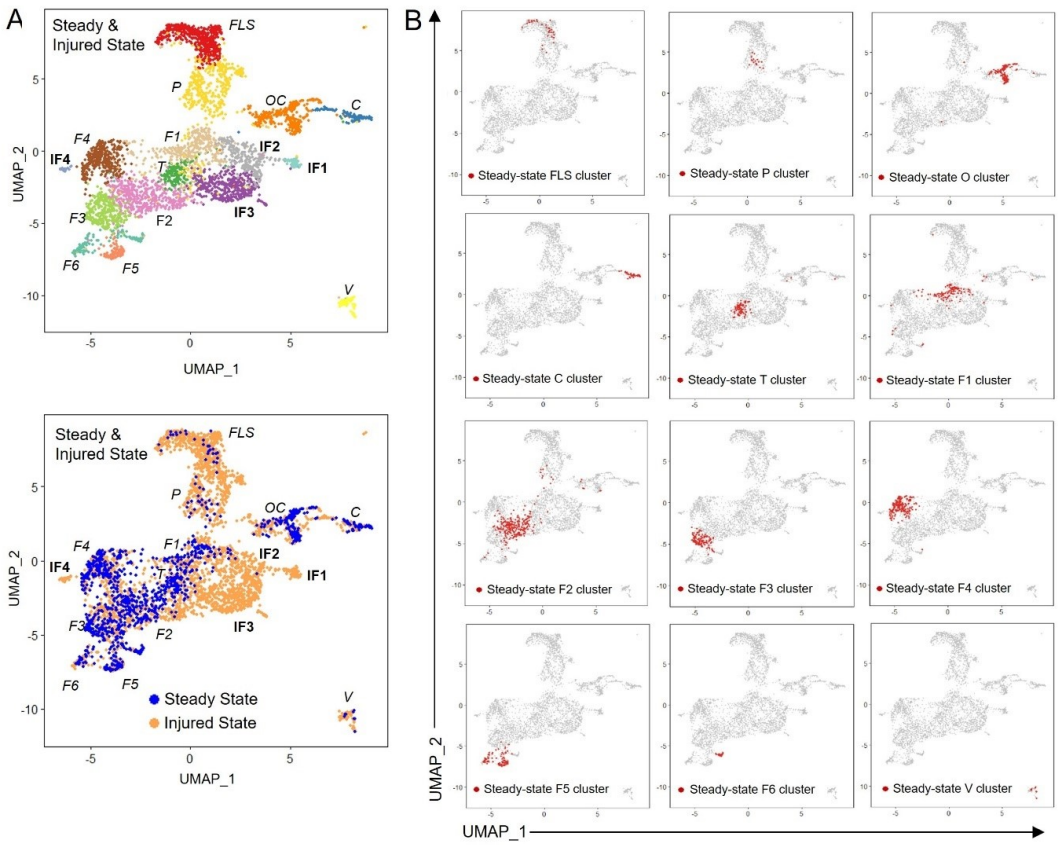

Supplementary Figure 12. Extended data Figure 3B,C. UMAP plots of integrated scRNA-seq data from steady-state and injured-state cells showing (A) Top: unsupervised clustering. Bottom: Colour coded by analysed state. Injury-induced fibroblast (IF) clusters are in bold; clusters with steady-state analogues in italics. (B) The location, in red, of steady-state cells within each of the clusters identified in steady-state (see Fig. 1) to verify cluster annotation. The location of steady-state cluster cells on the integrated uMAP correlates well with the integrated uMAP clustering and annotation, with the exception of clusters F5 and F6, which clustered differently between steady-state and integrated uMAP. FLS: Fibroblast-like synoviocytes; P: *Prg4*+ progenitors; O: Osteoblast-lineage cells; C: Chondrocyte-lineage cells; T: Tenocyte-lineage cells; F: Fibroblasts; V: Vascular smooth muscle cells.

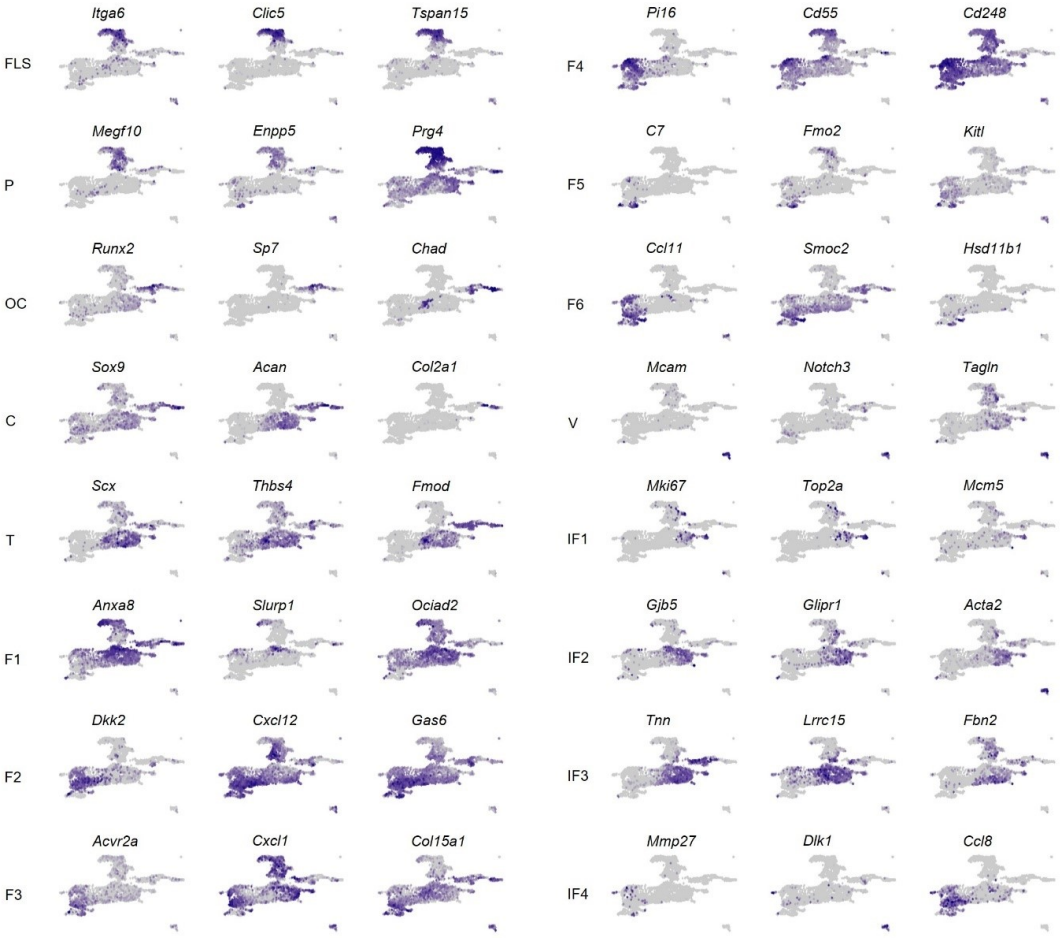

Supplementary Figure 13. Extended data Fig. 3B,C. UMAP plots showing the expression of selected DEGs for each cluster that identify specialised cell types or are dominant cluster-specific genes. FLS: Fibroblast-like synoviocytes; P: *Prg4*+ Progenitors; OC: Osteochondral-lineage cells; C: Chondrocyte-lineage cells; T: Tenocyte-lineage cells; F: Fibroblasts; V: Vascular smooth muscle cells; IF: Injury-induced fibroblasts.

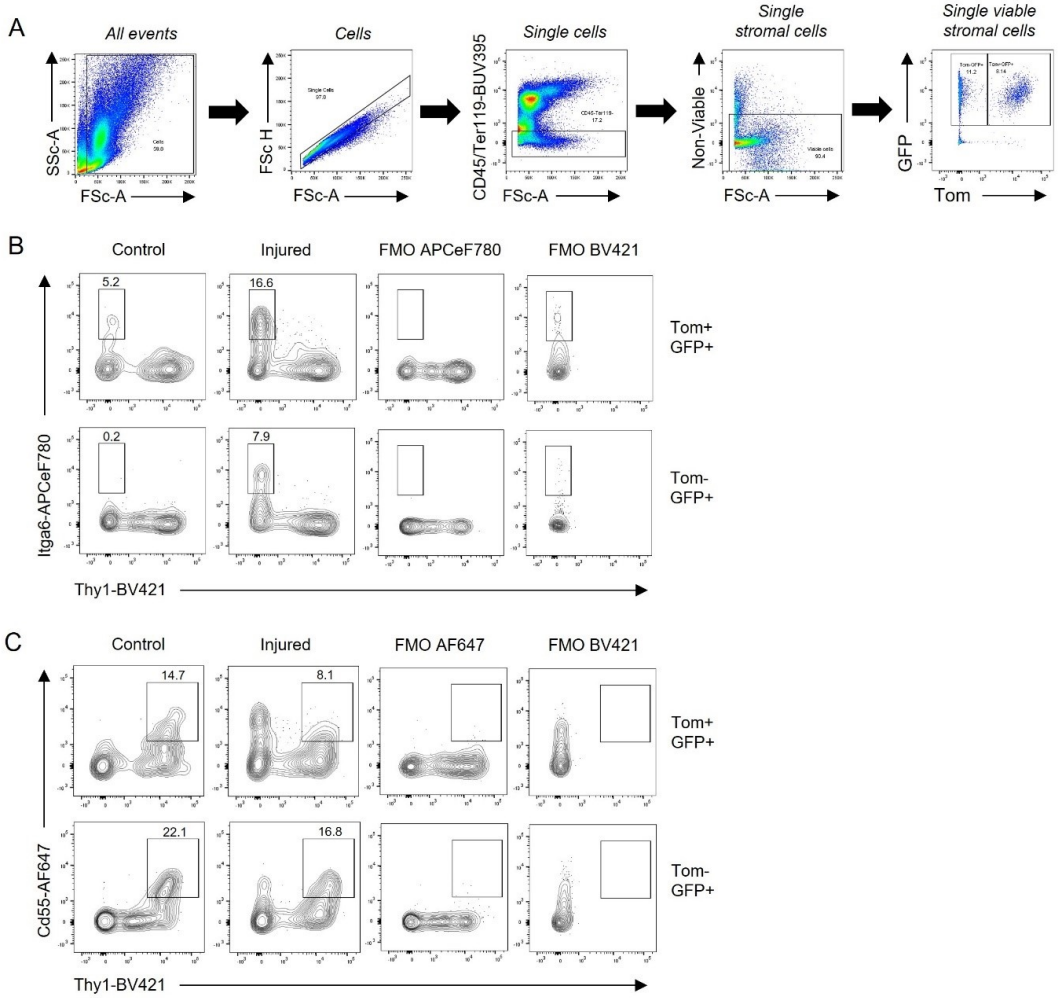

Supplementary Figure 14. Extended data Figure 3E. Freshly isolated cells from knees of 15-to-18-week-old *Gdf5-Cre;Tom;Pdgfrα-H2BGFP* mice 6 days after joint surface injury were analysed by flow cytometry (n=7). (**A**) Gating strategy to identify GFP+Tom+ and GFP+Tom- cells. Erythrocytes and debris were excluded based on Forward and Side Scatter profile. Doublets and aggregates were excluded based on Forward Scatter parameters. Haematopoietic cells and erythrocytes were further excluded based on CD45 and Ter119 staining. Dead cells were excluded based on viability dye staining. (**B,C**) Representative flow cytometry plots showing Itga6 and Thy1 expression (**B**) and Cd55 and Thy1 expression (**C**) within the GFP+Tom+ and GFP+Tom- cell populations. Injured: Cells isolated from injured knee; Control: Cells isolated from contralateral control knee. Gates were set using fluorescence-minus-one (FMO) controls.

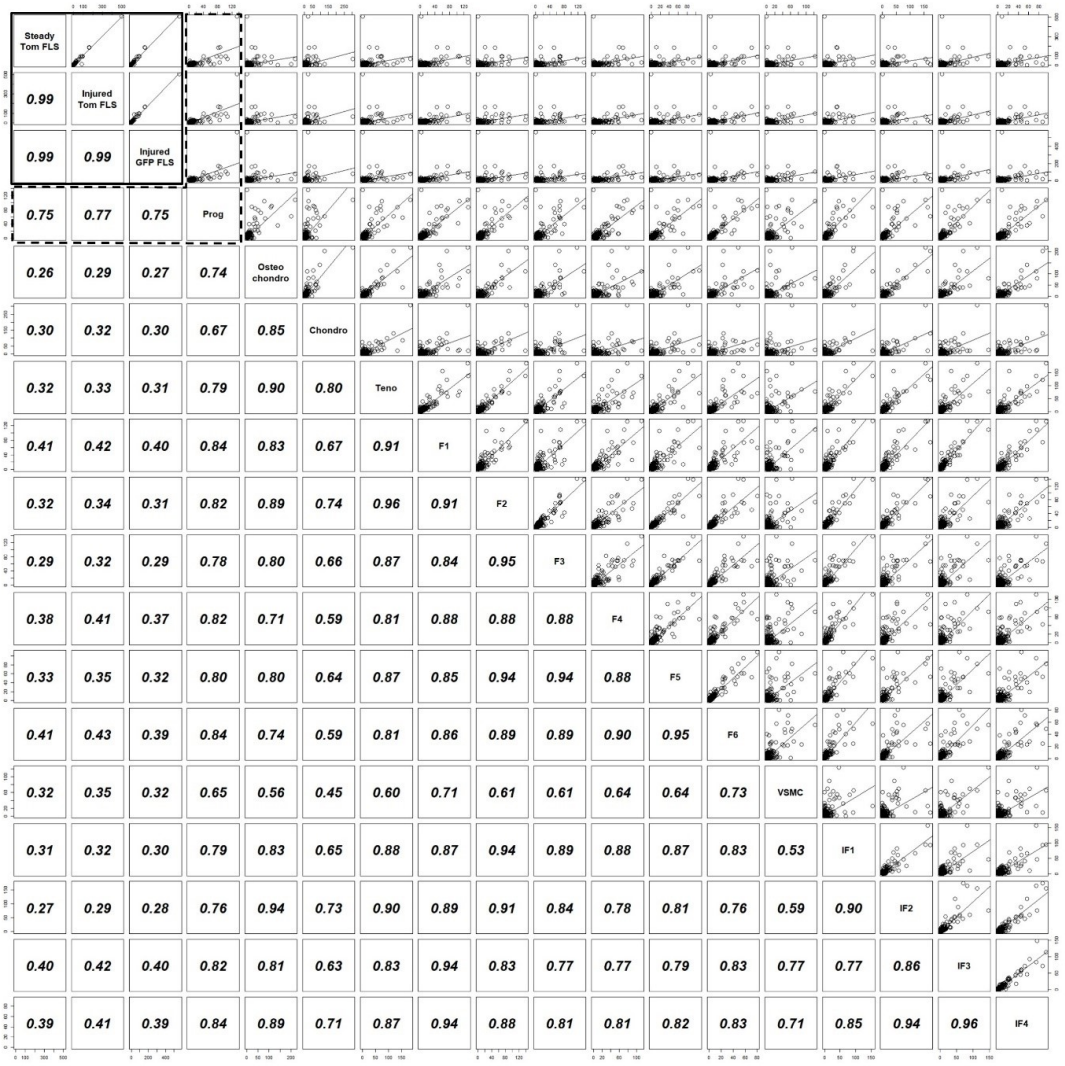

Supplementary Figure 15. Data relating to Figure 3. Pseudo-bulk transcriptome comparisons between FLS and *Prg4*+ progenitors. Average gene expression levels were calculated for the steady-state and injured-state Tom+ and Tom-GFP+ FLS and all cells within each identified integrated cell cluster. Solid black outline indicates comparisons between the steady-state and injured-state Tom+ and Tom-GFP+ FLS. Dotted black outline indicates comparison between the FLS and *Prg4*+ progenitors. FLS: Fibroblast-like synoviocytes; Prog: *Prg4*+ Progenitors; Osteo: Osteochondral-lineage cells; Chondro: Chondrocyte-lineage cells; Teno: Tenocyte-lineage cells; F: Fibroblasts; IF: Injury-induced fibroblasts; VSMC: Vascular smooth muscle cells.

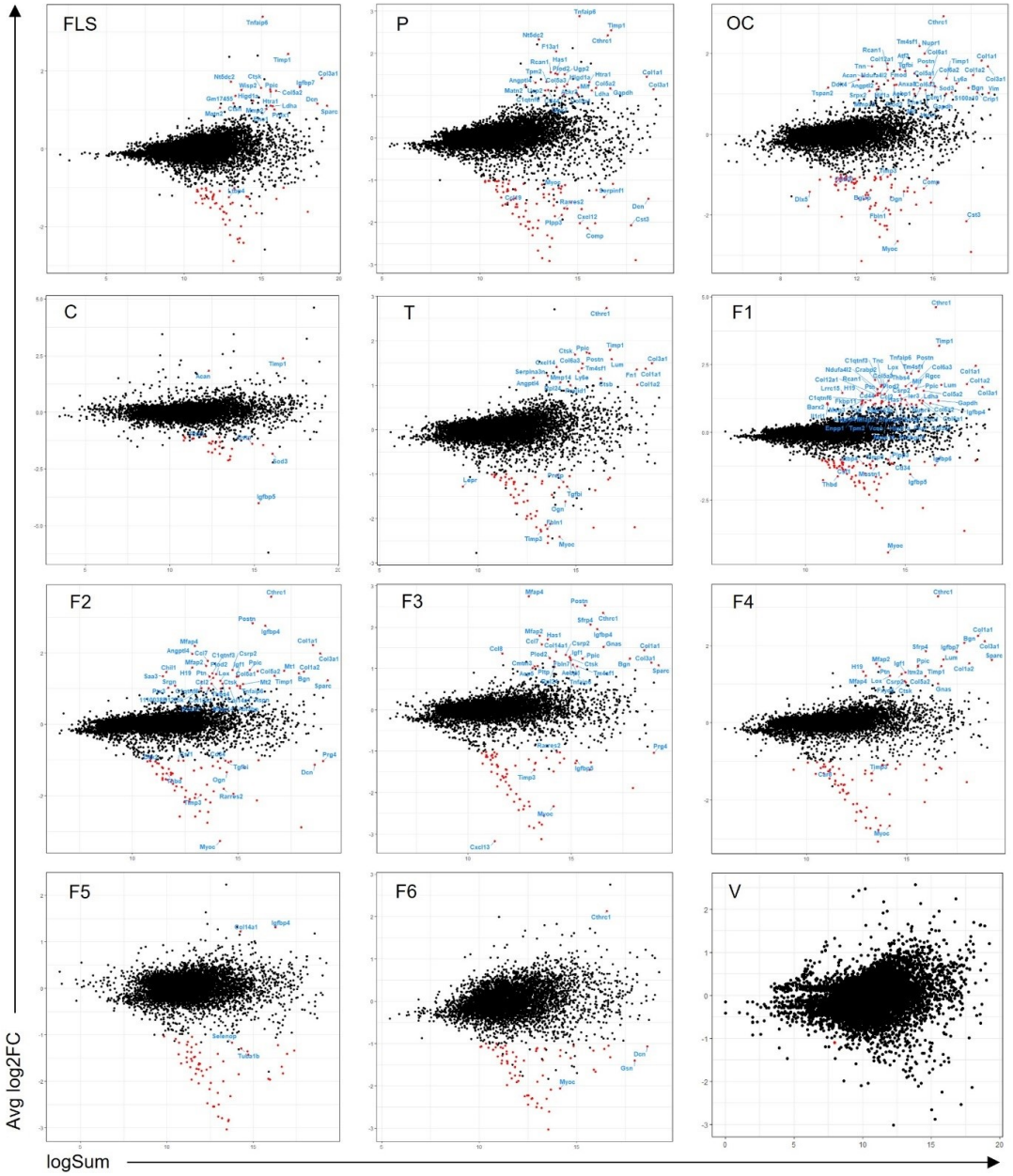

Supplementary Figure 16. Data relating to Figure 3. Transcriptomic changes between steady-state and injured-state cells within identified clusters. MA plots showing differentially expressed genes (log2FC > / < 1 and p<0.01; red points) following injury in each of the shared clusters**.** Significantly upregulated and selected downregulated genes are labelled. Majority of downregulated genes were predicted genes or pseudogenes (not shown). FLS: Fibroblast-like synoviocytes; P: *Prg4*+ Progenitors; OC: Osteochondral-lineage cells; C: Chondrocyte-lineage cells; T: Tenocyte-lineage cells; F: Fibroblasts; V: Vascular smooth muscle cells.

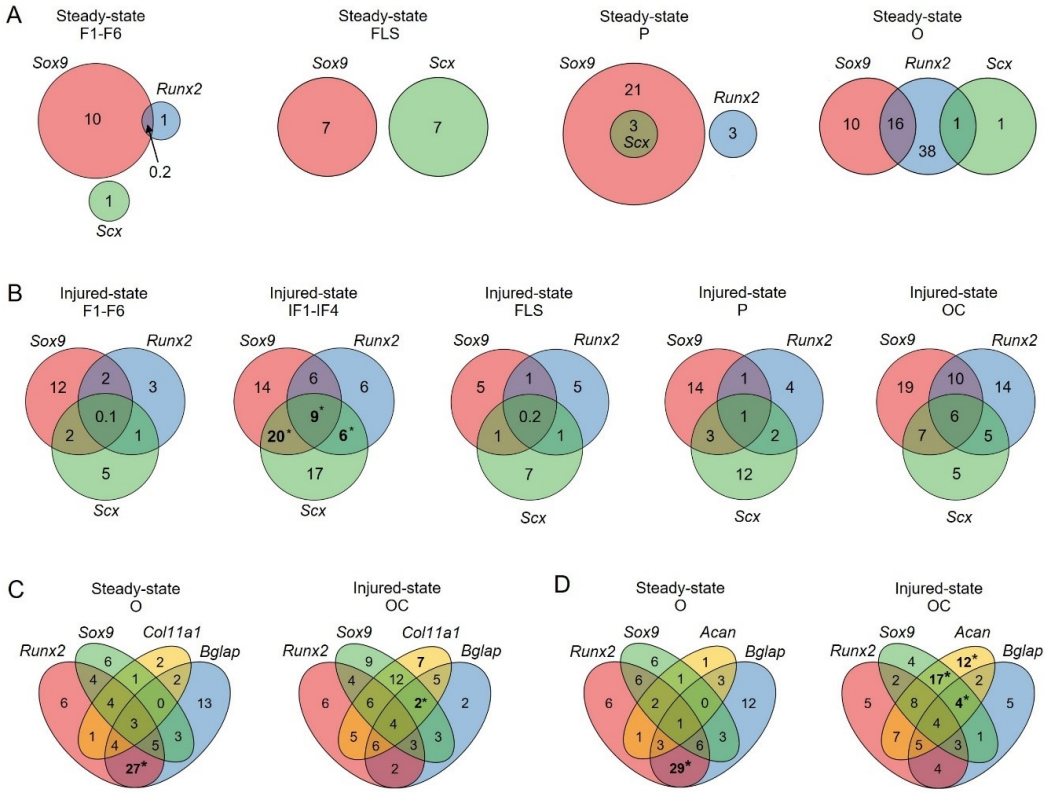

Supplementary Figure 17. Extended data Figure 3G. Venn diagrams showing the percentage of (**A**) steady-state cells and (**B**) injured-state cells within indicated clusters that express / co-express the skeletal lineage-specifying transcription factors *Sox9*, *Runx2* and *Scx*. *=FDR <0.05 between injured state F1-F6 and injured state IF1-IF4, negative binomial generalized linear model with Benjamini-Hochberg post-test. (**C,D**) Venn diagrams showing the percentage of osteochondral cells that express / co-express the genes (**C**) *Runx2*, *Sox9*, *Col11a1* and *Bglap* or (**D**) *Runx2*, *Sox9*, *Acan* and *Bglap* in steady-state and after injury. *=FDR <0.05 between steady-state O cluster and injured-state OC cluster, negative binomial generalized linear model with Benjamini-Hochberg post-test. FLS: Fibroblast-like synoviocytes; P: *Prg4*+ Progenitors; O: Osteoblast-lineage cells; OC: Osteochondral-lineage cells; F: Fibroblasts; IF: Injury-induced fibroblasts.

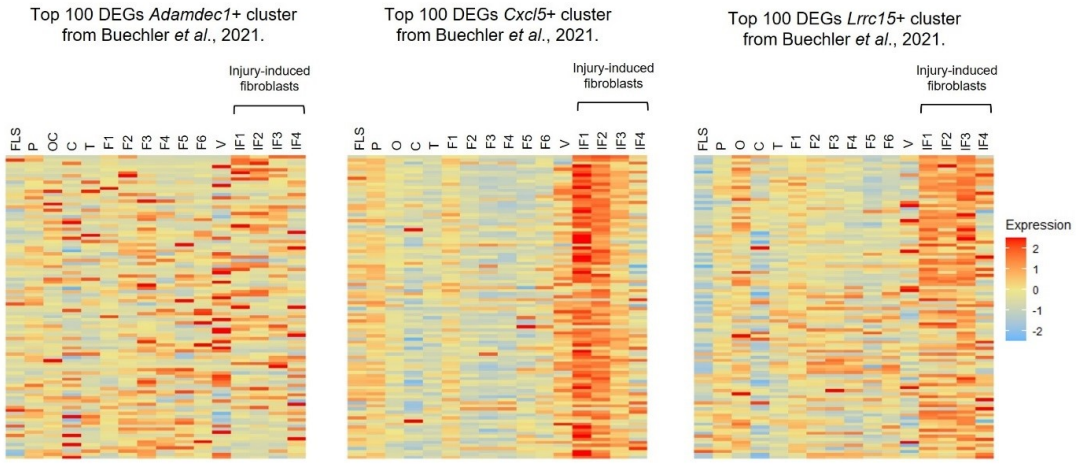

Supplementary Figure 18. Comparison of injury-induced fibroblast phenotype to previously identified perturbed fibroblast populations. Heatmaps showing expression of the top 100 DEGs of the *Adamdec1+*, *Cxcl5+* and *Lrrc15+* perturbed fibroblast populations identified by Buechler *et al*.[26] in the steady-state and injured-state integrated dataset. FLS: Fibroblast-like synoviocytes; P: *Prg4+* Progenitors; OC; Osteochondral-lineage cells; C: Chondrocyte-lineage cells; T: Tenocyte-lineage cells; F: Fibroblasts; IF: Injury-induced fibroblasts; V: Vascular smooth muscle cells.

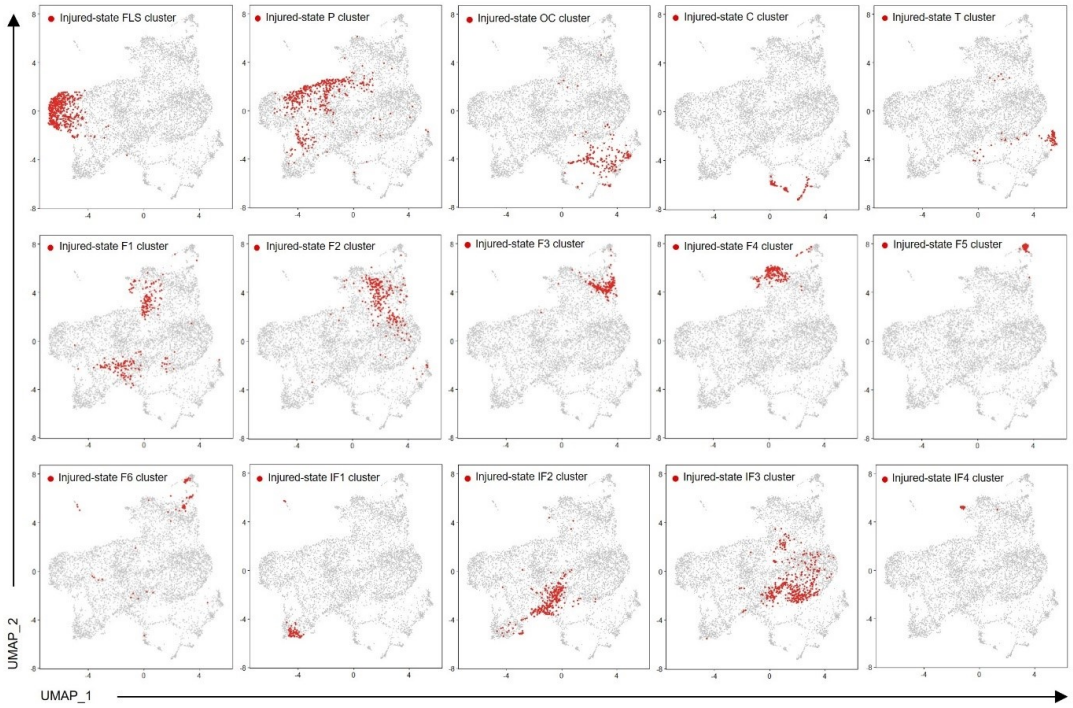

Supplementary Figure 19. Extended data Figure 4A. UMAP plots showing in red the location of injured-state clusters (Fig. 3) mapped onto the integrated injured-state and STIA dataset. FLS: Fibroblast-like synoviocytes; P: *Prg4*+ Progenitors; OC: Osteochondral-lineage cells; C: Chondrocyte-lineage cells; T: Tenocyte-lineage cells; F: Fibroblasts; IF: Injury-induced fibroblasts.

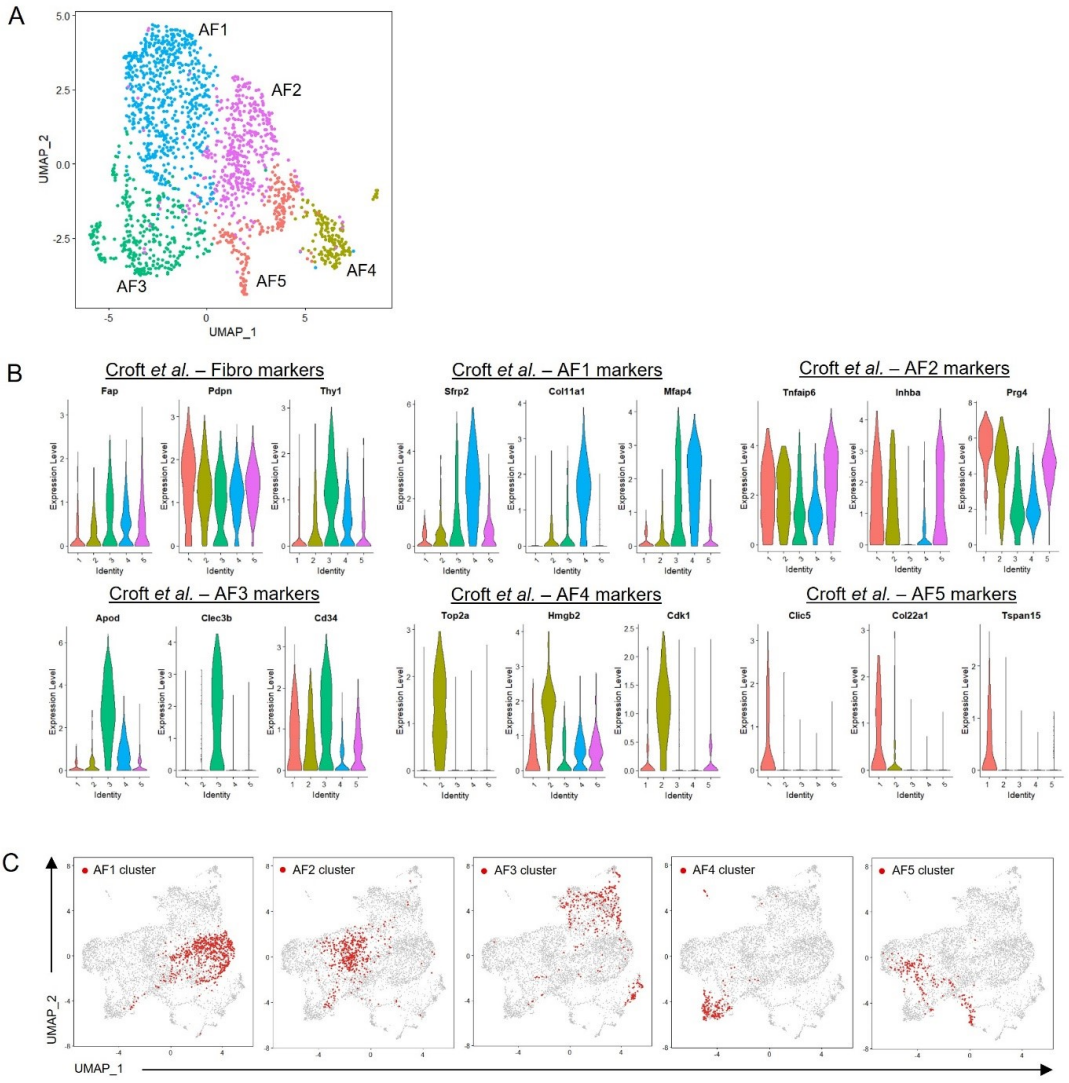

Supplementary Figure 20. Extended data Figure 4A. Identification of clusters in the STIA dataset. The serum transfer induced arthritis (STIA) scRNA-seq dataset was obtained from NCBI GEO GSE129087.[18] Data underwent QC, was down-sampled to consist of 1,725 cells and (**A**) clustered in an unbiased manner at a resolution that provided the same number of clusters as in the paper by Croft *et al*. [18]. (**B**) Clusters were annotated based upon the markers identified by Croft *et al*. [18] and (**C**) mapped, in red, onto the integrated injured-state and STIA dataset.

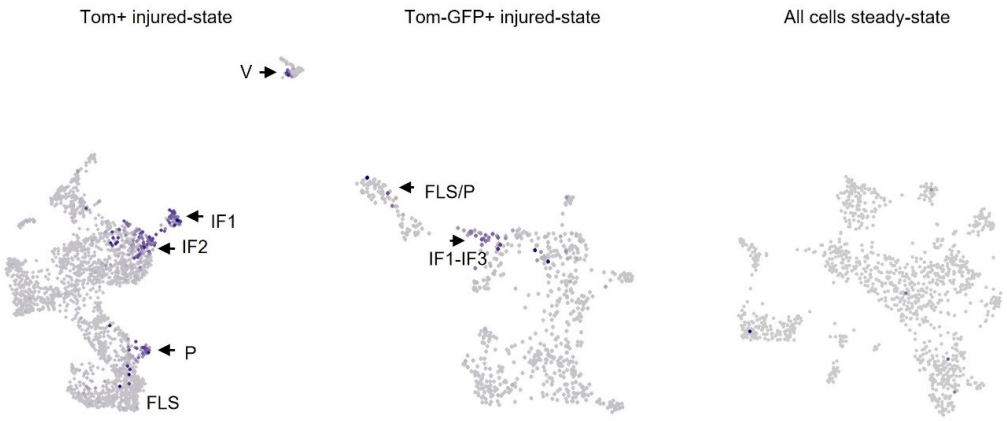

Supplementary Figure 21. Extended data Figure 5C. UMAP plots of cell cycle module score based on expression of *Mki67*, *Ccna2*, *Ccnb1*, *Ccnb2* and *Cdk1* for injured-state Tom+ cells, injured-state Tom-GFP+ cells, and steady-state Tom+ and Tom-GFP+ cells. Arrows indicate proliferating cell populations. FLS: Fibroblast-like synoviocytes; P: *Prg4*+ progenitors; IF: injury-induced fibroblasts. V: Vascular smooth muscle cells.

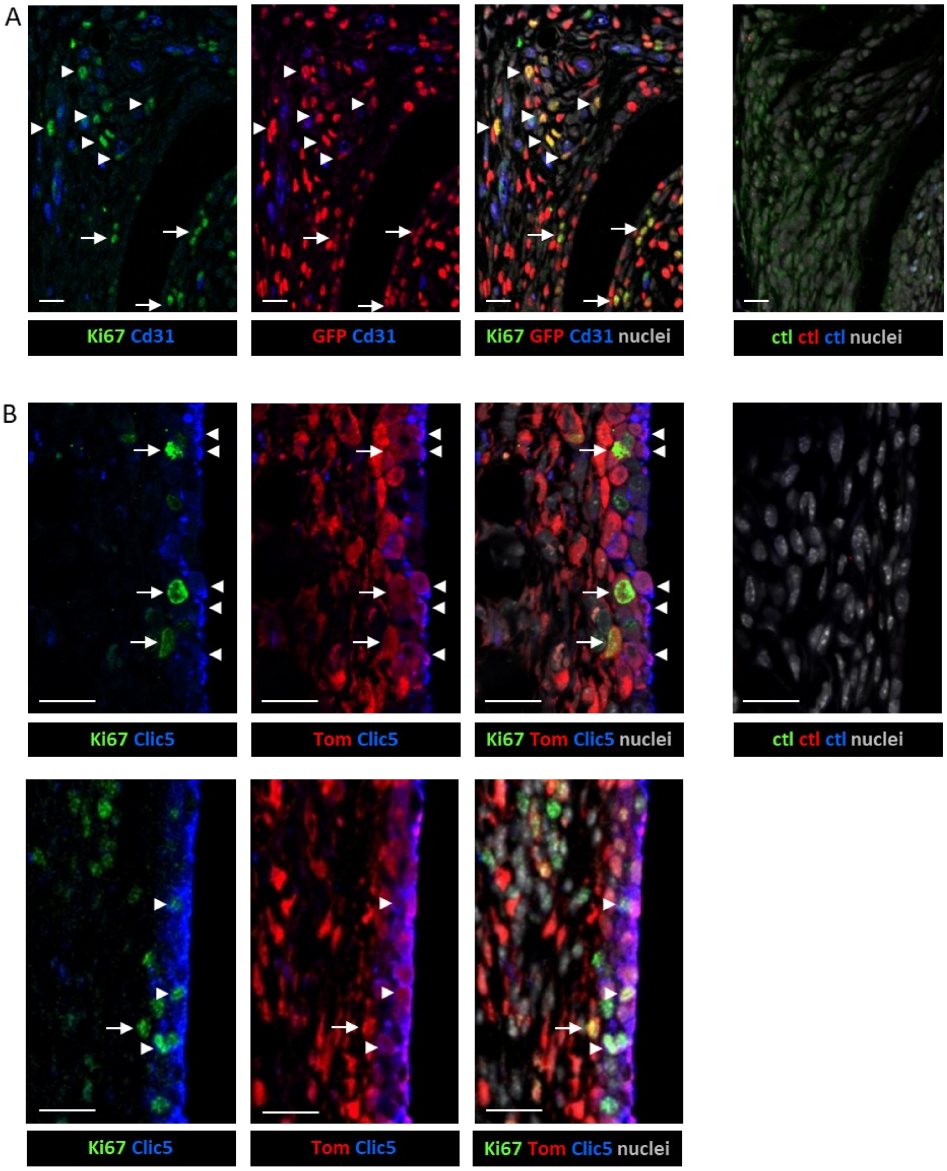

Supplementary Figure 22. Extended data Figure 5D,E. Immunofluorescence staining in *Gdf5-Cre*;*Tom;Pdgfrα-H2BGFP* mouse synovium 6 days after injury to locate proliferating fibroblasts. (**A**) Ki67+ and GFP+ proliferating fibroblasts in synovial lining (arrows), and near Cd31+ blood vessels in synovial sub-lining (arrowheads). The same microscopy image is shown from left to right with different fluorescence channels visualised as indicated. Tissue section stained with isotype negative control antibodies is shown on the right. Single-stained tissue sections served as additional controls (not shown). (**B**) Top: Ki67+Tom+Clic5- proliferating fibroblasts in synovial lining (arrows), adjacent to Clic5+Tom+ FLS (arrowheads). Bottom: Proliferating Ki67+Tom+Clic5- synovial lining fibroblast (arrow) and Ki67+Tom+Clic5+ FLS (arrowheads) in synovial lining. The same microscopy image is shown from left to right with different fluorescence channels visualised as indicated. Tissue section stained with isotype negative control antibodies is shown on the right. Single-stained tissue sections served as additional controls (not shown). All scale bars: 20 µm.

Supplementary Figure 23. Extended data Figure 6B. Analysis of regulon activity associated with *Thy1*+ fibroblast and FLS in separated (**A**) steady-state and (**B**) injured-state datasets. FLS: Fibroblast-like synoviocytes; P: *Prg4*+ progenitors; O: Osteoblast-lineage cells; OC: Osteochondral-lineage cells; C: Chondrocyte-lineage cells; T: Tenocyte-lineage cells; F: Fibroblasts; IF: Injury-induced fibroblasts; V: Vascular smooth muscle cells.

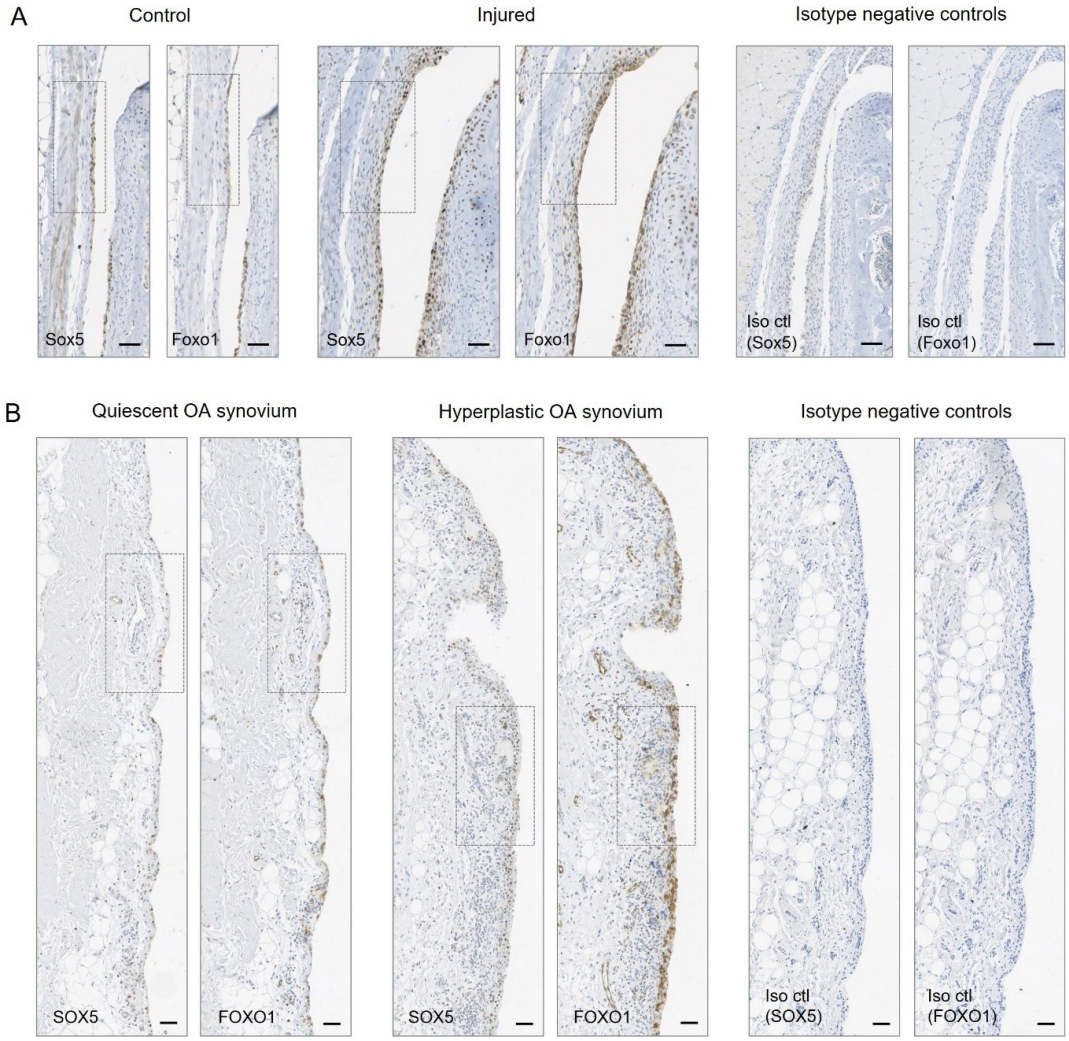

Supplementary Figure 24. Extended data Figure 6D,G. Detection of Sox5 and Foxo1 in mouse and human synovium. (**A**) Immunohistochemical detection of Sox5 and Foxo1 in synovium in near-consecutive tissue sections of 11-to-13-week-old mice 7 days post-injury (n=5) showing expression in synovial lining in control (unoperated contralateral control knee) and injured knees. Boxed areas indicate region shown in Fig. 6D. Iso ctl: sections stained with isotype negative control antibody. Scale bars: 50 µm. (**B**) Immunohistochemical detection of SOX5 and FOXO1 in near-consecutive tissue sections of human OA synovium obtained at arthroplasty (n=6), showing expression in quiescent and hyperplastic areas of synovial lining. Boxed areas indicate region shown in Fig. 6G. Scale bars: 20 µm.

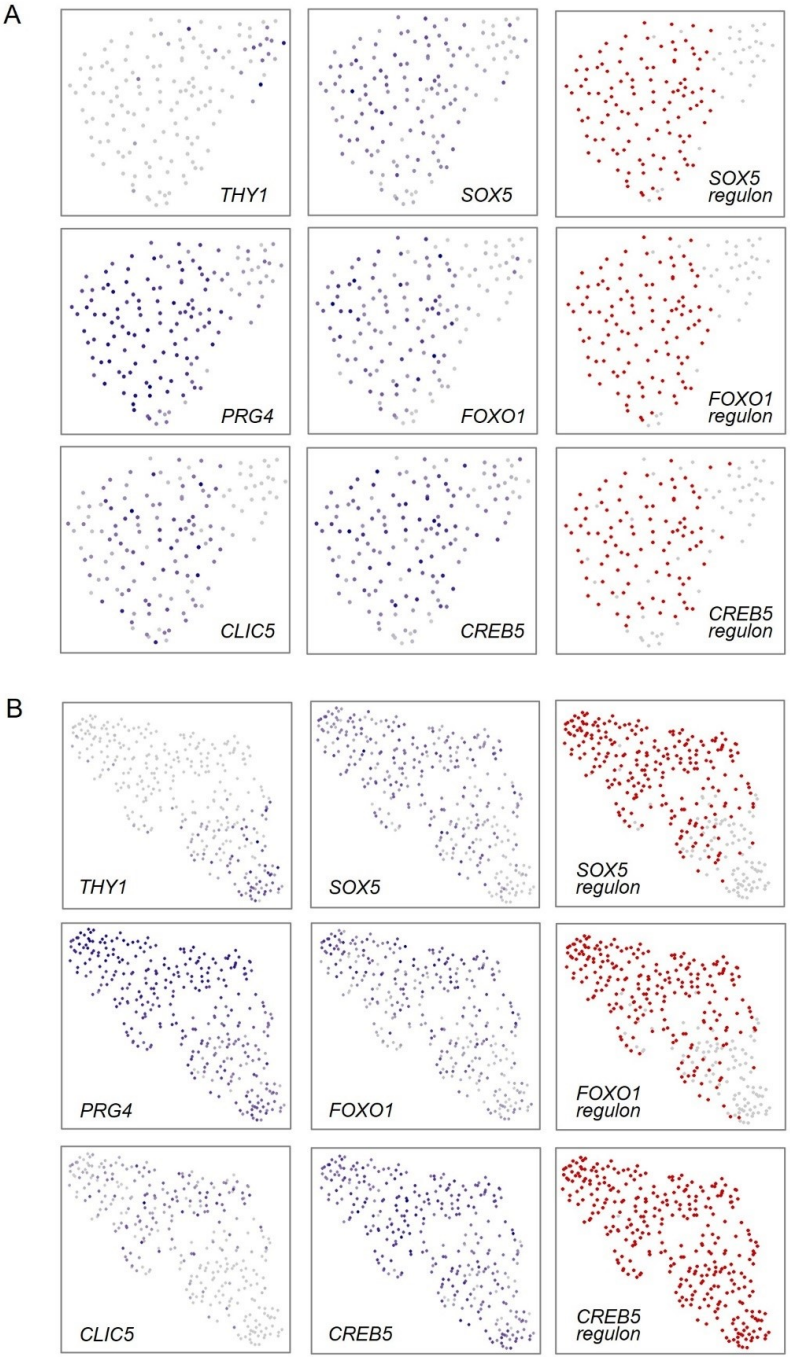

Supplementary Figure 25. Extended data Figure 6F. Identification of FLS regulon activity in additional human OA synovial cell datasets. UMAP plots showing expression of marker genes, transcription factors and FLS regulon activity in human OA scRNA-seq datasets from (**A**) Mizoguchi *et al*. (n=2 patients)[20] and (**B**) Zhang *et al*. (n = 3 patients).[21]

Supplementary Table 1. OA patient information

Patient	Age	Sex	Joint
1	65	M	Knee
2	81	M	Knee
3	65	F	Knee
4	79	F	Knee
5	68	F	Knee
6	65	F	Knee

Supplementary Table 2. Antibodies for immunohistochemistry and immunofluorescence staining

Antibody	Clone	Manufacturer	Cat. No.	Conjugation
mCherry (Tom)	Polyclonal	Sicgen Antibodies	AB0081-200	Unconjugated
GFP	Polyclonal	Abcam	ab13970	Unconjugated
Sox5	Polyclonal	Abcam	Ab94396	Unconjugated
Clic5	Polyclonal	Novus Biologicals (Bio-techne)	NBP1-80075	Unconjugated
Sox9	EPR14335-78	Abcam	ab185966	Unconjugated
Runx2	EPR14334	Abcam	ab192256	Unconjugated
Foxo1	C29H4	Cell Signalling	2880	Unconjuagted
Cd31	EPR17259	Abcam	ab182981	Unconjugated
Ki-67	Monoclonal	eBioscience	14-5698-82	Unconjugated
Rabbit IgG isotype control	Polyclonal	Abcam	ab37415	Unconjugated
Normal Rabbit IgG control	Polyclonal	R&D Systems (Bio-techne)	AB-105-C	Unconjugated
Normal Chicken IgY control	Polyclonal	R&D Systems (Bio-techne)	AB-101-C	Unconjugated
Normal Goat IgG control	Polyclonal	R&D Systems (Bio-techne)	AB-108-C	Unconjugated
Rabbit IgG XP® isotype control	DA1E	Cell Signaling Technology	3900	Unconjugated
Rat IgG1 isotype control	43414	R&D Systems (Bio-techne)	MAB005	Unconjugated
Goat anti-rabbit IgG (H&L)	Polyclonal	Vector Laboratories	BA-1000	Biotinylated
Horse anti-rabbit IgG (H&L)	Polyclonal	Vector Laboratories	BA-1100	Biotinylated
Streptavidin	1C2	Novus Biologicals (Bio-techne)	NBP1-04345B	Biotinylated
Donkey anti-rabbit IgG (H&L)	Polyclonal	Abcam	ab150065	Alexa Fluor®488
Donkey anti-goat IgG (H&L)	Polyclonal	Abcam	ab15029	Alexa Fluor®488
Goat anti-chicken IgY (H&L)	Polyclonal	Abcam	ab150173	Alexa Fluor®488
Donkey anti-goat IgG (H&L)	Polyclonal	Abcam	ab150136	Alexa Fluor®594
Donkey anti-rat IgG (H&L)	Polyclonal	Abcam	ab150156	Alexa Fluor®594
Donkey anti-rabbit IgG (H&L)	Polyclonal	Abcam	ab150067	Alexa Fluor®647

Supplementary Table 3. Antibodies for flow cytometry

Antibody	Clone	Manufacturer	Cat. No.	Conjugation
Cd55	RIKO-3	Biolegend	131806	Alexa Fluor®647
Cd49f (Itga6)	eBioGoH3	eBioscience	47-0495-82	APCef780
Cd90 (Thy1)	OX-7	BD Biosciences	563770	BV421

Supplementary Table 4. Samples analysed by scRNA-seq in this study.

Sample	Mouse	Cells	Condition	Cell number pre-QC	Cell number post-QC
1	1	Tom+	Steady state	333	297
2	2	Tom+	Steady state	547	489
3	2	Tom-GFP+	Steady state	394	376
4	3	Tom+	Injury	760	700
5	4	Tom+	Injury	848	752
6	5	Tom+	Injury	546	443
7	5	Tom-GFP+	Injury	539	434
8	6	Tom+	Injury	664	488
9	6	Tom-GFP+	Injury	339	217

Supplementary Table 5. Top 10 DEGs for each cluster in steady state.

Cluster	Gene	p_val	avg_log2FC	pct.1	pct.2	p_val_adj
FLS	F13a1	5.74E-171	2.888714	0.906	0.01	1.10E-166
FLS	Col22a1	3.79E-166	2.335707	0.75	0.003	7.26E-162
FLS	Clic5	3.34E-136	3.467433	0.875	0.016	6.39E-132
FLS	Gchfr	6.46E-104	1.111849	0.562	0.006	1.24E-99
FLS	Tspan15	4.99E-103	2.685473	0.875	0.03	9.56E-99
FLS	Tmem196	1.64E-102	0.800652	0.5	0.003	3.14E-98
FLS	Dlx3	9.02E-86	1.181168	0.781	0.028	1.73E-81
FLS	Itga6	2.17E-73	1.630272	0.781	0.038	4.15E-69
FLS	Fut9	6.10E-67	0.360444	0.312	0.002	1.17E-62
FLS	Rab37	1.91E-65	0.504096	0.281	0.001	3.66E-61

Cluster	Gene	p_val	avg_log2FC	pct.1	pct.2	p_val_adj
Osteo	Ibsp	3.31E-149	4.065684	0.773	0.028	6.33E-145
Osteo	Cdh11	2.08E-118	1.969991	0.773	0.062	3.98E-114
Osteo	Bglap	4.31E-106	4.935723	0.582	0.025	8.25E-102
Osteo	Fgfr2	5.61E-106	1.693455	0.738	0.065	1.07E-101
Osteo	Bglap2	3.66E-102	5.147283	0.582	0.028	7.00E-98
Osteo	Tnc	3.70E-101	2.352153	0.688	0.056	7.09E-97
Osteo	Runx2	1.03E-100	1.258095	0.546	0.021	1.97E-96
Osteo	Alpl	1.33E-98	2.982731	0.73	0.078	2.55E-94
Osteo	Cd200	3.62E-89	2.454558	0.872	0.182	6.94E-85
Osteo	Sp7	1.36E-75	1.152935	0.369	0.008	2.61E-71

Cluster	Gene	p_val	avg_log2FC	pct.1	pct.2	p_val_adj
Chondro	Meltf	1.85E-175	2.485438	0.795	0.005	3.53E-171
Chondro	Ppp1r1b	2.46E-169	1.956606	0.659	0	4.71E-165
Chondro	Mall	3.16E-159	1.639586	0.682	0.003	6.05E-155
Chondro	Hapln1	7.53E-150	2.635117	0.818	0.013	1.44E-145
Chondro	Ucma	4.61E-129	2.381635	0.545	0.002	8.84E-125
Chondro	Cytl1	2.01E-112	6.938956	0.591	0.008	3.86E-108
Chondro	Gdf6	1.06E-110	1.874056	0.432	0	2.02E-106
Chondro	Clec3a	1.12E-102	3.041147	0.591	0.011	2.15E-98
Chondro	Tspan13	5.37E-99	2.384974	0.75	0.027	1.03E-94
Chondro	Cpm	1.81E-89	1.720738	0.614	0.018	3.47E-85

Cluster	Gene	p_val	avg_log2FC	pct.1	pct.2	p_val_adj
Teno	Angptl7	8.10E-60	3.504045	0.422	0.024	1.55E-55
Teno	Uts2r	2.41E-53	1.093415	0.422	0.028	4.62E-49
Teno	Ccdc3	5.85E-53	1.865815	0.878	0.218	1.12E-48
Teno	Fibin	1.27E-43	2.653455	0.744	0.176	2.43E-39
Teno	Dkk3	4.67E-43	1.400572	0.8	0.207	8.95E-39
Teno	Cilp	6.26E-43	2.189124	0.744	0.169	1.20E-38
Teno	Prelp	3.43E-42	2.548272	0.978	0.753	6.56E-38
Teno	Kera	9.54E-39	2.452145	0.356	0.031	1.83E-34
Teno	Dcn	1.30E-37	1.523629	1	0.978	2.49E-33
Teno	Lox	1.12E-36	1.992322	0.767	0.228	2.15E-32

Cluster	Gene	p_val	avg_log2FC	pct.1	pct.2	p_val_adj
F1	S100a10	3.06E-52	1.428255	1	0.982	5.86E-48
F1	Anxa8	8.15E-47	2.119704	0.756	0.216	1.56E-42
F1	Tspo	5.49E-45	1.226833	0.992	0.885	1.05E-40
F1	Crip1	1.34E-42	1.406402	1	0.993	2.57E-38
F1	Ociad2	6.66E-42	1.149411	0.614	0.139	1.28E-37
F1	Anxa2	3.20E-40	1.20036	1	0.974	6.13E-36
F1	Slurp1	2.59E-37	2.127482	0.417	0.062	4.96E-33
F1	Txn1	5.84E-36	1.095678	1	0.931	1.12E-31
F1	Igfbp6	1.30E-34	1.418252	0.992	0.94	2.49E-30
F1	Crip2	1.03E-33	1.159756	0.992	0.87	1.97E-29

Cluster	Gene	p_val	avg_log2FC	pct.1	pct.2	p_val_adj
F2	Cxcl12	9.18E-57	1.642371	0.961	0.671	1.76E-52
F2	Ctsb	5.90E-45	0.857229	0.989	0.954	1.13E-40
F2	Pcolce	5.59E-43	0.952381	1	0.971	1.07E-38
F2	Gpnmb	1.93E-42	1.163044	0.831	0.422	3.70E-38
F2	Gas6	7.44E-42	0.959344	0.965	0.728	1.42E-37
F2	Dcn	5.56E-40	0.748553	1	0.973	1.07E-35
F2	Serping1	1.06E-38	1.067863	0.972	0.883	2.02E-34
F2	Serpina3n	6.33E-38	1.079861	0.803	0.468	1.21E-33
F2	Rarres2	9.36E-36	0.974022	0.986	0.838	1.79E-31

F2	C4b	3.15E-35	0.999104	0.743	0.343	6.03E-31

Cluster	Gene	p_val	avg_log2FC	pct.1	pct.2	p_val_adj
F3	Cxcl1	4.85E-47	2.556798	0.81	0.251	9.28E-43
F3	Lpl	4.23E-40	1.911208	0.871	0.36	8.09E-36
F3	Dpep1	4.80E-37	1.281209	0.75	0.222	9.20E-33
F3	Ccl11	2.16E-34	1.392893	0.681	0.177	4.15E-30
F3	Acvr2a	5.51E-34	1.046518	0.517	0.118	1.06E-29
F3	Ntrk2	2.89E-31	1.136963	0.802	0.314	5.54E-27
F3	Gsn	3.85E-31	1.135511	1	0.991	7.38E-27
F3	Col4a1	1.08E-30	1.632134	0.836	0.441	2.07E-26
F3	Fst	5.93E-28	1.331829	0.698	0.259	1.14E-23
F3	Bmper	3.56E-27	0.782675	0.543	0.143	6.82E-23

Cluster	Gene	p_val	avg_log2FC	pct.1	pct.2	p_val_adj
F4	Pi16	1.55E-109	4.035385	0.923	0.233	2.96E-105
F4	Car8	5.48E-107	1.89606	0.788	0.118	1.05E-102
F4	Efhd1	1.07E-86	1.603401	0.827	0.218	2.04E-82
F4	Anxa3	6.04E-85	2.043907	0.957	0.385	1.16E-80
F4	Aif1l	1.81E-81	1.181406	0.591	0.075	3.47E-77
F4	Mfap5	2.41E-73	1.773895	1	0.685	4.62E-69
F4	Cd248	8.39E-73	1.644116	0.995	0.561	1.61E-68
F4	Tek	2.15E-72	0.819107	0.5	0.047	4.11E-68
F4	Zyx	7.78E-71	1.524139	0.904	0.392	1.49E-66
F4	Sema3c	1.98E-70	1.717605	0.913	0.439	3.79E-66

Cluster	Gene	p_val	avg_log2FC	pct.1	pct.2	p_val_adj
F5	C7	9.63E-52	1.210175	0.324	0.016	1.84E-47
F5	Abcc9	3.85E-38	0.828005	0.324	0.03	7.38E-34
F5	Fmo2	3.56E-35	1.245506	0.342	0.04	6.82E-31
F5	Rbp1	4.40E-34	1.807167	0.568	0.152	8.43E-30
F5	F3	9.75E-33	2.368749	0.541	0.143	1.87E-28
F5	Kcnj8	3.67E-31	1.216805	0.351	0.05	7.03E-27
F5	Sparcl1	5.07E-24	1.738239	0.631	0.234	9.70E-20
F5	Gdf10	1.56E-21	1.546707	0.559	0.194	2.99E-17
F5	Kitl	4.87E-20	1.395803	0.387	0.104	9.33E-16
F5	Cygb	1.34E-19	1.461814	0.802	0.597	2.56E-15

Cluster	Gene	p_val	avg_log2FC	pct.1	pct.2	p_val_adj
F6	Hsd11b1	9.42E-72	1.727112	0.742	0.033	1.80E-67
F6	Vtn	3.15E-58	1.430101	0.581	0.023	6.04E-54
F6	Aldh1a2	1.30E-42	1.670248	0.484	0.024	2.49E-38
F6	Ret	1.95E-37	0.9342	0.484	0.029	3.73E-33
F6	Atp1a2	5.59E-37	1.142874	0.613	0.049	1.07E-32
F6	Cldn15	1.26E-36	0.74603	0.419	0.021	2.42E-32
F6	Ccl11	1.82E-36	3.358332	1	0.206	3.49E-32

F6	Hmcn2	1.27E-35	2.497802	0.968	0.18	2.43E-31
F6	D630033O11Rik	4.49E-35	1.156915	0.548	0.042	8.60E-31
F6	Prss12	8.49E-34	1.087155	0.452	0.029	1.63E-29

Supplementary Table 6. Top 10 DEGs for identified *Prg4*+progenitor and VSMC clusters in steady state.

Cluster	Gene	p_val	avg_log2FC	pct.1	pct.2	p_val_adj
Progenitor	Megf10	3.15E-22	0.756472	0.438	0.024	6.03E-18
Progenitor	Gm12695	2.45E-19	1.138587	0.5	0.038	4.69E-15
Progenitor	Enpp5	1.54E-18	0.767496	0.562	0.05	2.96E-14
Progenitor	Rspo2	9.32E-18	1.405092	0.625	0.064	1.78E-13
Progenitor	Cdkn2c	7.49E-15	0.917494	0.625	0.08	1.43E-10
Progenitor	Pla1a	2.35E-12	1.411035	0.75	0.143	4.51E-08
Progenitor	Marcksl1	7.55E-12	0.730894	0.5	0.062	1.45E-07
Progenitor	Sparcl1	9.54E-11	1.6785	0.938	0.262	1.83E-06
Progenitor	Nat8f1	1.37E-10	0.557503	0.438	0.055	2.62E-06
Progenitor	Pi15	8.59E-10	1.155656	0.812	0.208	1.64E-05

Cluster	Gene	p_val	avg_log2FC	pct.1	pct.2	p_val_adj
VSMCs	Gja4	4.82E-173	2.780155	0.667	0	9.22E-169
VSMCs	Tinagl1	1.30E-148	3.658437	0.667	0.001	2.48E-144
VSMCs	Kcnk3	8.00E-116	1.23995	0.444	0	1.53E-111
VSMCs	Rasgrp2	1.66E-104	1.910893	0.667	0.003	3.18E-100
VSMCs	Mcam	1.30E-103	1.512162	0.556	0.002	2.49E-99
VSMCs	Gucy1b1	3.11E-95	1.689412	0.667	0.004	5.95E-91
VSMCs	Myh11	6.25E-93	3.266787	0.444	0.001	1.20E-88
VSMCs	Timp4	2.88E-87	1.614912	0.333	0	5.51E-83
VSMCs	Nrip2	2.88E-87	1.452769	0.333	0	5.51E-83
VSMCs	Higd1b	2.88E-87	1.359717	0.333	0	5.51E-83

Supplementary Table 7. Top 10 DEGs for each cluster in integrated steady state and injured state.

Cluster	Gene	p_val	avg_log2FC	pct.1	pct.2	p_val_adj
FLS	Prg4	0	4.192193	1	0.423	0
FLS	Hbegf	0	4.118061	0.979	0.204	0
FLS	Rgcc	0	3.800575	0.992	0.352	0
FLS	F13a1	0	3.260149	0.988	0.094	0
FLS	Htra4	0	3.258303	0.985	0.215	0
FLS	Clic5	0	3.141345	0.973	0.041	0
FLS	Col22a1	0	2.66492	0.975	0.073	0
FLS	Cystm1	0	2.427589	0.927	0.077	0
FLS	Tspan15	0	2.312283	0.967	0.068	0
FLS	Pla1a	0	2.094637	0.934	0.177	0

Cluster	Gene	p_val	avg_log2FC	pct.1	pct.2	p_val_adj
Prog	Rspo2	9.41E-115	1.428591	0.724	0.269	1.80E-110
Prog	Nt5dc2	4.44E-94	1.470391	0.769	0.373	8.51E-90
Prog	Pla1a	2.10E-88	1.094779	0.656	0.222	4.01E-84
Prog	Tmem98	9.55E-84	0.79461	0.835	0.475	1.83E-79
Prog	Htra1	2.60E-83	0.96994	0.989	0.911	4.97E-79
Prog	Fn1	1.21E-79	0.974708	1	0.937	2.31E-75
Prog	Ctsb	2.51E-78	0.892483	0.998	0.976	4.80E-74
Prog	Htra4	7.22E-77	0.767449	0.697	0.261	1.38E-72
Prog	Ucp2	1.26E-75	0.935846	0.893	0.552	2.42E-71
Prog	Fbln7	3.06E-75	1.053359	0.947	0.614	5.87E-71

Cluster	Gene	p_val	avg_log2FC	pct.1	pct.2	p_val_adj
Osteochondro	Alpl	6.41E-266	2.46898	0.578	0.037	1.23E-261
Osteochondro	Mmp13	3.25E-260	3.963802	0.559	0.037	6.23E-256
Osteochondro	Fgfr2	2.27E-227	1.44952	0.638	0.07	4.34E-223
Osteochondro	Fmod	3.39E-174	2.439113	0.762	0.15	6.49E-170
Osteochondro	Cd200	3.76E-171	2.072584	0.708	0.138	7.20E-167
Osteochondro	Sp7	9.16E-170	0.823941	0.305	0.012	1.76E-165
Osteochondro	Cdh11	6.05E-162	1.579114	0.759	0.181	1.16E-157
Osteochondro	Ptprd	5.49E-144	1.140735	0.565	0.094	1.05E-139
Osteochondro	Galr2	2.15E-118	0.640802	0.302	0.024	4.11E-114
Osteochondro	1500015O10Rik	7.37E-118	1.860415	0.898	0.382	1.41E-113

Cluster	Gene	p_val	avg_log2FC	pct.1	pct.2	p_val_adj
Chondro	Col2a1	0	6.228617	0.658	0.009	0
Chondro	Snorc	0	4.390878	0.467	0.001	0
Chondro	Clec3a	0	3.836799	0.592	0.004	0
Chondro	Col11a2	0	3.195569	0.592	0.013	0
Chondro	Ucma	0	2.236359	0.525	0.003	0
Chondro	Meltf	0	2.1324	0.592	0.003	0
Chondro	Ppp1r1b	0	1.53759	0.575	0.001	0

Chondro	Cytl1	5.77E-307	6.400734	0.45	0.004	1.10E-302
Chondro	Col9a3	4.71E-303	3.295872	0.475	0.006	9.02E-299
Chondro	Col9a2	4.92E-291	2.698601	0.442	0.005	9.42E-287

Cluster	**Gene**	**p_val**	**avg_log2FC**	**pct.1**	**pct.2**	**p_val_adj**
Teno	Uts2r	1.76E-128	1.244781	0.485	0.042	3.37E-124
Teno	Cilp2	2.20E-126	1.519471	0.455	0.036	4.22E-122
Teno	Angptl7	2.49E-118	2.84857	0.257	0.009	4.77E-114
Teno	Comp	1.57E-77	2.504709	0.988	0.505	3.01E-73
Teno	Crispld2	6.42E-75	1.453325	0.844	0.263	1.23E-70
Teno	Ackr4	2.79E-74	0.706745	0.365	0.042	5.34E-70
Teno	Prelp	3.71E-74	2.416738	0.976	0.631	7.11E-70
Teno	Dcn	2.79E-70	1.942693	1	0.973	5.34E-66
Teno	Kera	2.17E-67	2.468773	0.509	0.098	4.16E-63
Teno	Vipr2	4.71E-65	0.567463	0.335	0.041	9.03E-61

Cluster	**Gene**	**p_val**	**avg_log2FC**	**pct.1**	**pct.2**	**p_val_adj**
F1	S100a10	3.53E-117	1.193676	1	0.986	6.75E-113
F1	Igfbp6	1.22E-94	1.59357	1	0.895	2.33E-90
F1	Anxa8	5.93E-83	1.475672	0.844	0.436	1.14E-78
F1	Crip1	6.88E-82	1.10051	1	0.987	1.32E-77
F1	Tspo	2.04E-80	0.97059	0.986	0.903	3.90E-76
F1	Emp1	1.95E-78	0.960788	0.992	0.871	3.73E-74
F1	Tmsb4x	2.85E-77	0.940177	0.997	0.969	5.45E-73
F1	Tppp3	1.57E-72	1.205264	0.97	0.71	3.01E-68
F1	Prelp	2.07E-72	1.148166	0.953	0.615	3.97E-68
F1	Anxa2	1.63E-71	0.946931	0.997	0.981	3.12E-67

Cluster	**Gene**	**p_val**	**avg_log2FC**	**pct.1**	**pct.2**	**p_val_adj**
F2	Gas6	5.56E-152	1.659649	0.976	0.601	1.06E-147
F2	Apod	1.37E-149	2.091537	0.936	0.407	2.63E-145
F2	Serping1	6.03E-137	1.68314	0.996	0.707	1.15E-132
F2	C3	1.90E-125	1.413437	0.919	0.385	3.63E-121
F2	C4b	5.30E-125	1.364737	0.838	0.327	1.01E-120
F2	Igf1	1.88E-120	1.745494	0.947	0.543	3.60E-116
F2	Cxcl12	9.24E-113	1.821489	0.974	0.654	1.77E-108
F2	C1s1	1.47E-105	1.061509	0.934	0.522	2.82E-101
F2	Cfb	7.50E-105	1.212355	0.746	0.289	1.44E-100
F2	Mgst1	1.39E-104	1.060967	0.934	0.502	2.66E-100

Cluster	**Gene**	**p_val**	**avg_log2FC**	**pct.1**	**pct.2**	**p_val_adj**
F3	Ntrk2	2.05E-161	1.300263	0.768	0.153	3.92E-157
F3	C3	2.63E-142	2.166307	0.971	0.402	5.03E-138
F3	C4b	1.36E-135	1.958287	0.912	0.341	2.60E-131
F3	Gm2564	2.16E-134	1.695882	0.758	0.174	4.14E-130
F3	Ccl19	1.50E-128	1.345777	0.69	0.143	2.88E-124

F3	Entpd2	9.31E-128	1.675424	0.908	0.339	1.78E-123
F3	Apod	1.04E-118	2.003309	0.958	0.426	1.99E-114
F3	Dpep1	2.18E-117	1.22852	0.569	0.106	4.18E-113
F3	Icam1	2.09E-109	1.316798	0.706	0.208	3.99E-105
F3	Ccl11	1.14E-104	1.511605	0.507	0.089	2.18E-100

Cluster	Gene	p_val	avg_log2FC	pct.1	pct.2	p_val_adj
F4	Pi16	0	4.214291	0.915	0.15	0
F4	Efhd1	1.81E-246	1.552535	0.74	0.106	3.47E-242
F4	Tek	4.25E-227	0.781211	0.462	0.029	8.13E-223
F4	Scara5	2.34E-191	1.726887	0.904	0.262	4.49E-187
F4	1700019D03Rik	3.12E-177	1.446628	0.858	0.249	5.98E-173
F4	Dpp4	9.11E-168	0.90987	0.555	0.079	1.74E-163
F4	Cadm3	1.42E-164	1.510233	0.883	0.278	2.71E-160
F4	Cd34	4.21E-164	1.879422	0.997	0.616	8.06E-160
F4	Cd248	1.60E-162	1.828725	0.992	0.642	3.06E-158
F4	Zfp385a	2.68E-159	1.504881	0.803	0.246	5.13E-155

Cluster	Gene	p_val	avg_log2FC	pct.1	pct.2	p_val_adj
F5	C7	0	2.170172	0.66	0.008	0
F5	Abcc9	2.84E-187	1.41048	0.67	0.037	5.43E-183
F5	Gdf10	5.75E-150	3.003916	0.962	0.127	1.10E-145
F5	Fmo2	1.01E-142	1.706508	0.594	0.041	1.94E-138
F5	F3	7.08E-126	3.102675	0.849	0.121	1.36E-121
F5	Kcnj8	4.94E-125	1.680578	0.585	0.045	9.47E-121
F5	Inmt	1.32E-113	1.143862	0.283	0.009	2.52E-109
F5	C2	3.94E-87	1.428263	0.575	0.068	7.54E-83
F5	Rbp1	6.68E-84	2.321247	0.896	0.223	1.28E-79
F5	Atp1a2	1.95E-73	0.690957	0.33	0.023	3.73E-69

Cluster	Gene	p_val	avg_log2FC	pct.1	pct.2	p_val_adj
F6	Ccl11	2.23E-44	2.532614	0.446	0.107	4.27E-40
F6	Abca8a	5.85E-40	1.348558	0.497	0.146	1.12E-35
F6	Hmcn2	5.34E-36	1.667374	0.414	0.113	1.02E-31
F6	Gsn	1.23E-32	1.593795	0.955	0.979	2.35E-28
F6	Myoc	1.86E-25	1.496215	0.522	0.195	3.57E-21
F6	Dpep1	2.79E-23	1.314804	0.382	0.13	5.34E-19
F6	AW112010	8.19E-23	0.991697	0.261	0.064	1.57E-18
F6	Ltbp4	1.13E-22	1.712527	0.713	0.574	2.16E-18
F6	Entpd2	1.57E-20	1.267053	0.624	0.371	3.01E-16
F6	Tmem204	7.97E-20	0.686135	0.255	0.067	1.53E-15

Cluster	Gene	p_val	avg_log2FC	pct.1	pct.2	p_val_adj
VSMC	Fabp4	0	5.027236	0.821	0.023	0
VSMC	Tinagl1	0	3.119222	0.917	0.005	0
VSMC	Notch3	0	2.438523	0.881	0.024	0

VSMC	Gja4	0	2.332056	0.75	0.002	0
VSMC	Esam	0	2.312816	0.905	0.004	0
VSMC	Myh11	0	2.242495	0.667	0.002	0
VSMC	Higd1b	0	2.09126	0.738	0	0
VSMC	Bcam	0	1.905123	0.75	0.014	0
VSMC	Mcam	0	1.851284	0.845	0.009	0
VSMC	Gucy1a1	0	1.850627	0.726	0.008	0

Cluster	**Gene**	**p_val**	**avg_log2FC**	**pct.1**	**pct.2**	**p_val_adj**
IF1	Rad51ap1	0	0.733068	0.8	0.013	0
IF1	Lrr1	7.02E-259	0.425761	0.55	0.007	1.34E-254
IF1	Mybl2	3.42E-242	0.390336	0.483	0.006	6.55E-238
IF1	Mcm5	5.14E-240	0.867321	0.9	0.031	9.84E-236
IF1	Top2a	1.43E-234	1.455163	0.867	0.029	2.73E-230
IF1	Pbk	1.11E-232	1.226563	0.817	0.025	2.12E-228
IF1	Uhrf1	1.89E-226	0.878371	0.817	0.027	3.61E-222
IF1	Clspn	8.51E-226	0.724775	0.767	0.022	1.63E-221
IF1	Hist1h1b	6.48E-222	0.996719	0.467	0.006	1.24E-217
IF1	Dscc1	1.41E-218	0.593203	0.633	0.015	2.70E-214

Cluster	**Gene**	**p_val**	**avg_log2FC**	**pct.1**	**pct.2**	**p_val_adj**
IF2	Gjb5	1.10E-199	0.7378	0.681	0.082	2.10E-195
IF2	Glipr1	3.86E-135	0.625788	0.611	0.097	7.40E-131
IF2	Cenpa	6.24E-135	1.799363	0.509	0.069	1.20E-130
IF2	Pclaf	1.22E-134	0.737422	0.456	0.049	2.34E-130
IF2	Gjb3	1.25E-128	0.310034	0.281	0.015	2.39E-124
IF2	Ccnb2	4.41E-128	1.131655	0.467	0.059	8.45E-124
IF2	Bcat1	6.45E-126	0.797317	0.804	0.204	1.24E-121
IF2	Acta2	7.86E-124	1.101911	0.684	0.141	1.50E-119
IF2	Birc5	1.17E-119	1.189635	0.432	0.053	2.25E-115
IF2	Il1rl1	8.12E-119	1.094216	0.474	0.064	1.55E-114

Cluster	**Gene**	**p_val**	**avg_log2FC**	**pct.1**	**pct.2**	**p_val_adj**
IF3	C1qtnf3	6.49E-222	2.919563	0.848	0.201	1.24E-217
IF3	Tnn	1.27E-191	1.422573	0.873	0.205	2.44E-187
IF3	Postn	1.18E-175	2.313526	0.983	0.458	2.25E-171
IF3	Cthrc1	1.09E-166	2.229164	0.99	0.543	2.09E-162
IF3	Col12a1	1.51E-154	1.565005	0.945	0.371	2.89E-150
IF3	Col1a1	1.06E-148	1.543449	1	0.955	2.02E-144
IF3	Col1a2	5.76E-141	1.393105	1	0.874	1.10E-136
IF3	Capn6	8.75E-133	0.759305	0.656	0.155	1.68E-128
IF3	Ptn	9.44E-130	1.660086	0.89	0.353	1.81E-125
IF3	Lgals1	4.07E-127	1.042633	1	0.98	7.80E-123

Cluster	**Gene**	**p_val**	**avg_log2FC**	**pct.1**	**pct.2**	**p_val_adj**
IF4	Mmp27	1.19E-98	0.563316	0.5	0.009	2.27E-94

IF4	Col6a5	1.78E-97	1.046239	0.636	0.016	3.41E-93
IF4	Draxin	3.14E-78	0.404489	0.318	0.005	6.00E-74
IF4	Dlk1	9.87E-78	3.36091	0.682	0.025	1.89E-73
IF4	Cpz	1.10E-62	1.508402	0.818	0.048	2.11E-58
IF4	Plac8	1.94E-51	3.420075	1	0.099	3.71E-47
IF4	Wnt16	6.32E-47	0.863145	0.773	0.054	1.21E-42
IF4	Mcoln2	1.23E-45	0.429844	0.409	0.015	2.35E-41
IF4	Ccl8	1.11E-37	2.731665	1	0.13	2.12E-33
IF4	C430049B03Rik	1.71E-36	1.519104	0.682	0.057	3.28E-32

Supplementary Table 8. *Foxm1* Regulon

Cep55	*Racgap1*	*Hmgb2*	*Mxd3*	*Dock5*	*Asf1b*
Mki67	*Ncapd2*	*Ndc80*	*Ska1*	*Tacc3*	

Supplementary Table 9. *Pole3* Regulon

Acaca	*Acbd3*	*Adam12*	*Adcy7*	*Arntl*	*Baz1b*
C2cd3	*C87436*	*Ccbe1*	*Ccne1*	*Chaf1b*	*Chn2*
Fam98a	*Fancl*	*Gart*	*Gemin6*	*Gins2*	*Gpr153*
Hat1	*Hist1h1e*	*Hjurp*	*Hmgb3*	*Hmgcr*	*Ier3ip1*
Irx3	*Lsm3*	*Lsm5*	*Mbtps2*	*Mcm3*	*Mcm4*
Mcm7	*Mdn1*	*Med10*	*Moxd1*	*Myh10*	*Nfkb2*
Ogg1	*Pcdh19*	*Pla2g4a*	*Plk4*	*Poc5*	*Polg*
Ppp1r7	*Ptpn4*	*Racgap1*	*Rpa2*	*Ruvbl2*	*Sephs1*
Skp2	*Slc25a44*	*Smad2*	*Smchd1*	*Snrpd1*	*Steap1*
Tbx3					

Supplementary Table 10. *Pole4* Regulon

Ccne1	*Gins2*	*Mcm3*	*Rbm3*	*Enah*	*Ung*
Gap43	*Dtl*	*Uhrf1*	*Cenpk*	*Mcm2*	*Mcm5*
Orc6	*Pcna*	*Rad51*	*Psat1*	*Siva1*	

Supplementary Table 11. *Hif1a* Regulon

Ankrd11	*Kdm2b*	*190002N15Rik*	*Sgk1*	*Abl2*	*Ankrd17*
Btg3	*Copa*	*Ddx3x*	*Dlc1*	*Gas5*	*Lmna*
Lysmd3	*Mbnl2*	*Nr4a2*	*Prrc2c*	*Rpl3*	*Srpr*
Srsf6	*Stat3*	*Tmem39a*	*Tnks2*	*Uso1*	*Vegfa*
Xpr1	*Socs2*	*Tnfaip3*	*Adcy7*	*Ak2*	*Anp32b*
Arcn1	*Arhgef19*	*Cacna1c*	*Cald1*	*Calu*	*Cblb*
Chn2	*Clip1*	*Cltc*	*Cnnm4*	*Cog3*	*Ddit4*
Dhrs3	*Dnajc1*	*Dock9*	*Dyrk2*	*En1*	*Eri3*
Ext1	*Fam117b*	*Foxp4*	*Gadd45b*	*Golga4*	*H19*
Hnrnpa0					

Supplementary Table 12. *Nfactc4* Regulon

Vegfa	*Angptl2*	*Antxr1*	*C1qtnf6*	*Chd3*	*Dhx57*
Fbn1	*Glis3*	*Kcnj15*	*Lrig3*	*Meg3*	*Nfatc2*

Prrx2	*Psd3*	*Rin3*	*Tgfb3*	*Tnn*	*Vcan*
Col12a1	*Dkk3*	*Igfbp2*	*Kcnma1*	*Nfatc4*	*Olfml3*
Thbs2	*Mtmr11*	*C1qtnf3*	*Prkd2*	*Srpx2*	*Arsj*
Olfml2b	*Hmcn1*	*Itga2*	*Aspn*	*Fzd2*	

Supplementary Table 13. *Cebpd* Regulon

Arhgap32	*C2*	*Cntfr*	*Gpc3*	*Sfrp2*	*Adipoq*
Angpt1	*Cadm3*	*Col6a6*	*Dkk2*	*Fgf7*	*Flrt2*
Fmo1	*Hdac7*	*Mgst1*	*Ntrk2*	*Opcml*	*Ankrd11*
Chd2	*Eif4a2*	*Foxp1*	*Pdp1*	*Spop*	*Tmcc3*
Arid5a	*Arl5b*	*Atf3*	*Atp8b1*	*Btg1*	*Btg2*
Ccl7	*Cxcl1*	*Cyr61*	*Dusp1*	*Fam110b*	*Fos*
Fosb	*Fosl2*	*Gadd45g*	*Gem*	*Ier2*	*Irs2*
Jun	*Kdm6b*	*Klf6*	*Klf9*	*Map3k8*	*Mllt10*
Myc	*Nckap5l*	*Nfil3*	*Nfkbiz*	*Per1*	*Sgk1*
Slc38a2	*Spry2*	*Trib1*			

Supplementary Table 14. *Klf4* Regulon

Cadm3	*Atf3*	*Cdkn1a*	*Fosb*	*Has1*	*Mafk*
Osr2	*Arl4a*	*Insig1*	*Maff*	*Rab11fip5*	*Tob1*
Bdnf	*Camkk1*	*Coro2b*	*Erf*	*Klf3*	*Mtmr12*
Mtmr3	*Ncoa3*	*Pak4*	*Stk40*	*Chst1*	*Tmem158*
Cry2	*Wnt2*	*Rbm38*	*Rusc2*	*Klf13*	*Cd248*
Msx1	*Ndrg1*	*Timp3*	*Trip10*	*Ugdh*	*Zfp385a*
Arap1	*Tacc2*	*Spsb1*	*Mical1*	*Hdac4*	*Scara5*
Stmn4	*Bbc3*				

Supplementary Table 15. *Irf1* Regulon

Cntfr	*Dkk2*	*Tbx5*	*Atf3*	*Ccnl1*	*Irf1*
Klf9	*Map3k8*	*Mllt10*	*Sbno2*	*Zfp36l1*	*Il6*
Cxcl10	*H2-Q7*	*Stx11*	*Tnfaip3*	*Hk2*	*Pogz*
Socs7	*Twist2*	*Acsl1*	*Pparg*	*Nr2f2*	*Psmb8*
Tcirg1	*Pik3r1*	*Tifa*	*Tap2*	*H2-Q6*	*Plxna2*
Deptor	*Rnf19b*	*Cebpd*	*Dtx3l*	*Esr1*	*Nampt*
Pcdh18	*Uba7*				

Supplementary Table 16. *Sox5* Regulon

Col4a1	*Hipk2*	*Limch1*	*Lmo4*	*Pbx1*	*Sox11*
Traf1	*Zeb2*	*Zfp385b*	*Sparcl1*	*Prune2*	*Calcrl*
Mfap3l	*Rtn1*	*Rspo2*	*Col22a1*	*Fut9*	*Hcn1*
Sox5	*Ugp2*	*Efnb2*	*Gpr1*	*Itgb8*	*Clic5*
Pcbd1					

Supplementary Table 17. *Foxo1* Regulon

Dcaf15	*Mrpl53*	*Tet2*	*Usp38*	*Als2*	*Ankrd11*
Ccnk	*Cdc14b*	*Ctnnd1*	*Dnajb4*	*Eif4a2*	*Exoc2*
Fbxo33	*Fbxo42*	*Fbxw7*	*Gpbp1*	*Gripap1*	*Homer1*

Hoxa11	*Jarid2*	*Midn*	*Slc30a9*	*Smchd1*	*Tiprl*
Ubn2	*Zfhx3*	*Zfp503*	*Zfp655*	*Bhlhe40*	*Cttnbp2nl*
Hsph1	*Ier2*	*Junb*	*Klf4*	*Nckap5l*	*Nfkbiz*
Ppp1r10	*Sbno2*	*Trib1*	*810055G02Rik*	*Adipor1*	*Aftph*
Ahnak	*Aldoa*	*Ankrd17*	*Arf6*	*Arhgef10l*	*Arih2*
Arl4a	*BC005537*	*Becn1*			

Supplementary Table 18. *Creb5* Regulon

Abr	*Adamtsl1*	*Ap2a2*	*Arrb1*	*Atp6v0c*	*Bend6*
Casp3	*Cdk6*	*Cdr2l*	*Ckb*	*Clcn3*	*Clcn5*
Creb5	*Daam1*	*Dbndd2*	*Dennd4b*	*Egfr*	*Elmo1*
Epdr1	*Fahd2a*	*Fn1*	*Fyn*	*Gabarapl2*	*Homer1*
Hspb8	*Igfbp5*	*Igsf9b*	*Laptm4b*	*Map1lc3a*	*Mknk2*
Mmp28	*Nacc2*	*Nhs*	*Pfdn1*	*Ppp2r5b*	*Ptpre*
Rab10	*Rela*	*Rnd2*	*Sbsn*	*Sema4c*	*Slc6a9*
Sox11	*Thbd*	*Timp3*	*Tmbim1*	*Tmod1*	*Trps1*
Ubap1	*Vat1*	*Zfhx2*			

References

1 Rountree RB, Schoor M, Chen H, *et al.* BMP receptor signaling is required for postnatal maintenance of articular cartilage. *PLoS Biol* 2004;**2**:e355. doi:10.1371/journal.pbio.0020355

2 Madisen L, Zwingman TA, Sunkin SM, *et al.* A robust and high-throughput Cre reporting and characterization system for the whole mouse brain. *Nat Neurosci* 2010;**13**:133–40. doi:10.1038/nn.2467

3 Snippert HJ, van der Flier LG, Sato T, *et al.* Intestinal Crypt Homeostasis Results from Neutral Competition between Symmetrically Dividing Lgr5 Stem Cells. *Cell* 2010;**143**:134–44. doi:10.1016/j.cell.2010.09.016

4 Roelofs AJ, Zupan J, Riemen AHK, *et al.* Joint morphogenetic cells in the adult mammalian synovium. *Nat Commun* 2017;**8**:15040. doi:10.1038/ncomms15040

5 Eltawil NM, De Bari C, Achan P, *et al.* A novel in vivo murine model of cartilage regeneration. Age and strain-dependent outcome after joint surface injury. *Osteoarthritis Cartilage* 2009;**17**:695–704. doi:10.1016/j.joca.2008.11.003

6 Roelofs AJ, De Bari C. Immunostaining of Skeletal Tissues. In: *Methods in molecular biology (Clifton, N.J.)*. Humana Press 2019. 437–50. doi:10.1007/978-1-4939-8997-3_25

7 Gnerre S, Maccallum I, Przybylski D, *et al.* High-quality draft assemblies of mammalian genomes from massively parallel sequence data. *Proc Natl Acad Sci U S A* 2011;**108**:1513–8. doi:10.1073/pnas.1017351108

8 Young MD, Behjati S. SoupX removes ambient RNA contamination from droplet-based single-cell RNA sequencing data. *Gigascience* 2020;**9**:1–10. doi:10.1093/gigascience/giaa151

9 Butler A, Hoffman P, Smibert P, *et al.* Integrating single-cell transcriptomic data across different conditions, technologies, and species. *Nat Biotechnol* 2018;**36**:411–20. doi:10.1038/nbt.4096

10 La Manno G, Soldatov R, Zeisel A, *et al.* RNA velocity of single cells. *Nature* 2018;**560**:494–8. doi:10.1038/s41586-018-0414-6

11 Bergen V, Lange M, Peidli S, *et al.* Generalizing RNA velocity to transient cell states through dynamical modeling. *Nat Biotechnol* Published Online First: 2020. doi:10.1038/s41587-020-0591-3

12 Cao J, Spielmann M, Qiu X, *et al.* The single-cell transcriptional landscape of mammalian organogenesis. *Nature* 2019;**566**:496–502. doi:10.1038/s41586-019-0969-x

13 Street K, Risso D, Fletcher RB, *et al.* Slingshot: cell lineage and pseudotime inference for single-cell transcriptomics. *BMC Genomics* 2018;**19**:477. doi:10.1186/s12864-018-4772-0

14 Chen Y, Lun ATL, Smyth GK. From reads to genes to pathways: Differential expression analysis of RNA-Seq experiments using Rsubread and the edgeR quasi-likelihood pipeline. *F1000Research* 2016;**5**:1–51. doi:10.12688/F1000RESEARCH.8987.2

15 Aibar S, González-Blas CB, Moerman T, *et al.* SCENIC: Single-cell regulatory network inference and clustering. *Nat Methods* 2017;**14**:1083–6. doi:10.1038/nmeth.4463

16 Gustavsen JA, Pai S, Isserlin R, *et al.* Rcy3: Network biology using cytoscape from within r [version 1; peer review: 2 approved]. *F1000Research* 2019;**8**:1–20. doi:10.12688/f1000research.20887.1

17 Hu H, Miao YR, Jia LH, *et al.* AnimalTFDB 3.0: A comprehensive resource for annotation and prediction of animal transcription factors. *Nucleic Acids Res* 2019;**47**:D33–8. doi:10.1093/nar/gky822

18 Croft AP, Campos J, Jansen K, *et al.* Distinct fibroblast subsets drive inflammation and damage in arthritis. *Nature* 2019;**570**:246–51. doi:10.1038/s41586-019-1263-7

19 Chou CH, Jain V, Gibson J, *et al.* Synovial cell cross-talk with cartilage plays a major role in the pathogenesis of osteoarthritis. *Sci Rep* 2020;**10**:1–14. doi:10.1038/s41598-020-67730-y

20 Mizoguchi F, Slowikowski K, Wei K, *et al.* Functionally distinct disease-associated fibroblast subsets in rheumatoid arthritis. *Nat Commun* 2018;**9**:1–11. doi:10.1038/s41467-018-02892-y

21 Zhang F, Wei K, Slowikowski K, *et al.* Defining inflammatory cell states in rheumatoid arthritis joint synovial tissues by integrating single-cell transcriptomics and mass cytometry. *Nat Immunol* 2019;**20**:928–42. doi:10.1038/s41590-019-0378-1

22 Schumacher BL, Block JA, Schmid TM, *et al.* A novel proteoglycan synthesized and secreted by chondrocytes of the superficial zone of articular cartilage. *Arch Biochem Biophys* 1994;**311**:144–52. doi:10.1006/abbi.1994.1219

23 Zhang C, Gao Y, Jadhav U, *et al.* Creb5 establishes the competence for Prg4 expression in articular cartilage. *Commun Biol* 2021;**4**:332. doi:10.1038/s42003-021-01857-0

24 Khan IM, Salter DM, Bayliss MT, *et al.* Expression of clusterin in the superficial zone of bovine articular cartilage. *Arthritis Rheum* 2001;**44**:1795–9. doi:10.1002/1529-0131(200108)44:8<1795::AID-ART316>3.0.CO;2-K

25 Li L, Newton PT, Bouderlique T, *et al.* Superficial cells are self-renewing chondrocyte progenitors, which form the articular cartilage in juvenile mice. *FASEB J* 2017;**31**:1067–84. doi:10.1096/fj.201600918R

26 Buechler MB, Pradhan RN, Krishnamurty AT, *et al.* Cross-tissue organization of the fibroblast lineage. *Nature* 2021;**593**:575–9. doi:10.1038/s41586-021-03549-5